Development of a 6-DOF Trajectory Simulation Model for Asymmetric Projectiles

AAA Altufayl

orcid.org/0000-0001-9374-433X

Dissertation submitted in partial fulfilment of the requirements for the degree *Master of Science in Mechanical Engineering* at the North-West University

Supervisor: Prof WL den Heijer

Graduation Ceremony: May 2019

Student number: 27359999

بِسْمِ اللهِ الرَّحْمَنِ الرَّحِيم

﴿قَالُوا سُبْحَانَكَ لَا عِلْمَ لَنَا إِلَّا مَا عَلَّمْتَنَا إِنَّكَ أَنتَ الْعَلِيمُ الْحَكِيم﴾

(سورة البقرة، الآية 32)

الحمْد لله حمدًا كثيرًا طيّبًا مباركًا فيه، مِلْءَ السّمَاوَاتِ وَمِلْءَ الْأَرْضِ وَمِلْءَ مَا شِئْتَ مِنْ شَيْءٍ بَعْدُ، أَهْلَ الثّنَاءِ وَالْمَجْدِ لَا مَانِعَ لِمَا أَعْطَيْ وَلَا مُعْطِي لِمَا مَنَع وَلَا يَنْفَعُ ذَا الْجَدِّ مِنْه الْجَدُ، الحمْد لله كما ينبغي لِجَلال وجْهِه وعظيمِ سُلْطَانه، لَهُ الحَمْدُ كُلْه، وإِليهِ يُرجعُ الأمر كُلّه، والصّلاةُ والسلامُ على المَبْعُوثِ رَحمَةً للعالمين.

ACKNOWLEDGEMENTS

This study would not have been possible had it not been for the endeavour of many individuals. I wish to express my deepest gratitude towards the following people and institutions:

Prof. Willem L den Heijer, my supervisor, to whom I'm greatly indebted for his support, guidance, and encouragement.

Mr. Louis Du Plessis, my co-supervisor, whose encouragement, guidance and support from the initial to the final level enabled me to develop an understanding of the subject, and without him this thesis would not have been completed or written. One simply could not wish for a better or friendlier supervisor. I am indebted to him more than he knows.

Raney Almehmadi, Naif Alotaibi, Shehab Alzahrani, Saad Alqarni, Abdulaziz Bin Sultan, Motassm A. Aldoegre , my colleagues in MIC, for being great colleagues, a constant source of support and inspiration. Their unselfish cooperation and much needed help has helped me to complete this task.

Thanks to all members of the MIC for the opportunity, support, and for the payment of my study fees.

Thanks to the product development team at RDM, for their support, help, and encouragement.

Lastly, my deepest gratitude goes to my parents and siblings for their unflagging love and support throughout my life; this dissertation would have been simply impossible without them. I am indebted to my father, Abdulrahman Altufayl, for his care and love. I cannot ask for more from my mother, Nawal Alolit, as she is simply perfect. Mother, I love you. Thank you to my two children, Daniyah and Abdulrahman, for their ability to make me smile on the bad days and keep me unfocused. Most importantly, thank you to my wife Abrar who never stopped pushing me towards success and believed in me even when I was doubtful.

ABSTRACT

Key terms: Asymmetric projectiles, spin-stabilized projectile, six degree of freedom trajectory model, stability of projectile, flight dynamics, impact dispersion, mass asymmetries, aerodynamic asymmetries.

Precision is important to modern artillery where long range cannons can fire unguided and guided projectiles for many kilometres. Precision projectiles are in demand, because it is both cost effective (increasing the chance to hit the target with the first shot) and reduce collateral damage (minimises the risk of hitting friendly forces). This requires accurate prediction of the flight path using trajectory simulation models. The so-called 6-DOF projectile exterior ballistic model is the most complex simulation model and allows for the modelling of all the projectile motions.

The aim of this study was to develop and verify the correctness of a 6 Degrees-of-Freedom trajectory simulation model known as 6-DOF, by conducting case studies to gain insight in the flight behaviour of mortar bombs.

This literature study provided valuable insight on the various trajectory simulation models. The information from this literature was used to define models to be incorporated in a 6-DOF trajectory simulation that can be used to analyse both symmetric and asymmetric projectiles.

Based on the case studies selected in the verification part used for this study, the input data requirements for each case study selected for modelling purposes, were entered into the 6-DOF model and output results were generated. The 6-DOF output results were compared to results from other simulation programs, as well as the results that predicted by analytical solutions.

The 6-DOF model produced similar outputs, within a difference of +0.36% to +0.49% in range and - 0.31% to -2.70% in drift, to that of the PRODAS V3 program. The differences between the results from the two programs are relatively small, except for drift. In addition, the results illustrated that the 6-DOF model and WinFast program produce comparable results when starting with the same initial parameters.

Lastly, the 6-DOF model program was conducted case studies to find possible causes for the flight behaviour of real test results captured during the dynamic firing of mortar bombs. The results of the cases study indicated good agreement with experimental results. The 6-DOF results matches the radar data captured during dynamic testing.

GLOSSARY OF TERMS AND ABBREVIATIONS

Here are the Terms that are used in this Master thesis.

GLOSSARY OF TERMS

BALCO	The Standard 6-DOF Simulation Model used within NATO
BATES	Battlefield Artillery Target Engagement System
DOF	Degrees of Freedom
ELEV	Elevation Angle
FT	Firing Table
MDP	Meteorological Datum Plane
Modelling	Using a Computer Program Version of a Mathematical Model for a Physical System.
MPMM	Modified Point Mass Model
MSL	Mean Sea Level
MV	Muzzle Velocity
NABK	NATO Armaments Ballistics Kernel
ODE	Ordinary Differential Equation
PI	Practice Inert
PLT	Projectile Linear Theory
PMM	Point Mass Model
PRJ	Projectile
Prodas V3	Projectile Design and Analysis Software by Arrow Tech
QE	Quadrant Elevation, see also ELEV
RDM	Rheinmetall Denel Munition
RT	Range Tables, see also FT
Temp	Temperature
WinFast	Program used by RDM for Trajectory Analysis and The Preparation of Range Tables
WNB	Natural Pitch Frequency in The Body frame

ABBREVIATIONS

Cd_0	Zero Yaw Drag Coefficient
$Cd_{\alpha 2}$	Quadratic Yaw Drag Coefficient
Cd_b	Base Drag Coefficient [Note that base drag is already included in Cd_0, but also given separately for use in Base Bleed modeling]

Cl	Roll Moment Coefficient: [$Cl = Cl_{\delta} * \delta$]
CL_{α}	Lift Force Coefficient
$CL_{\alpha 3}$	Cubic Lift Force Coefficient
Cl_{p}	Spin Damping Moment Coefficient
Cm_{α}	Pitch Moment Coefficient
$Cm_{\alpha 3}$	Cubic Pitch Moment Coefficient
$Cm_{p\alpha}$	Magnus Moment Coefficient
$Cm_{p\alpha 3}$	Cubic Magnus Moment Coefficient
Cm_{q}	Pitch damping moment coefficient
$Cm_{d\alpha/dt}$	Damping Moment due to the Rate of Change in Yaw Angle
Cspin	Base Bleed Spin Burn Rate Coefficient see also Aspin, Bspin
Cy_{pa}	Magnus force coefficient
Cy_{pa3}	Cubic Magnus force coefficient
d	Reference Length = Projectile Diameter
D	Drag Force
Db	Diameter at Base
Fmag	Magnus Force
ICAO	International Civil Aviation Organization
It	Transverse (Lateral) Moment of Inertia
Ix	Axial Moment of Inertia
L	Lift Force
M	Mass
Mach	Mach Number = Velocity / (Acoustic Velocity)

Mmag	Magnus Moment
Mp	Spin Damping Moment
Mq	Pitch Damping Moment
MSL	Mean Sea Level
MV	Muzzle Velocity
Mα	Pitch (Overturning) Moment due to Yaw
Mδ	Roll Moment due to Fin or Nubb Deflection Angle
NABK	NATO Artillery (Armaments) Ballistic Kernel see (STANAG 4537, 2010)
p	Spin Rate
Pb	Base Pressure
Pa	Ambient Free Stream Pressure
q	Pitch Rate
S	Reference Area = π * Diameter^2 / 4
V	Velocity
$\vec{V}$	Velocity Vector
$\hat{X}$	Unit Vector along the projectile axis of symmetry

GREEK and Other SYMBOLS

ρ	Atmospheric density		
α	Yaw Angle [also called Angle of Attack or Incidence]		
γ	Specific Heat Ratio	=	Cp/Cv

CONVENTIONS and MATH OPERATIONS

$\rightarrow$	An arrow above any symbol is used to identify a Vector
$\wedge$	This is used to identify a unit vector
$\otimes$	This symbol is used to indicate the Vector (Cross) Product
*	This symbol is used for Scalar Product (Multiplication)

TABLE OF CONTENTS

LIST OF TABLES

LIST OF FIGURES

CHAPTER 1 INTRODUCTION

1.1 Title

Development of a 6-DOF trajectory simulation model for asymmetric projectiles.

1.2 Topic

This dissertation focuses on the theoretical and practical aspects of the stability of symmetric and asymmetric projectiles during flight. The relevant mathematical equations are used to develop a simulation model to analyse the performance observed during dynamic flight tests. The conducted research highlights the factors that play important roles in the stability of a projectile during flight. A six-degrees-of-freedom, [6-DOF], trajectory simulation proved itself indispensable for such an analysis and the development of specifications for the design and manufacturing tolerances of projectiles and missiles.

1.3 Background

Initially, exterior ballistics existed more as an art or craft before it developed into a science. The technical art of it emanated as simple throwing mechanisms. After years of continuous and evolutionary development, exterior ballistics were established as a branch of science, especially after the growing body of knowledge gathered during the renaissance era in the sixteenth and seventeenth century. Isaac Newton was one of the prominent scientists in this era, and one of those who contributed a great deal to make exterior ballistics into the science we know today. The most important contributions are the laws of motion and the effect of aerodynamics on a projectile. Through the years, ballisticians developed an interest in armament development and the goals are still the same, to primarily extend range and improve accuracy on target (Mccoy, 1998).

“The modern science of the exterior ballistics has evolved as a specialized branch of the dynamics of rigid bodies, moving under the influence of gravitational and aerodynamic forces and moments” (Mccoy, 1998). The development of a better understanding of exterior ballistics lad to the establishment of guidelines for stability and an increase in the accuracy of the projectiles.

Precision is important for modern artillery where long range cannons can fire unguided and guided projectiles for many kilometres. Precision projectiles are in demand, because they are cost effective (increasing the chance to hit the target with the first shot) and reduce collateral damage (minimizes the risk of hitting friendly forces) (Fresconi *et al.*, 2010; Maurice Lee

Rasmussen, 1964; Sterne, 1944). This requires accurate prediction of the flight path using trajectory simulation models. Different models can be used to predict the flight path as discussed in chapter 2. The so-called 6-DOF projectile exterior ballistic model is the most complex simulation model and allows for the modelling of all the projectile motions. The first 6-DOF projectile exterior ballistic model was constructed by pioneering English ballisticians Fowler, Gallop, Lock and Richmond in 1920 (Mccoy, 1998). Various scientists and ballisticians have since improved on this model.

1.4 Rationale

Ballistic munitions, which is indeed any flying object, are meant to cause extensive damage. Projectiles and mortar bombs are relatively inexpensive when compared to guided missiles which is self-propelled projectiles, with the ability to control or correct the projectile trajectory after being fired. Without corrections to the flight path, the impact accuracy of ballistic munitions deteriorates as the range increases. The effectiveness of ballistic munitions such as projectiles and mortar bombs therefore reduce significantly as the impact accuracy degraded through external disturbances and instabilities during flight. (“Impact accuracy” is used as a measure for the deviation of the actual impact point from the desired impact on the target). These external disturbances include variation in atmospheric conditions such as temperature, air pressure, density, and wind direction, firing platform motion, aiming errors, gun tube problems, and variations in propellant and projectiles (Dykes, 2011). A 6-DOF simulation model can be used to analyse the contribution of all these external influences to allow for the evaluation of the behaviour of projectiles. In addition, the 6-DOF simulation model can be used during the design process to derive specifications for allowable manufacturing tolerances, and asymmetries to ensure that the performance goal with respect to stability and greater accuracy is achieved. This 6-DOF simulation model is developed to achieve satisfactory agreement with published data and verified against experiments and other trajectory simulation codes to be used with confidence for projectile trajectory analysis under various conditions.

1.5 Justification

A 5-DOF simulation program is sufficient and computationally effective to study the behaviour of symmetric projectiles. To study the effect of body fixed asymmetries however, it is imperative to use a 6-DOF simulation model. Developing a new 6-DOF simulation model allows for the study of asymmetries and instabilities not treated in the “standard available 6-DOF programs”.

1.6 Degrees of Freedom

Six degrees of freedom is a specific parameter count for the number of degrees of freedom an object has in three-dimensional space. It means that there are six parameters or ways that the object can move. A 6-DOF simulation model has three rotations and three translations. The three translations components (x, y, z) describe the position of the projectile's centre of mass and the three Euler angles (φ, θ, ψ) describe the orientation of the projectile, as illustrated in Figure 1.

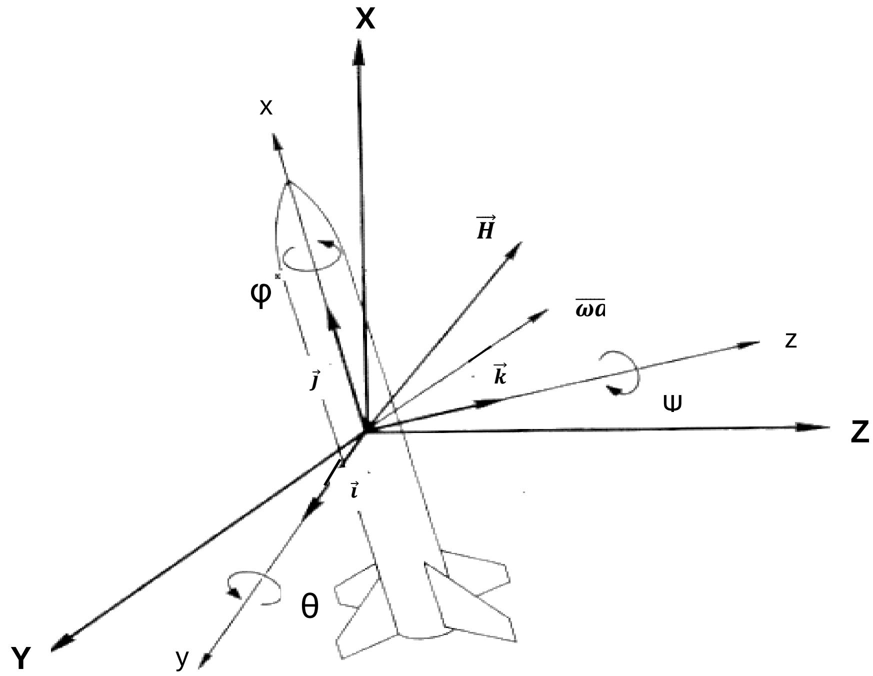

Figure 1 : Axis System (6-DOF) (Vaughn, 1969).

The motion of a symmetric projectile can adequately be described using an aeroballistics axis system. This is an axis system that share all angular motion of the projectile, but do not spin around the axis of symmetry, essentially rendering it to a five-degrees-of-freedom model. For the analysis of an asymmetric projectile it is however necessary to consider angular motion around all the axes, since these asymmetries would be body fixed and rotate with the projectile. Therefore, when considering a 6-DOF simulation, care should be taken to ensure that all the expected asymmetries are treated properly and addressed.

1.7 Problem Statement

There are 6-DOF trajectory simulation models available addressing some of the shortcomings in the classical tri-cyclic description of motion. It was however, deemed necessary to develop a new 6-DOF trajectory model that can be used during the research to address simultaneously the challenges associated with:

- Projectiles experiencing high angles of attack and hence require nonlinear description of its aerodynamic properties
- Projectiles with asymmetries of both aerodynamic and inertia properties

Such a model can be verified against available analytic solutions, (as given by the tri-cyclic description of motion) and existing 6-DOF simulation programs for symmetric programs. The new 6-DOP simulation program will then be used during the research to evaluate combinations of asymmetries to match the "unexpected" projectile behaviour observed during dynamic firing tests.

In future the new 6-DOF simulation program to be developed during this research can also be adapted to study new aerodynamic properties (not presently treated in existing 6-DOF models) such as the Yaw Moments experienced by a projectile during Pitch presently associated with vortex shedding on spinning projectiles (Nielsen, 1988).

However, there are several factors that affect a projectile's stability during flight. Classically the stability of spinning projectiles is determined by the dynamic stability factor [Sd] and gyroscopic stability factor [Sg], as illustrated in Figure 2. The derivation of the illustrated stability region is based on the tri-cyclic motion of the projectile. The name "tri-cyclic" stems from the fact that the angular motion of the projectile is described as the sum of three rotating vectors.

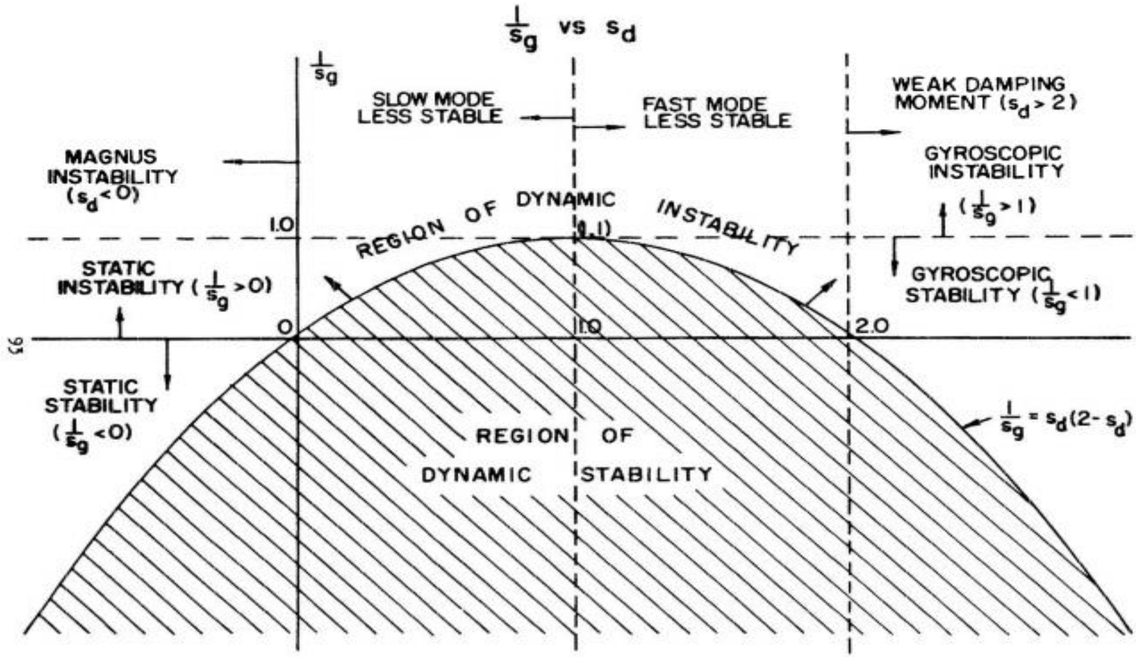

Figure 2 : **Graphic Presentation of Stability Criteria (Murphy, 1963).**

The stability criteria as illustrated in Figure 2, specify the conditions that will satisfy stable pitch and yaw motion of the projectile. These motions are oscillating motions and stability requires that it should be damped. The classic stability criteria as derived by (Murphy, 1963) is based on assumptions of linearity regarding aerodynamic properties, and limited allowance for asymmetries at a constant flight velocity. Although very useful, it is limited to the analysis of the pitch and yaw motion due to linear forces, and moments along short segments of the flight path. Using a 6-DOF trajectory simulation model allows for the study of non-linear properties and various asymmetries encountered along the entire flight path. It allows for more complex modelling and the study of requirements for stability beyond what is treated in the classical tri-cyclic motion from a mathematical perspective.

1.8 The Objectives

<u>The primary objective of this research is to:</u>

(1) Present a detailed description of the forces and moments associated with symmetric and asymmetric projectiles.

(2) Develop a simulation program incorporating these equations.

(3) Verify the accuracy of this simulation program by:

(a) Comparing the translational motion of a symmetric projectile with the results of a simpler model.

(b) Compare the angular motion of an asymmetric projectile with the analytic solutions noted by (Murphy, 1963; Regan, 1984; Vaughn, 1969).

(c) Compare the results with predictions in other 6-DOF simulation programs and case studies published in literature.

(4) Use the program for a diagnostic evaluation of real test data captured for mortar projectiles with asymmetries and conduct a systematic analysis of the effects of asymmetries on the flight trajectory of mortar bombs.

1.9 Research Methodology and Experimental Procedure

1.9.1 The main phases of this research study consist of:

(1) A literature study of 6-DOF simulation programs and the models required to predict forces and moments for symmetric and asymmetric projectiles.

(2) Develop and verify the correctness of a 6-DOF simulation program.

(3) Using the 6-DOF simulation model to conduct case studies to gain insight in the flight behaviour of mortar bombs.

1.9.2 Method used during research study

(1) In the literature study important references to 6-DOF simulation and the modelling of the forces and moments for these simulations will be identified. A critical review of the literature will be used to identify the short-comings in the available models and define models to be incorporated in the 6-DOF simulation program.

(2) A 6-DOF simulation program will be developed using Matlab and based on the models identified during the literature study phase. This 6-DOF simulation program will be validated by comparing predicted results with (a) results from analytical results for simplified case studies (b) results published in literature for case studies and (c) results obtained by other 6-DOF simulation programs that are commercially available.

(3) On completion of the 6-DOF program validation phase, the program will be used to conduct case studies to identify possible causes for the flight behavior of real test results captured during the dynamic firing of mortar bombs. The correlation between the test data

and predicted performance will be used to obtain insight in the accuracy of this simulation program and conclude with comments on the adequacy of models to analyse stability and asymmetries.

1.10 Research Contributions

(1) Present a detailed description of the forces and moments associated with symmetric and asymmetric projectiles.

(2) Study in depth non-linear and “non-standard” aerodynamic properties for symmetric and asymmetric projectiles.

(3) Analyse the external disturbances and instabilities observed during flight, using a 6-DOF simulation model to evaluate and identify possible causes for the observed behaviour of projectiles.

(4) Establish a design tool to derive specification for manufacturing tolerances and allowable asymmetries to ensure that the desired performance goals with respect to range and accuracy are achieved.

(5) This research provides a cost-effective tool that can be used to predict the behavior of the projectiles.

(6) This research provides a description of parameters that affect the flight trajectory of mortar bombs, and the generic presentation thereof that contributes to failure analysis in cases where “strange” behavior is observed during dynamic tests of mortar bombs.

1.11 Scope and Limitations of research

(1) The 6-DOF model can be used to predict the movement of projectiles only and cannot be used with aircraft, ships and robot movement, which requires its own models.

(2) All the data which the author will use in this model consist of actual test data from Rheinmetall Denel Munition (RDM). However, the model will not be limited to RDM’s projectiles, but future studies would require data for other projectiles.

(3) Due to the expected complexity of the 6-DOF model, the simulation time on standard PC computers is expected to be relatively long.

(4) Verification and the study of real test cases will be limited to data available for projectiles of RDM.

CHAPTER 2: LITERATURE SURVEY

2.1 Introduction

Since the ballisticians started to use computers in the ballistic science, many theories and models have been developed to simulate trajectory of projectiles. These models range from the extremely simple to very complex models. The degree of complexity usually depends upon the degrees of freedom which the model is based on, and the specific simulation requirements. This chapter describes the development of these simulation models, starting with a simple model which is point mass trajectory model (PMM) that only includes gravity and drag forces. This is followed secondly by the modified point mass model (MPMM) which include the most essential forces and moments such as drag, gravity, lift, the Magnus force, and the Coriolis acceleration terms. While essentially still a PMM, it is modified to approximate yawing motion through the so-called “Yaw-of-Repose”. This model has become the international standard for artillery trajectory simulations (STANAG 4355, 2009). The next level of complexity is presented by the 5-DOF model. The 5 DOF model account for translation in three dimensions and rotations around the two axes (pitch and yaw) and include all forces and moments experienced by an axially symmetric projectile. Although the projectile spin about the axis of symmetric is included, the angle of rotation about this axis is irrelevant. Lastly, the 6-DOF model, which account for translation in three dimensions and rotations around the three axes (pitch, yaw and spin), and include forces and moments experienced by both axially symmetric and asymmetric projectiles. All the trajectory simulation models have the general layout as illustrated in Figure 3.

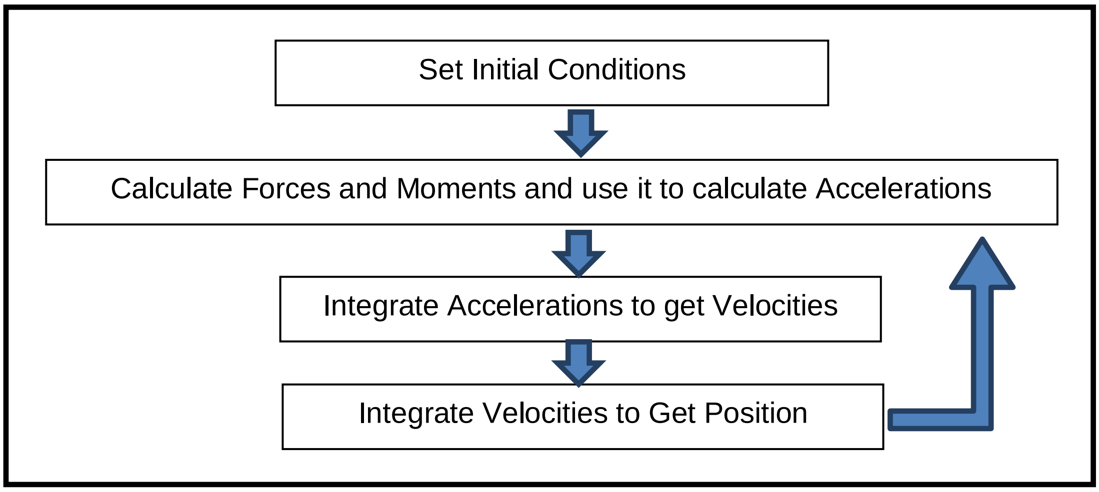

Figure 3: General elements of all trajectory simulations.

2.2 TRAJECTORY MODELS

2.2.1 Point Mass Trajectory Model

The Point Mass Trajectory Model is the simplest trajectory simulation model and if the flight is restricted to a plane as illustrated in Figure 4, it essentially becomes a 2-DOF trajectory simulation model.

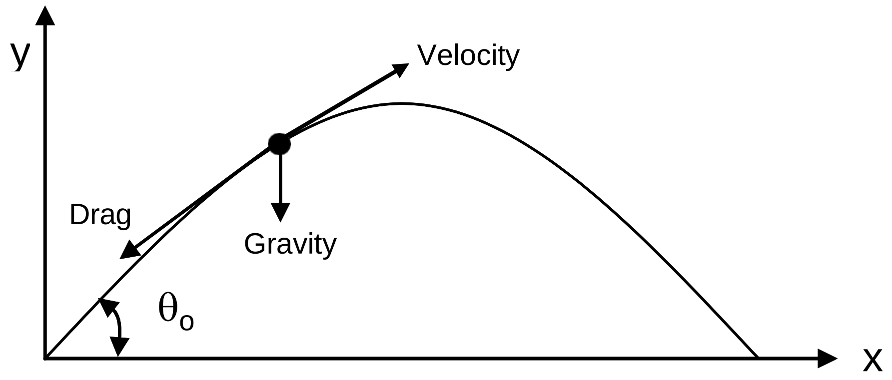

Figure 4: Forces Acting on the Projectile in a Point Mass Model (Fann, 2006)

The 2-DOF means translation along the horizontal axis, x (range) and vertical axis, y (height) as illustrated in Figure 4. The projectile is treated as a point mass in the point mass trajectory model. This means that the translation of the centre of gravity is simulated without considering the angular motion of the projectile around its centre of gravity. It is assumed that the projectile's axial axis is aligned with the trajectory. This means that the pitch and yaw is neglected. Despite the simplicity of the model, it can account for the effect that weather conditions may have on the trajectory. Furthermore, this model proved to be very efficient in terms of computing resources and time, as well as being very useful in predicting nominal trajectories and analyse the performance (Fann, 2006).

This model uses the body forces (as illustrated in Figure 4) to calculate the acceleration experienced by the projectile. Integration of this acceleration allows for the prediction of velocity and position along the trajectory. The force parallel to the trajectory shown in Figure 4, can be a combination of atmospheric drag force and thrust if the projectile is fitted with a rocket motor. The accuracy of the trajectory prediction is dependent on the time step, especially if first order integration routines are used. For these schemes a smaller time step is required to improve accuracy and will increase simulation run time. A solution might also be to use higher order integration schemes such as the Runga-Kutta schemes (Hoffman, 1992; Hawley & Blauwkamp, 2010). For constant gravity and no drag, this model has an analytic solution that will also be used as one of the verification case studies of the 6-DOF model. However, if flight is not restricted to a plane, the PMM becomes a 3-DOF trajectory simulation model allowing for translation in the Z-axis (cross-wise) direction as well.

2.2.2 Modified Point Mass Model (MPMM)

The modified point mass model is implemented in trajectory programs such as the NATO Armaments Ballistics Kernel (NABK), (STANAG 4537, 2010) and the Battlefield Artillery Target Engagement System (BATES) (Fann, 2006). This model has become an international standard for artillery trajectory simulations (STANAG 4355, 2009).

“The MPMM is representing the flight of spin-stabilised, dynamically stables, conventional projectiles, possessing at least axial symmetry. The mathematical modelling is accomplished, mainly by: (a) including only the most essential forces and moments, (b) approximating the actual yaw by the yaw of repose, neglecting transient yawing motion, and (c) applying fitting factors to some of the above forces to compensate for the neglect of other forces and moments and for the yaw approximation. All vectors have as a frame of reference a right-handed, orthonormal, ground-fixed, Cartesian coordinate system with unit vectors $(\vec{1}, \vec{2}, and\, \vec{3})$” as illustrated in Figure 5 (STANAG 4355, 2009).

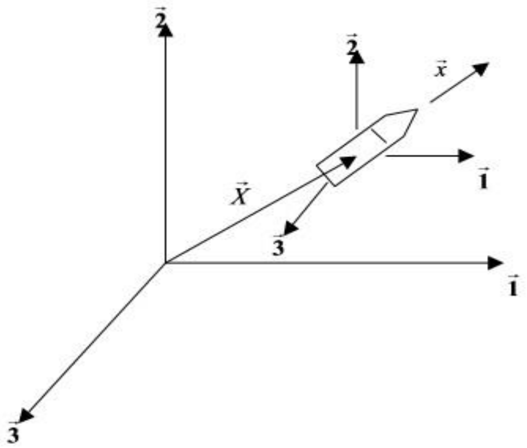

Figure 5 : Cartesian coordinate system with Unit Vectors (STANAG 4355, 2009)

The acceleration equation in MPMM contains the drag, thrust, gravity, lift, Magnus force, and the Coriolis acceleration terms, where the 2-DOF or 3-DOF only contains the drag, thrust and gravity terms. The MPMM provides means to predict drift due to (approximate) the effect of yaw while retaining computational efficiency and has become an international standard for ballistic simulations (STANAG 4355, 2009). It also includes moment terms: Magnus moment, spin damping moment and pitch damping moment.

2.2.3 5-DOF Trajectory Model (STANAG 4355, 2009)

The 5-DOF trajectory simulation model accounts for translation in three-dimensional space as well as rotation around the Y and Z axis (pitch and yaw angular motion). For symmetric projectiles, the 5-DOF has no limitation because there is not any forces and moments linked to the roll orientation of the projectile and the 5-DOF will render the same results as a full 6-DOF trajectory simulation.

In addition, the spin around the axial axis is treated independently accounting for its contribution towards “gyroscopic stiffness”, but not for any forces and moments linked to the rotation around the axial axis of symmetry. However, it provides the same accuracy as a full 6-DOF trajectory model without the need to use the extremely small integration timestep required especially for projectiles with a high spin rate. This makes it an efficient trajectory model but is limited to the simulation of symmetric projectiles (STANAG 4355, 2009).

For typical rocket configurations, experiencing a relatively low spin rate compared to spin stabilised projectiles, the 5-DOF trajectory model has become an international standard (STANAG 4355, 2009). Computational efficiency is maintained because these rockets experience relatively low rates of angular motion.

2.2.4 6-DOF Trajectory Model

(1) A full 6-DOF flight dynamics model by (Gkritzapis *et al.*, 2007) was proposed for the accurate prediction of short- and long-range trajectories of spin-stabilised projectiles. The projectile is assumed to be both rigid (non-flexible) and is axially symmetric in its spin axis. It allows for launches at low and high elevation angles and takes in consideration the most significant force and moment variations as well as gravity and Magnus Effect. This paper provides an excellent description of a typical 6-DOF model, but its major short-coming is that it is limited to the simulation of symmetric projectiles.

(2) Development and evaluation of a 6-DOF model of a 155 mm artillery projectile by Marcus Thuresson in Sept 2015 (Thuresson, 2015). In this Master Thesis, the author evaluated a 6-DOF model of a 155 mm artillery projectile and compared it to a modified point mass trajectory model for the same projectile. The models were simulated using the software FLAMES, that uses a spherical earth model, terrain data and measured atmospheric conditions. The model’s results were accurate in range but had a 35% error in drift compared to the firing-table of a 155 mm projectile. When the model was compared to a modified point mass model and to real test data, the Mean Distance Error (MDR) to target was about 250 m. A plausible reason for this distance error is that the data used in this

thesis was not very accurate. The thesis showed a large difference in the angle of attack between the different models for simulation of trajectories launched at high elevation as well as when there was a wind present. The results for the 6-DOF model showed that 90 % of all projectiles hit within a 50 m x 75 m ellipse, at a simulated fire distance of about 16 km. This study provides useful information regarding the accuracy obtained by 6-DOF simulation models, but the short-coming is again limited allowance for asymmetries and options to evaluate non-linear and "non-standard" aerodynamic properties.

(3) Projectile linear theory for aerodynamically asymmetric projectiles was proposed by John W. Dykes in December 2011 (Dykes, 2011). The scope of this thesis was to create analytical tools that were capable of quantifying aerodynamically asymmetric projectile performance. It demonstrates the capability of these models to accurately account for aerodynamic asymmetries and gain insight into the flight mechanics of several aerodynamically asymmetric projectiles. One of these analytical tools was a 6-DOF flight dynamic model, which used a point-force lifting surface aerodynamic model, that was developed to replicate flight characteristics observed from measured results of common projectiles. From this model that was developed, stability of symmetric projectiles is validated and show that the classical and extended Projectile Linear Theory dynamic model (PLT model) yielded identical results. Results show that aerodynamic asymmetries can sometimes cause instabilities and other times cause a significant increase in dynamic mode damping. Moreover, it can cause increase and/or decrease in mode frequency. Partially asymmetric (single plane) configurations were shown to cause epicyclic instabilities as the asymmetries became severe, while fully asymmetric (two plane) can grow unstable in either the epicyclic modes or the roll/yaw mode. Another significant result showed that the model can capture aerodynamic lifting-surface periodic aspects to evaluate dynamic stability requirements for asymmetric projectiles. This thesis provides useful insight into asymmetric aspects and should be complemented with an ability to evaluate "non-standard" aerodynamic models in order to study the behaviour of mortar bombs not previously seen in published case studies.

(4) BALCO. This 6-DOF simulation model was presented at the International Symposium on Ballistics in 2016 (Wey et al., 2016) as the standard 6-DOF to be used within NATO. It was developed at the Institute of Saint Louis and provides a good benchmark for "best practices" regarding 6-DOF simulation. It's short-coming however, is also limitation regarding asymmetric properties and the flexibility to analyse instabilities not covered by the classical tri-cyclic motion theories.

(5) Zipfel Modelling and Simulation of Aerospace Vehicle Dynamics (Zipfel, 2007). This is an excellent reference providing basic information on the various models often encountered in simulation of flight trajectories. It was also one of the basic references used for the definition of the BALCO code discussed in (4) above. Zipfel provides valuable information on the different reference coordinate frames required in trajectory simulations and the transformation between the various reference frames.

2.2.5 Integration schemes

(1) Numerical Methods for Engineer and Scientist (Hoffman, 1992). In this book, the author provided many of the basic problems that arise in all branches of engineering and science. These problems include: solution of systems of linear algebraic equations, Eigen problems, solution of nonlinear equations, polynomial approximation and interpolation, numerical differentiation and difference formulas, and numerical integration. It also provided the numerical solutions and methods which can be used to solve mathematical problems that cannot be solved by exact methods. In addition, this book has expressed many numerical algorithms such as Runge-Kutta 4^{th} order method in the form of a computer program. The 4th order Runge-Kutta integration technique is one of the popular integration techniques used in the trajectory simulation models.

(2) A Six-Degree-Of-Freedom Digital Computer Program For Trajectory Simulation (Duncan & Ensey , 1964). This model was proposed for the accurate prediction in digital simulation to simulate the trajectory of an unguided, fin-stabilised, wind sensitive rocket. Especially to study both theoretical and empirical performance characteristics of unguided rockets. This document gives an excellent description of the structure of typical 6-DOF model in general with the description of each part. One of these parts was the integration routine which showed how the equations of motion are numerically integrated by the fourth order Runge-Kutta integration technique, and how to check the validity of the integration. This model provides valuable information on the structures required in the trajectory simulation models.

2.2.6 Timestep

Effect of the mathematical model and integration step on the accuracy of the results of computation of artillery projectile flight parameters (Baranowski, 2013). The scope of this paper is to develop software that is capable of simulating the flight of 155 mm artillery projectile and to conduct comprehensive research on the influence of integration step on the accuracy and time of computation of projectile trajectory. This paper showed how the size of the integration step influenced the accuracy of results. It also provided useful insight into the strategies for adjusting the integration step during simulation.

2.3 Conclusion

This literature study provides valuable insight on the various trajectory simulation models. The information from this literature was used to define models to be incorporated in a 6-DOF trajectory simulation that can be used to analyse both symmetric and asymmetric projectiles as described in chapter 3.

CHAPTER 3: MODEL DEVELOPMENT

3.1 Introduction

Over the last few years many theories and simulation models have been developed to simulate mortar, artillery, and missile trajectories. These models range from the extremely simple to the very complex, the complexity usually depending on the specific simulation requirements. The 6-DOF trajectory simulation model is one of the more complex models. This model accounts for all the translational and rotational motion of a body in three-dimensional space, the equations of motion account for:

- Translation in the X, Y and Z direction.
- Rotation as described by yaw, pitch and roll (Angular motion around the X, Y and Z axis).

If the 6-DOF model is used to simulate the trajectory of an axially symmetric projectile, (where no forces or moments are linked to the angular orientation around the axial axis of symmetry), this model should give the same results as the 5-DOF model introduced in the previous paragraph (2.2.3). In the case of analysing the flight trajectory of an asymmetric projectile, (where there might be forces and moments linked to the angular rotation around the axial axis), the 6-DOF is needed. The 6-DOF model can account for forces and moments linked to the roll orientation of the projectile and that makes it ideally suited for the simulation of asymmetric projectiles. The asymmetries usually accounted for are, see (Glover, Hagan, 1971):

- Aerodynamic asymmetries [i.e. Normal force and Yaw-Moment at zero angle of attack, Un-equal Pitch and Yaw Forces and Moments and Rolling moments].
- Inertial asymmetries [i.e. Radial off-set in the CoG, Principle axis not aligned with the axial axis of symmetry and Unequal moments of inertia around the two lateral transverse axes].
- Thrust misalignments.

This chapter describes a six-degree-of-freedom trajectory simulation providing a breakdown of the model that was implemented by the author, to simulate the ballistic trajectories of mortar bombs, artillery projectiles and unguided rockets. Ballistic flight means that guidance along the flight path is not considered. This chapter provide complete detail on the theoretical models used to calculate forces and moments as well as all the transformations between the various coordinate frames that were implemented. Flexibility (to handle various projectile configurations) and modularity (to allow for validation of different parts of the simulation program), were used during the development of the 6-DOF simulation program.

The model is programmed in MATLAB language. It consists of a main function (Main6), three subfunctions (INIT6, AERODYN6, and DYNAMIC6) and a group of small subfunctions each designed for a specific task. A detail description of the projectile model that was used is given in paragraph 3.6.

3.2 Structure of 6-DOF Trajectory Simulation Model

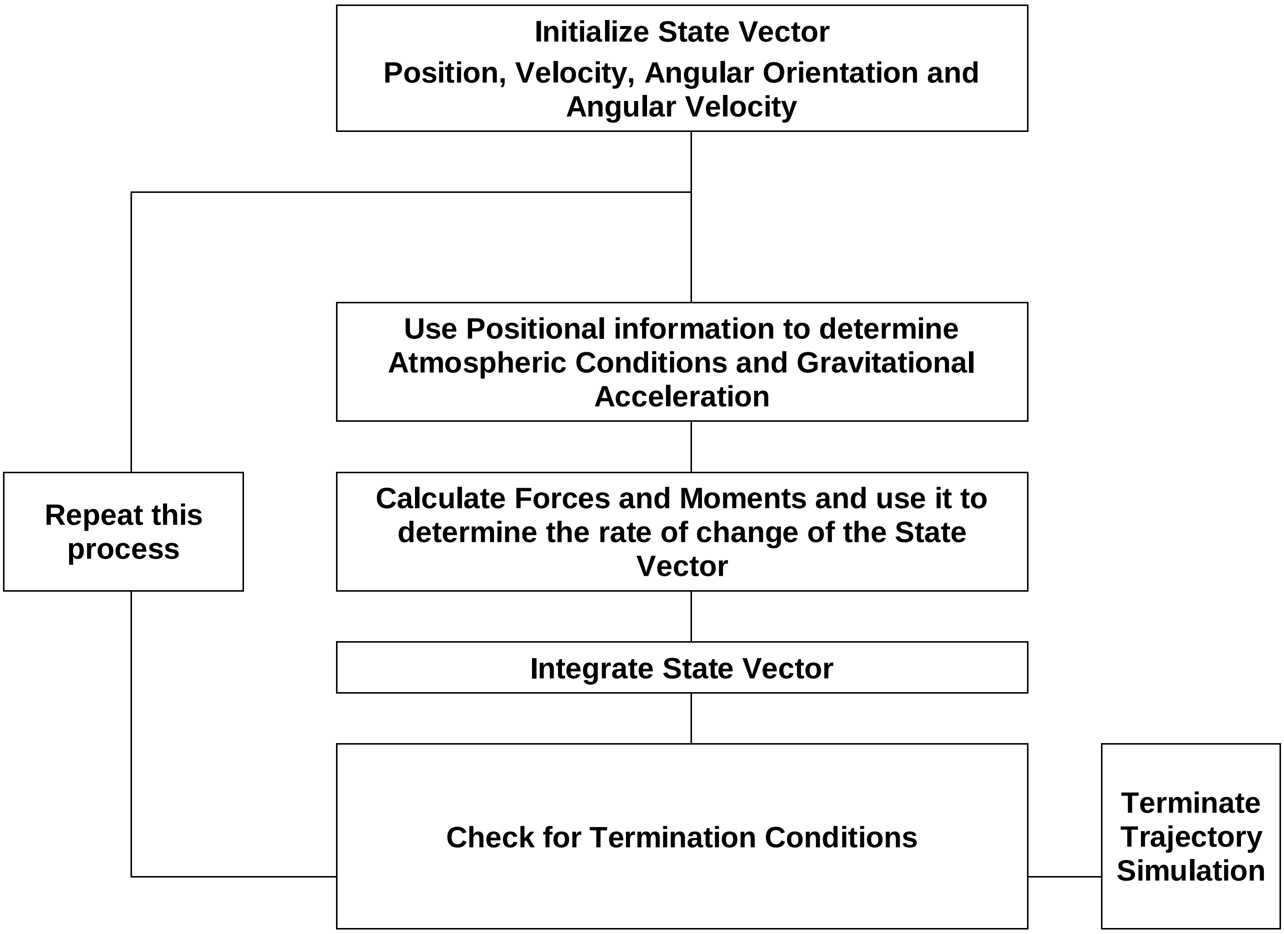

Figure 6: Typical structure of 6-DOF trajectory simulations.

3.3 Earth Model

3.3.1 Flat Earth Constant Gravity Model

The “Flat Earth Model” is characterised by a constant gravity model and the value often used is: (Wertz, 1978; Zipfel, 2007)

$$Gravity\ Acceleration\ = 9.81\frac{m}{s^2}$$

3.3.2 Spherical Earth Model – Inverse Square Gravity Model

If the earth is assumed to be spherical symmetric, the strength of its gravitational field is inversely proportional to the square of the distance from the centre of the Earth as illustrated in Figure 7 (Wertz, 1978; Zipfel, 2007; STANAG 2211, 2016).

$$\vec{G} = -\mu * \frac{\vec{R}}{\|R^3\|}\ ,\ where\colon\ \mu = 3.986005 * 10^{14}$$

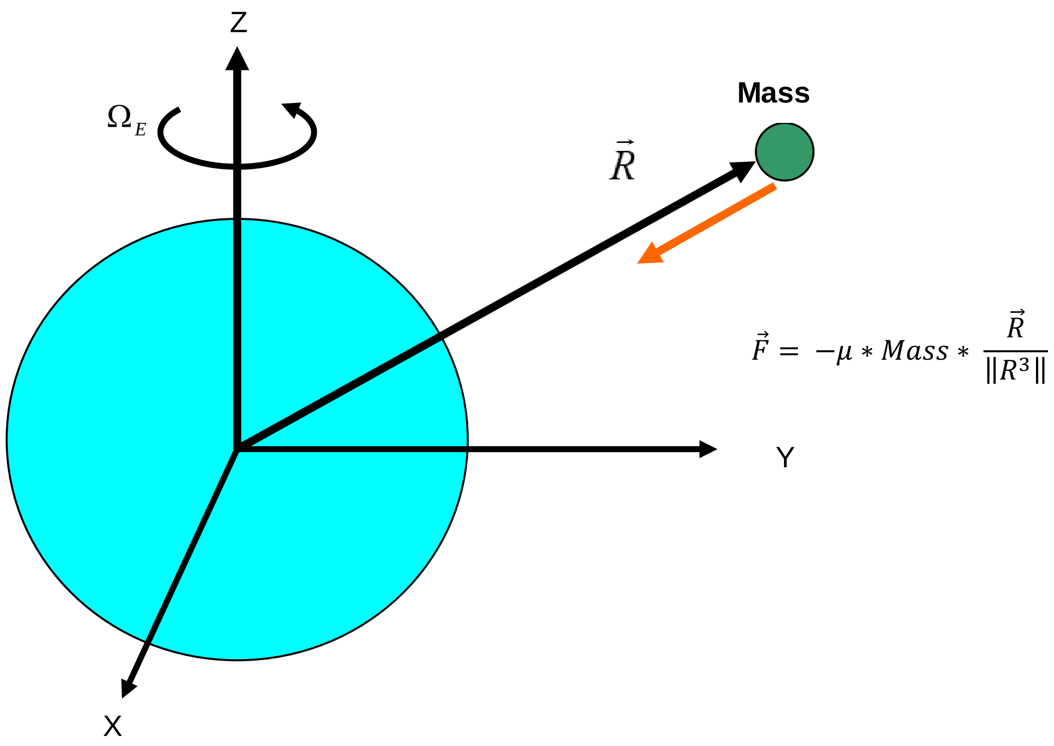

Figure 7: Illustration of spherical Earth model

3.3.3 Oblate Earth Model – Ellipsoidal Earth Model

The earth is basically an oblate spheroid because of combined centrifugal and gravitational accelerations. The basic reference earth model is a spheroid. This is an ellipse rotated about its minor axis to represent the flattening of the earth as illustrated in Figure 8. The ellipse is defined by: (Wertz, 1978; Zipfel, 2007; STANAG 2211, 2016).

- Equatorial radius: $R_E = 6378140\ m$
- Polar radius: $R_P = 6356755\ m$
- Ellipticity of flattening: $f = \frac{R_E - R_P}{R_E} = \frac{1}{298.257}$

The geocentric earth radius at any given geocentric latitude (LatC), is given by:

- Geocentric radius: $R_{LatC} = \frac{R_E}{\sqrt{1 + Sin^2(LatC) * \left(\frac{{R_E}^2 - {R_P}^2}{{R_P}^2}\right)}}$

Positions on the earth are usually described in terms of the geodetic reference frame. Figure 8 illustrates the difference between geocentric- and geodetic latitude.

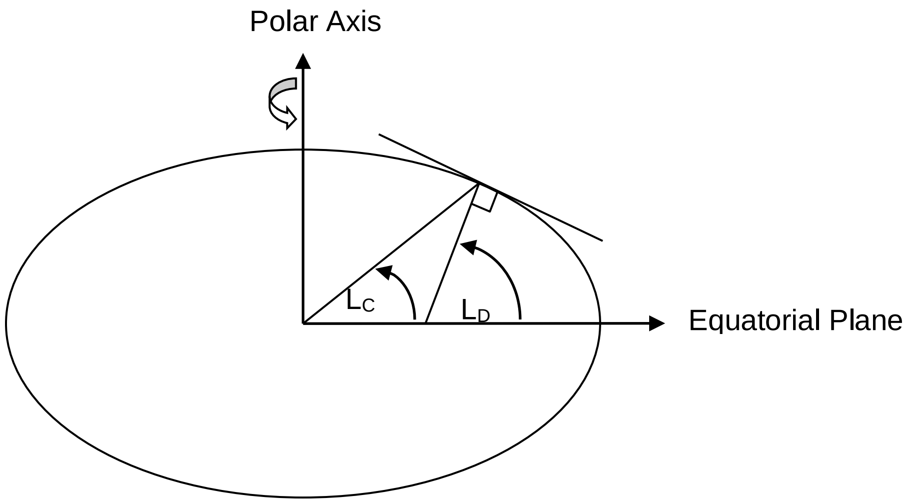

Figure 8: Illustration of oblate or ellipsoidal Earth model

The relationship between the Geocentric and Geodetic latitude is given by:

$$\tan(LatG) = \left[\frac{1}{1-f}\right]^2 * \tan(LatC), \quad where\ f\ is\ the\ Earth\ Flattening$$

For most trajectory calculations an ellipsoidal earth model proved to be sufficient and the gravitational potential, (U), is given by (see (Wertz, 1978:126)).

$$U \cong \frac{\mu}{R_C} * \left[U_0 + U_{J2}\right]$$

$$U_0 = -1$$

$$U_{J2} = \left(\frac{R_E}{R_C}\right)^2 * J2 * \frac{[3 * \cos^2(\theta) - 1]}{2}$$

Where:

R_E is the Equatorial radius and R_C is the Geocentric radius to the point of interest

$J2 = 1082.63 * 10^{-6}$

$\theta = Co - elevation\ Angle$, see Figure 9.

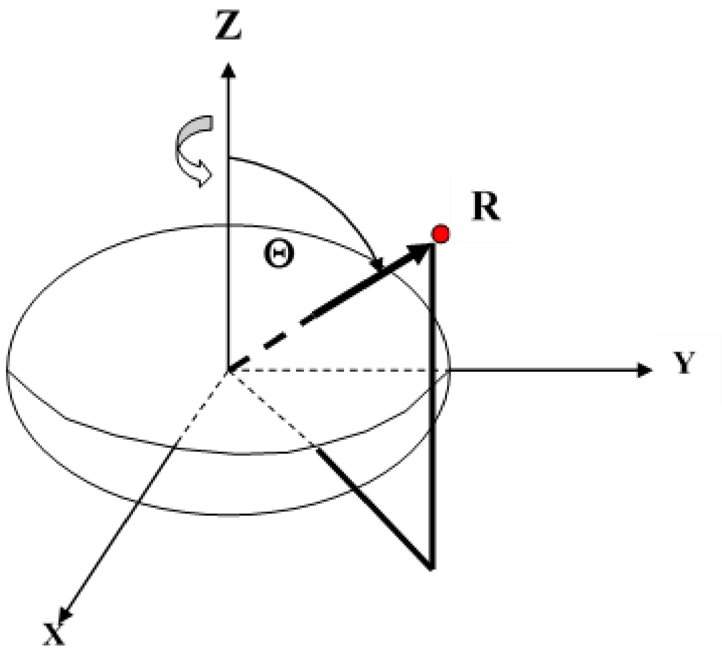

Figure 9 : Illustration of Co-Elevation angle used by (Wertz, 1978)

The gravitational acceleration at any point is given by:

$$\vec{G} = -\nabla U$$

In terms of components relative to an inertial reference frame with origin at the centre of the Earth and Z-axis point north along the rotational axis of the Earth:

$$G_X = -\left(\frac{\mu}{r^3}\right) * \left\{1 + \left(\frac{3 * J2 * {R_E}^2}{2 * r^2}\right) * \left(1 - \frac{5 * Z^2}{r^2}\right)\right\} * X$$

$$G_Y = -\left(\frac{\mu}{r^3}\right) * \left\{1 + \left(\frac{3 * J2 * {R_E}^2}{2 * r^2}\right) * \left(1 - \frac{5 * Z^2}{r^2}\right)\right\} * Y$$

$$G_Z = -\left(\frac{\mu}{r^3}\right) * \left\{1 + \left(\frac{3 * J2 * {R_E}^2}{2 * r^2}\right) * \left(3 - \frac{5 * Z^2}{r^2}\right)\right\} * Z$$

$$r = \sqrt{X^2 + Y^2 + Z^2}$$

For typical trajectory simulations, it would be sufficient to use the oblate earth model. For general satellite orbital simulations, it might be necessary to use “higher order” gravity models. For validation purposes it might be necessary to use the simple constant gravity model, allowing for comparison with analytic trajectory solutions. The basic model used internationally for artillery trajectory simulation i.e. the Modified Point Mass Model, (see (STANAG 4355, 2009), approximate the oblate earth model by using:

$$G = 9.80665 * [1 - 0.0026 * \cos(2 * Latitude)]$$

It is important to note that this model provides an effective gravity, approximating the combined effect of the oblate earth gravity model and the centrifugal acceleration due to the rotation of the earth.

3.4 Earth Atmospheric Model

If the earth’s atmosphere is modelled as a hydrostatic equilibrium, meaning that the lower layers (near the surface of the earth), carry the weight of the layers above it, one expects to find an exponential decrease in atmospheric pressure and density as the height above the surface of the earth increases. The vertical structure of the atmosphere is illustrated in Figure 10. For trajectory simulations it is important to account for especially:

- Variation in atmospheric density.
- Variation in the speed of sound (linked to atmospheric temperature).
- Variation in atmospheric winds.

Meteorological data (MET data) is gathered by flying MET balloons recording temperature humidity, and pressure as it ascends through the atmosphere. In addition, its flight path is tracked as it is carried by the prevailing atmospheric winds and this information is used to obtain wind data at various altitudes. Presently artillery projectiles are designed to obtain a range of up to 60 km and for these ballistic trajectories the projectile has an apex height of about 36 km. Accurate simulation would therefore require MET data up to that altitude.

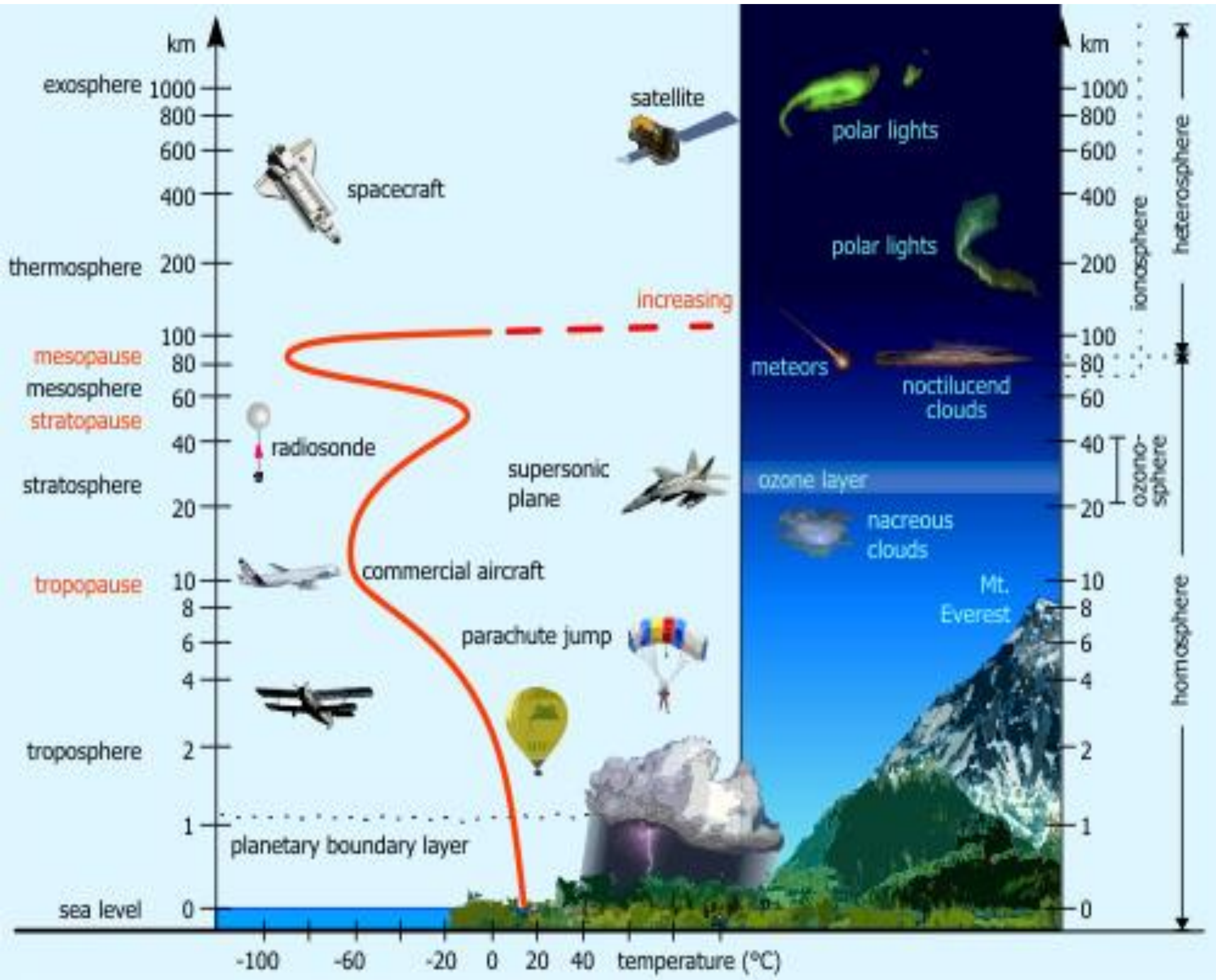

Figure 10 : **Vertical structure of the atmosphere (Venegas, 2018)**

3.4.1 Standard ICAO Atmospheric Model

The standard meteorological model of the International Civil Aviation Organisation [ICAO MET] and (ISO 2533, 1975) is often used as a standard reference. A summary of essential MET data from the ICAO standard MET is given in Table 1 up to a height of 100 km.

Table 1: Summary of ICAO MET condition used in simulation

Height [m MSL]	Press [Pa]	Density [Kg/m3]	Sound Speed [m/ses]
0	101330	1.22500	340.29
500	95461	1.16730	338.37
1000	89876	1.11170	336.44
1500	84560	1.05810	334.49
2000	79501	1.00660	332.53
2500	74692	0.95695	330.56
3000	70121	0.90925	328.58
3500	65780	0.86340	326.59
4000	61660	0.81935	324.59
4500	57753	0.77704	322.57
5000	54048	0.73643	320.55
6000	47218	0.66011	316.45
7000	41105	0.59002	312.31
8000	35652	0.52579	308.11
9000	30801	0.46706	303.85
10000	26500	0.41351	299.53
12000	19399	0.31194	295.07
14000	14170	0.22786	295.07
16000	10353	0.16647	295.07
18000	7565	0.12165	295.07
20000	5529	0.08891	295.07
22000	4048	0.06451	296.38
24000	2972	0.04694	297.72
28000	1616	0.02508	300.39
30000	1197	0.01841	301.71
34000	663	0.00989	306.49
38000	377	0.00537	313.67
40000	287	0.00399	317.19
44000	169	0.00226	324.12
48000	102	0.00132	329.80
50000	80	0.00103	329.80
55000	43	0.00056	326.70
60000	22	0.00031	320.61
70000	6	0.00009	297.14
80000	1	0.00002	269.44
100000	0.03	4.974E-09	269.44

3.4.2 Standard Formats of Meteorological Data

There are two important formats of meteorological data used internationally for ballistic trajectory predictions:

- Ballistic meteorological message, usually used with firing tables to calculate the launch parameters (Gun Elevation and Line of Fire), that is required to reach a certain target. The METB2 message is used for surface to air ballistic calculations and the METB3 as illustrated Figure 11 is used for surface to surface ballistic calculations. This format provides an average of the atmospheric variations encountered by the projectile along its entire flight path and is suited for quick estimations and manual calculations using sensitivities published in the firing tables of the projectile. It is however not suitable for simulation programs requiring prevailing atmospheric information at every height along the trajectory (STANAG 4061, 2000). A detail description of the data in the Ballistic MET file is provided in APPENDDIX A.

SPECIMEN OF BALLISTIC METEOROLOGICAL MESSAGE

METB30	512018	070954	013992		
000000	971021	015702	971021	025906	972021
036009	972022	045810	975022	055711	975023
065813	977018	076115	981013	086319	987006
096321	991002	106429	991002	110136	991999
120137	991997	130132	991992	140129	991992
150127	991992				

Figure 11: Example of a Ballistic METB3 file (STANAG 4061, 2000)

- Standard artillery computer meteorological message – METCM as illustrated in Figure 12. The format of this meteorological message is defined in STANAG 4082 This is the MET data usually used with trajectory simulation programs such as the Modified Point Mass, 5-DOF and 6-DOF programs. This MET data essentially supply the average atmospheric conditions for certain zones, where the zones are linked to specific atmospheric heights (STANAG 4082, 2012). A detailed description of the data in the Computer MET file is provided in APPENDDIX A.

METCM0	512018	070952	013972
00310004	29770972	01290013	29560961
02306014	29040933	03357014	28340890
04396007	28090837	05502008	28040787
06450015	27810742	07475013	27440696
08520013	27050653	09582018	26730613
10575017	26430575	11566016	26100538
12571015	25620487	13588009	25000427
14611011	24270372	15354012	23570323

Figure 12: Example of a Computer MET File (STANAG 4082, 2012)

3.4.3 Examples of Practical MET data files

Although there are the standard MET formats as discussed in the previous paragraph, the format of the data obtained from weather stations often differ substantially. An example of the MET data captured at 150 m intervals at the Alkantpan test range is shown in Table 2.

Table 2: Example of Alkantpan MET file – data at 150 m intervals

GPM_AGL [m]	Press [hPa]	Temp [C]	RelHum %	Wdirn [°]	Wspeed [m/s]
0	895.1	11.0	56.0	0	6.0
150	879.4	22.2	17.1	40	5.1
300	864.3	22.3	19.6	26	4.2
450	849.5	21.9	20.2	319	2.6
600	834.9	20.7	21.1	276	4.1
750	820.4	19.6	21.2	268	6.9
900	806.2	18.6	24.3	280	9.6
1050	792.2	18.3	27.2	290	10.5
1200	778.4	17.0	29.4	297	9.6
1350	764.8	15.4	31.8	302	8.5
1500	751.3	14.0	33.8	317	8.4
1650	738.0	12.7	35.5	320	9.3
1800	724.9	11.7	38.5	310	10.3
1950	712.0	10.4	40.8	303	10.5
2100	699.3	9.0	43.9	299	10.6
2250	686.7	7.6	48.1	298	12.0
2400	674.3	6.5	49.4	299	13.5
2550	662.0	5.2	54.4	299	15.1
2700	650.0	3.8	59.3	300	16.5
2850	638.0	2.4	65.1	302	17.0
3000	626.3	0.9	71.1	304	16.7
3150	614.7	-0.5	74.9	301	16.6
3300	603.2	-1.3	51.0	296	15.6
3450	592.0	-2.1	26.5	287	13.6
3600	580.9	-2.8	14.0	281	13.3
3750	570.0	-2.5	14.0	280	13.6

For practical applications a trajectory simulation should be able to handle various MET data formats.

3.5 Reference Frames and Transformations between Frames

3.5.1 Introduction to Reference Frames

Newton's laws governing projectile motion are generally known by its forms:

- Force = [Mass] * [Acceleration].
- Moment = [Moment of Inertia] * [Angular Acceleration].

The above is only applicable to the description of the projectile motion relative to an inertial reference frame or axis system. For every problem this Inertial Reference Frame should be selected so that it is "sufficiently inertial" for the specific case. For many problems, looking at relatively short flight trajectories (i.e. < 10km), it might be sufficient to select an earth fixed reference frame as an inertial frame. For most ballistic trajectories it is sufficient to select the inertial reference frame at the centre of the earth, but not rotating with the earth. This might even be sufficient for satellite orbit simulation. For interplanetary travel one would have to select the inertial frame at the centre of the sun or even at the centre of gravity of our galaxy (Diebel,2006; Zipfel, 2007).

- For trajectory simulations there are basically three "primary" sets of reference frames:
  - Inertial reference frame [A non-rotating frame with origin at the centre of the Earth].
  - An earth fixed frame with origin fixed at the launch point. Where X-axis is horizontally in the launch direction, Y-axis is horizontally (positive left), and Z-axis is vertical (positive upwards).
  - A body fixed frame with origin at the centre of gravity of the projectile. This frame is spinning with the projectile, sharing all its angular motions.
- To describe the transformations between these frames and the various forces and moments affecting the trajectory, several other "secondary" frames are often also used:
  - A frame with origin at the center of the earth but rotating with the earth after launch.
  - An aero ballistic frame with origin at the projectile centre of gravity, aligned with the geometric axial axis of the projectile and the component of flow perpendicular to the axial axis of the projectile. This axis is not spinning with the projectile.
  - A local level, local north frame at projectile position.

Diebel provides a very concise/useful summary of various transformation schemes between the various reference frames.

3.5.2 Inertial Reference Frame [IF]

Note: Before launch this frame has one of its axes pointing to the meridian that pass through the launch point and therefore rotates with the earth. This rotation stops at the moment the projectile is launched at time =zero and from that point in time it does not rotate with the earth (Diebel,2006; Zipfel, 2007).

- Origin At the centre of the earth (In the plane of the equator).
- Zi Along the rotating axis of the earth pointing north.
- Xi In the equatorial plane pointing towards the meridian that passes through the launch point [LP].
- Yi Completing the right-handed cartesian coordinate frame: $\vec{Y}_i = \vec{Z}_i \; X \; \vec{X}_i$.

3.5.3 Earth Rotating Reference Frame [EF]

Note: After launch at time = zero, this frame rotates with the earth.

- Origin At the centre of the earth (In the plane of the equator).
- Ze Along the rotating Axis of the earth pointing north.
- Xe In the equatorial plane pointing towards the meridian that passes through the launch point [LP].
- Ye Completing the right-handed cartesian coordinate Frame: $\vec{Y}_e = \vec{Z}_e \; X \; \vec{X}_e$.

3.5.4 Earth Fixed Launch Frame [LF]

Note: This frame is also fixed to the earth at the launch point and therefore rotates with the earth. For most ballistic trajectories, this is the frame used to describe the trajectory from the launch point [LP] up till it reach the intended target point [TP].

- Origin At the launch point on the earth surface [Geoid].
- Zl Perpendicular to the earth geoid with nadir pointing into space.

- Xl Tangential to the surface of the earth pointing in the launch direction.
- Yl Completing the right-handed cartesian coordinate frame: $\vec{Y}_l = \vec{Z}_l \, X \, \vec{X}_l$.

3.5.5 Local Level Local North Frame [NF]

This reference frame is introduced, because Atmospheric Meteorological Data [Temperature, Density, Wind and Wind Direction], is often supplied in terms of the local position of the projectile and referenced to north.

- Origin At the centre of gravity of the projectile.
- Zn Along the geocentric nadir pointing into space.
- Xn Perpendicular to Zn and pointing towards true north.
- Yn Completing the right-handed cartesian coordinate frame: $\vec{Y}_n = \vec{Z}_n \, X \, \vec{X}_n$.

3.5.6 Body Frame [BF]

This reference frame is fixed to the projectile and share all its translational and angular motions. The initial orientation of this frame is described for a projectile in a horizontal position at the launch point with its nose aligned with the launch direction.

- Origin At the centre of gravity of the projectile
- Xb Along the axial axis of the projectile pointing towards the nose. For a projectile in the horizontal position, (before elevated to the launch elevation), the Xb axis points in the launch direction and is therefore aligned with the Xl axis.
- Zb Perpendicular to Xb, pointing towards the centre of the earth (for the projectile still in a horizontal position at the launch point).
- Yb Completing the right-handed cartesian coordinate frame: $\vec{Y}_b = \vec{Z}_b \, X \, \vec{X}_b$.

3.5.7 Aero-Ballistic Frame [AF]

This reference frame is fixed to the projectile and share all its translational motions. With respect to angular motions, it shares the pitch and yaw motion of the projectile, but not the spin around the axial axis of the projectile. This frame is convenient for the description of aerodynamic forces and moments.

- Origin On the geometric centerline of the projectile at the axial position of the center of gravity.
- Note: For an asymmetric projectile, the centre of gravity might have a radial off-set from the geometric axis.
- Xa along the Axial Axis of the projectile pointing towards the nose, aligned with the Xb axis.
- Za in the plane that contains the flow perpendicular to axial axis of the projectile.
- Ya Completing the right-handed cartesian coordinate frame: $\vec{Y}_a = \vec{Z}_a \, X \, \vec{X}_a$

The flow perpendicular to the axial axis of a projectile is given by the components equation.

$$V_{Rel-Yb} \; and \; V_{Rel-Zb}$$

The angle between the body axes and the aero-ballistic axes, as shown in Figure 13, is given by (Zipfel, 2007:79):

$$\beta = Tan^{-1}\left[\frac{Vrel_{Yb}}{Vrel_{Zb}}\right]$$

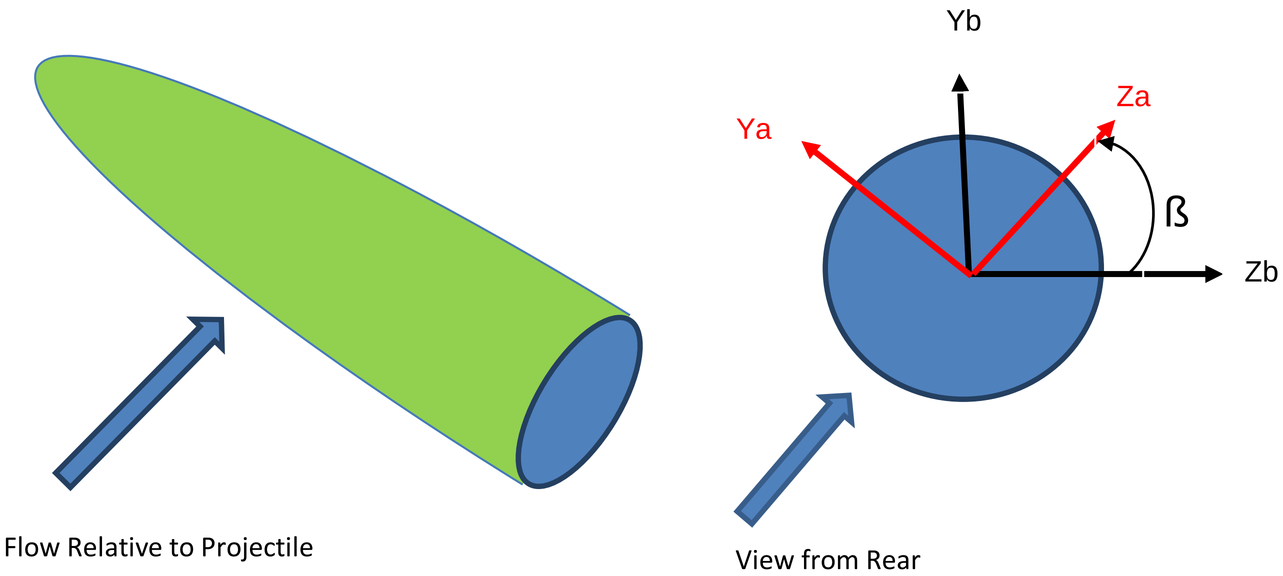

Figure 13: Illustration of Aero-Ballistic Axes

Note that the angle β is the positive rotation around the Xa–axis that is required to align the Za–axis with the Zb–axis.

3.5.8 Transformation between Inertial and Earth Frame: IF2EF and EF2IF

These frames are aligned at launch, but thereafter the earth frame rotates with the earth. This angle of rotation is given by:

$$Ang = \Omega_{Earth} * (Time\ of\ Flight)$$

$$IF2EF: \begin{Bmatrix} X_e \\ Y_e \\ Z_e \end{Bmatrix} = \begin{bmatrix} Cos(Ang) & Sin(Ang) & 0 \\ -Sin(Ang) & Cos(Ang) & 0 \\ 0 & 0 & 1 \end{bmatrix} * \begin{Bmatrix} X_i \\ Y_i \\ Z_i \end{Bmatrix}$$

$$EF2IF: \begin{Bmatrix} X_i \\ Y_i \\ Z_i \end{Bmatrix} = \begin{bmatrix} Cos(Ang) & -Sin(Ang) & 0 \\ Sin(Ang) & Cos(Ang) & 0 \\ 0 & 0 & 1 \end{bmatrix} * \begin{Bmatrix} X_e \\ Y_e \\ Z_e \end{Bmatrix}$$

3.5.9 Transformation between Earth Frame and the Launch Frame: EF2LF and LF2EF

Both these frames rotate with the earth and their relative orientation is determined by:

- Geodetic Latitude of the Launch Point, Latg, [Note that North of the Equator is positive]
- The Launch Azimuth [i.e. the Launch Direction given as Clockwise from North]

The orientation of the launch frame relative to the rotating earth frame can be described by the following consecutive Euler rotations:

$$First\ a\ rotation\ around\ the\ Ey - Axis\ of: \qquad \varphi = \left\{\frac{\pi}{2} - Lat_g\right\}$$

$$Then\ a\ rotation\ around\ the\ new\ Z - Axis\ of: \qquad \theta = \{\pi - Azim\}$$

$$And\ Finally\ a\ rotation\ around\ the\ new\ X - Axis\ of: \qquad \psi = \{0\}$$

EF2LF:

$$\begin{Bmatrix} X_L \\ Y_L \\ Z_L \end{Bmatrix} = \begin{bmatrix} \mathrm{Cos}(\theta) * \mathrm{Cos}(\varphi) & \mathrm{Sin}(\theta) & -\mathrm{Cos}(\theta) * \mathrm{Sin}(\varphi) \\ -\mathrm{Cos}(\psi) * \mathrm{Sin}(\theta) * \mathrm{Cos}(\varphi) + \mathrm{Sin}(\psi) * \mathrm{Sin}(\varphi) & \mathrm{Cos}(\psi) * \mathrm{Cos}(\theta) & \mathrm{Cos}(\psi) * \mathrm{Sin}(\theta) * \mathrm{Sin}(\varphi) + \mathrm{Sin}(\psi) * \mathrm{Cos}(\varphi) \\ \mathrm{Sin}(\psi) * \mathrm{Sin}(\theta) * \mathrm{Cos}(\varphi) + \mathrm{Cos}(\psi) * \mathrm{Sin}(\varphi) & -\mathrm{Sin}(\psi) * \mathrm{Cos}(\theta) & -\mathrm{Sin}(\psi) * \mathrm{Sin}(\theta) * \mathrm{Sin}(\varphi) + \mathrm{Cos}(\psi) * \mathrm{Cos}(\varphi) \end{bmatrix} * \begin{Bmatrix} X_E \\ Y_E \\ Z_E \end{Bmatrix}$$

And likewise, the orientation of the rotating earth frame relative to the launch frame can be described by the following consecutive Euler rotations:

$$First\ a\ rotation\ around\ the\ Ey - Axis\ of: \qquad \varphi = \{Azim - \pi\}$$

$$Then\ a\ rotation\ around\ the\ new\ Z - Axis\ of: \qquad \theta = \left\{Lat_g - \frac{\pi}{2}\right\}$$

$$And\ Finally\ a\ rotation\ around\ the\ new\ X - Axis\ of: \qquad \psi = \{0\}$$

LF2EF:

$$\begin{Bmatrix} X_L \\ Y_L \\ Z_L \end{Bmatrix} = \begin{bmatrix} \mathrm{Cos}(\theta) * \mathrm{Cos}(\varphi) & \mathrm{Cos}(\theta) * \mathrm{Sin}(\varphi) & -\mathrm{Sin}(\theta) \\ -\mathrm{Cos}(\psi) * \mathrm{Sin}(\varphi) + \mathrm{Sin}(\psi) * \mathrm{Sin}(\theta) * \mathrm{Sin}(\varphi) & \mathrm{Cos}(\psi) * \mathrm{Cos}(\varphi) + \mathrm{Sin}(\theta) * \mathrm{Sin}(\varphi) & \mathrm{Sin}(\psi) * \mathrm{Cos}(\theta) \\ \mathrm{Sin}(\psi) * \mathrm{Sin}(\varphi) + \mathrm{Cos}(\psi) * \mathrm{Sin}(\theta) * \mathrm{Cos}(\varphi) & -\mathrm{Sin}(\psi) * \mathrm{Cos}(\varphi) + \mathrm{Cos}(\psi) * \mathrm{Sin}(\theta) * \mathrm{Sin}(\varphi) & \mathrm{Cos}(\psi) * \mathrm{Cos}(\theta) \end{bmatrix} * \begin{Bmatrix} X_E \\ Y_E \\ Z_E \end{Bmatrix}$$

3.5.10 Transformation between Inertial Frame and the Body Frame: IF2BF and BF2IF

The orientation of the body frame relative to the inertial frame can be described by the following consecutive Euler rotations and illustrated in Figure 14:

$$First\ a\ rotation\ around\ the\ Ix - Axis\ of: \qquad \psi$$

$$Then\ a\ rotation\ around\ the\ new\ Y - Axis\ of: \qquad \theta$$

$$And\ Finally\ a\ rotation\ around\ the\ new\ Xb - Axis\ of: \qquad \varphi$$

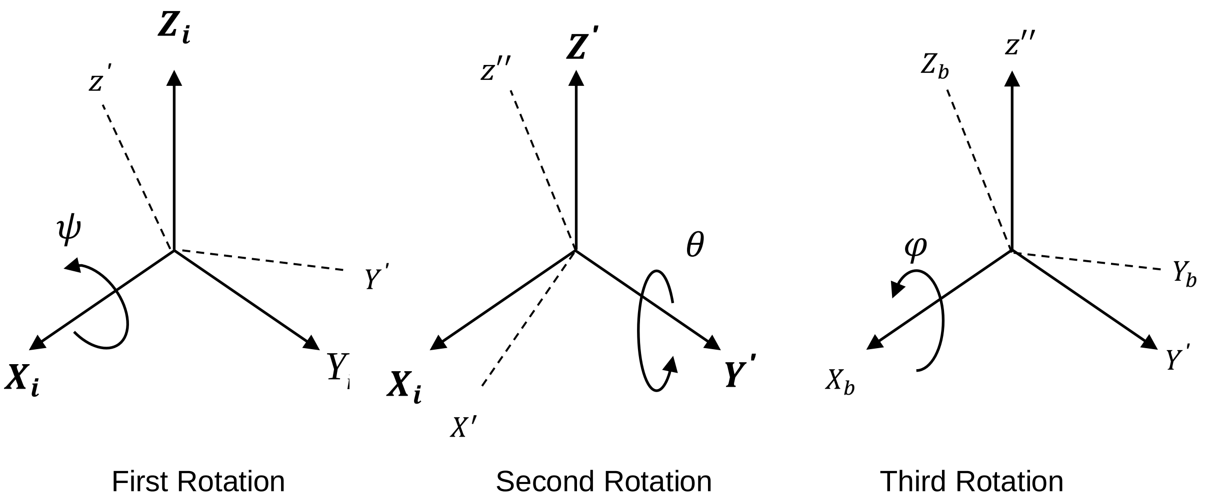

Figure 14: Illustration of Euler 1-2-1 Transformation

$$[Third] \quad * \quad [Second] \quad * \quad [First]$$

$$\begin{bmatrix} X \\ Y \\ Z \end{bmatrix}_b = \begin{bmatrix} 1 & 0 & 0 \\ 0 & \cos(\emptyset) & \sin(\emptyset) \\ 0 & -\sin(\emptyset) & \cos(\emptyset) \end{bmatrix} * \begin{bmatrix} \cos(\theta) & 0 & -\sin(\theta) \\ 0 & 1 & 0 \\ \sin(\theta) & 0 & \cos(\theta) \end{bmatrix} * \begin{bmatrix} 1 & 0 & 0 \\ 0 & \cos(\psi) & \sin(\psi) \\ 0 & -\sin(\psi) & \cos(\psi) \end{bmatrix} * \begin{bmatrix} X \\ Y \\ Z \end{bmatrix}_i$$

IF2BF:

$$\begin{Bmatrix} X_B \\ Y_B \\ Z_B \end{Bmatrix} = \begin{bmatrix} \mathrm{Cos}(\theta) & \mathrm{Sin}(\theta) * \mathrm{Sin}(\psi) & -\mathrm{Sin}(\theta) * \mathrm{Cos}(\psi) \\ \mathrm{Sin}(\varphi) * \mathrm{Sin}(\theta) & \mathrm{Cos}(\varphi) * \mathrm{Cos}(\psi) - \mathrm{Sin}(\varphi) * \mathrm{Cos}(\theta) * \mathrm{Sin}(\psi) & \mathrm{Cos}(\varphi) * \mathrm{Sin}(\psi) + \mathrm{Sin}(\varphi) * \mathrm{Cos}(\theta) * \mathrm{Cos}(\psi) \\ \mathrm{Cos}(\varphi) * \mathrm{Sin}(\theta) & -\mathrm{Sin}(\varphi) * \mathrm{Cos}(\psi) - \mathrm{Cos}(\varphi) * \mathrm{Cos}(\theta) * \mathrm{Sin}(\psi) & -\mathrm{Sin}(\varphi) * \mathrm{Sin}(\psi) + \mathrm{Cos}(\varphi) * \mathrm{Cos}(\theta) * \mathrm{Cos}(\psi) \end{bmatrix} * \begin{Bmatrix} X_i \\ Y_i \\ Z_i \end{Bmatrix}$$

And likewise, the orientation of the inertial frame relative to the body frame can be described by the following consecutive Euler rotations, (note simply the reverse order):

$$First\ a\ rotation\ around\ the\ Xb - Axis\ of: \qquad -\varphi$$

$$Then\ a\ rotation\ around\ the\ new\ Y - Axis\ of: \qquad -\theta$$

$$And\ Finally\ a\ rotation\ around\ the\ new\ Xi - Axis\ of: \qquad -\psi$$

BF2IF:

$$\begin{Bmatrix} X_i \\ Y_i \\ Z_i \end{Bmatrix} = \begin{bmatrix} \mathrm{Cos}(\theta) & \mathrm{Sin}(\theta) * \mathrm{Sin}(\varphi) & \mathrm{Sin}(\theta) * \mathrm{Cos}(\varphi) \\ \mathrm{Sin}(\psi) * \mathrm{Sin}(\theta) & \mathrm{Cos}(\psi) * \mathrm{Cos}(\varphi) - \mathrm{Sin}(\psi) * \mathrm{Cos}(\theta) * \mathrm{Sin}(\varphi) & -\mathrm{Cos}(\psi) * \mathrm{Sin}(\varphi) - \mathrm{Sin}(\psi) * \mathrm{Cos}(\theta) * \mathrm{Cos}(\varphi) \\ -\mathrm{Cos}(\psi) * \mathrm{Sin}(\theta) & \mathrm{Sin}(\psi) * \mathrm{Cos}(\varphi) + \mathrm{Cos}(\psi) * \mathrm{Cos}(\theta) * \mathrm{Sin}(\varphi) & -\mathrm{Sin}(\psi) * \mathrm{Sin}(\varphi) + \mathrm{Cos}(\psi) * \mathrm{Cos}(\theta) * \mathrm{Cos}(\varphi) \end{bmatrix} * \begin{Bmatrix} X_L \\ Y_L \\ Z_L \end{Bmatrix}$$

3.5.11 Initial Orientation of the Body Reference Frame:

To describe the initial orientation of the body frame relative to the inertial frame the following sequence of rotations are used and illustrated in Figure 15:

$$First\ a\ rotation\ around\ the\ Iy - Axis\ of: \qquad A_1 = -(Lat_{LP} + \frac{\pi}{2})$$

$$Then\ a\ rotation\ around\ the\ new\ Z - Axis\ of: \qquad A_2 = Azimuth$$

$$And\ Finally\ a\ rotation\ around\ the\ new\ Yb - Axis\ of: \quad A_3 = Elevation$$

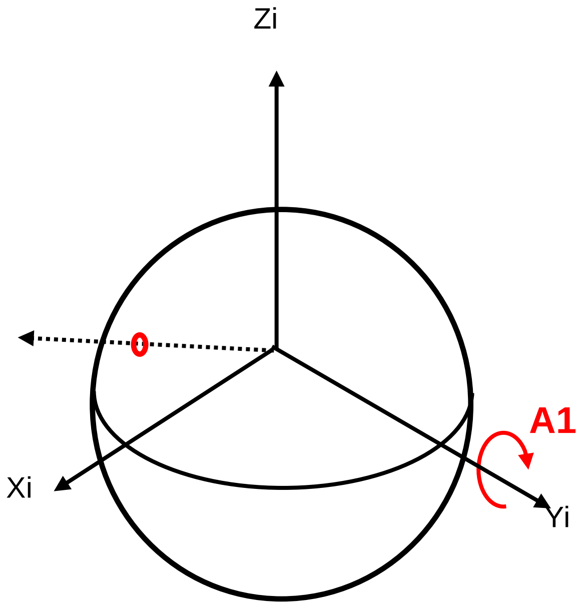

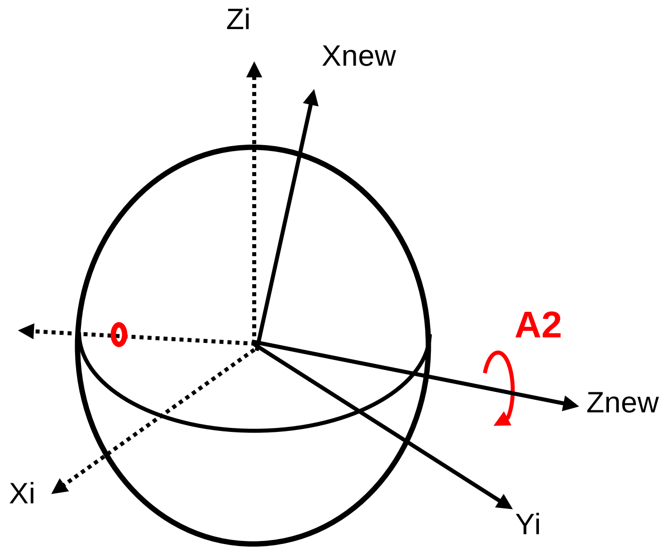

$$Rotation\ around\ Yi = -\left(Lat_{LP} + \frac{\pi}{2}\right) \qquad Rotation\ around\ Znew = \ Azim$$

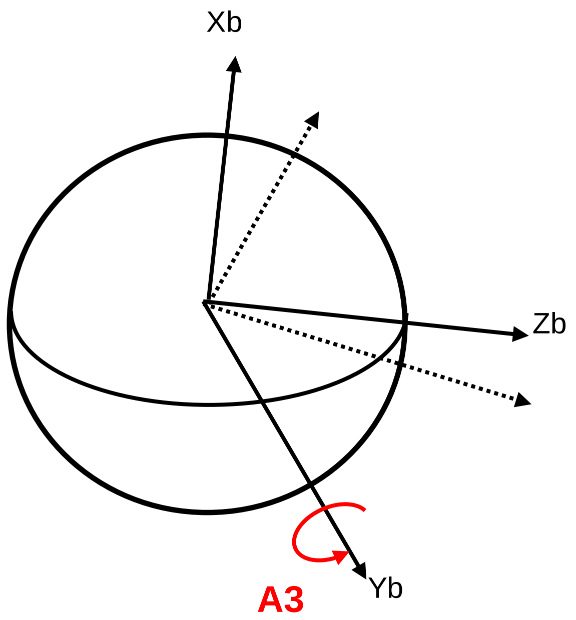

$$Rotation\ Yb = \ Elev$$

Figure 15: **Illustration of the sequence of the initial orientation of the Body Frame relative to the Inertial Frame**

The transformation matrix for this 2-3-2 Euler transformation is (Diebel, 2006):

$$\begin{Bmatrix} X_B \\ Y_B \\ Z_B \end{Bmatrix} = \begin{bmatrix} \mathrm{Cos(A3)} * \mathrm{Cos(A2)} * Cos(A1) - Sin(A3) * Sin(A1) & \mathrm{Cos(A3)} * \mathrm{Sin(A2)} & -\mathrm{Cos(A3)} * \mathrm{Cos(A2)} * \mathrm{Sin(A1)} - \mathrm{Sin(A3)} * \mathrm{Cos(A1)} \\ -\mathrm{Sin(A2)} * \mathrm{Cos(A1)} & \mathrm{Cos(A2)} & \mathrm{Sin}(A2) * \mathrm{Sin(A1)} \\ \mathrm{Sin(A3)} * \mathrm{Cos(A2)} * \mathrm{Cos(A1)} & \mathrm{Sin(A3)} * \mathrm{Sin(A2)} & -\mathrm{Sin(A3)} * \mathrm{Cos}(A2) * \mathrm{Sin(A1)} + \mathrm{Cos(A3)} * \mathrm{Cos(A1)} \end{bmatrix} * \begin{Bmatrix} X_i \\ Y_i \\ Z_i \end{Bmatrix}$$

If the projectile is launched with an initial $Pitch\ Angle\ (\alpha)\ and\ Yaw\ Angle\ (\beta)$, the angular rotations are modified as:

$$First\ a\ rotation\ around\ the\ Iy - Axis\ of: \qquad A_1 = -(Lat_{LP} + \frac{\pi}{2})$$

$$Then\ a\ rotation\ around\ the\ new\ Z - Axis\ of: \quad A_2 = Azimuth + \ \beta/COS(Elev)$$

$$And\ Finally\ a\ rotation\ around\ Yb - Axis\ of: \quad A_3 = Elevation + \ \alpha$$

NB: This strategy still requires some correction because it lead to errors in launches at high elevation and from high latitude.

These rotations are used to construct the direction cosine matrix for the transformation between the inertial axis, IF, and the body axis, BF, at the time of launch. Once the components of the directional cosinus matrix have been calculated, using the 2-3-2 Euler transformation described above, it is used to determine the initial values of Psi, Tet and Phi rotation of the 1-2-1 Euler Transformation from IF-2-BF:

$$Tet = ACOS\{DC(1,1)\}$$

$$PSI = ATAN\left\{\frac{DC(1,2)}{-DC(1,3)}\right\}$$

$$PHI = ATAN\left\{\frac{DC(2,1)}{DC(3,1)}\right\}$$

The convention used to define pitch and yaw angles, $\{\boldsymbol{\alpha} \text{ and } \boldsymbol{\beta}\}$, is illustrated in Figure 16.

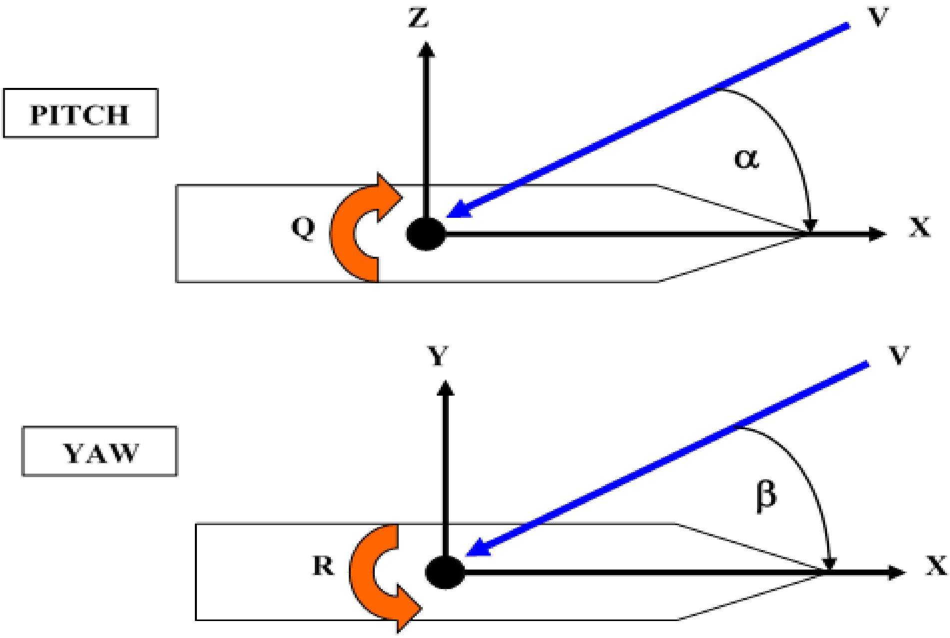

Figure 16 : Illustration of Pitch and Yaw angles

Kinematic equations for the Euler 1-2-1 transformation If2BF:

If $\{\boldsymbol{X},\boldsymbol{Y},\boldsymbol{Z}\}_i$represents inertial axis and the angular velocity of the $\{\boldsymbol{X},\boldsymbol{Y},\boldsymbol{Z}\}_b$- axis are given by:

$$[\vec{\Omega}_b] = \begin{bmatrix} P \\ Q \\ R \end{bmatrix}$$

The same transformation sequence used to derive transformation matrix equations can be used to derive the kinematic relationship between the Euler angular velocities and the angular velocities around the body axis: [i.e. P, Q, R].

$$[Third] \quad * \quad [Second] \quad * \quad [First]$$

$$\begin{bmatrix} P \\ Q \\ R \end{bmatrix}_b = \begin{bmatrix} 1 & 0 & 0 \\ 0 & cos(\emptyset) & sin(\emptyset) \\ 0 & -sin(\emptyset) & cos(\emptyset) \end{bmatrix} * \left[\begin{bmatrix} \frac{d\emptyset}{dt} \\ 0 \\ 0 \end{bmatrix} + \begin{bmatrix} cos(\theta) & 0 & -sin(\theta) \\ 0 & 1 & 0 \\ sin(\theta) & 0 & cos(\theta) \end{bmatrix} * \left\{ \begin{bmatrix} 0 \\ \frac{d\theta}{dt} \\ 0 \end{bmatrix} + \begin{bmatrix} 1 & 0 & 0 \\ 0 & cos(\psi) & sin(\psi) \\ 0 & -sin(\psi) & cos(\psi) \end{bmatrix} * \begin{bmatrix} 0 \\ 0 \\ \frac{d\psi}{dt} \end{bmatrix} \right\}_i \right]$$

$$[Third] \quad * \quad [Second]$$

$$\begin{bmatrix} P \\ Q \\ R \end{bmatrix}_b = \begin{bmatrix} 1 & 0 & 0 \\ 0 & cos(\emptyset) & sin(\emptyset) \\ 0 & -sin(\emptyset) & cos(\emptyset) \end{bmatrix} * \left[\begin{bmatrix} \frac{d\emptyset}{dt} \\ 0 \\ 0 \end{bmatrix} + \begin{bmatrix} cos(\theta) & 0 & -sin(\theta) \\ 0 & 1 & 0 \\ sin(\theta) & 0 & cos(\theta) \end{bmatrix} * \left\{ \left[\begin{bmatrix} 0 \\ \frac{d\theta}{dt} + sin(\psi) * \frac{d\psi}{dt} \\ cos(\psi) * \frac{d\psi}{dt} \end{bmatrix} \right] \right\} \right]$$

$$[Third]$$

$$\begin{bmatrix} P \\ Q \\ R \end{bmatrix}_b = \begin{bmatrix} 1 & 0 & 0 \\ 0 & cos(\emptyset) & sin(\emptyset) \\ 0 & -sin(\emptyset) & cos(\emptyset) \end{bmatrix} * \begin{bmatrix} \frac{d\emptyset}{dt} - sin(\theta) * cos(\psi) * \frac{d\psi}{dt} \\ \frac{d\theta}{dt} + sin(\psi) * \frac{d\psi}{dt} \\ cos(\theta) * cos(\psi) * \frac{d\psi}{dt} \end{bmatrix}$$

$$= \begin{bmatrix} -sin(\theta) * cos(\psi) & 0 & 1 \\ cos(\emptyset) * sin(\psi) & cos(\emptyset) & 0 \\ cos(\emptyset) * cos(\theta) * cos(\psi) - sin(\emptyset) * sin(\psi) & -sin(\emptyset) & 0 \end{bmatrix} * \begin{bmatrix} \frac{d\psi}{dt} \\ \frac{d\theta}{dt} \\ \frac{d\emptyset}{dt} \end{bmatrix}$$

From the equation above, the Euler angular velocities can be solved in terms of the angular velocity components around the body axis as:

$$\begin{bmatrix} \frac{d\psi}{dt} \\ \frac{d\theta}{dt} \\ \frac{d\emptyset}{dt} \end{bmatrix} = \begin{bmatrix} 0 & \frac{sin(\emptyset)}{cos(\theta)} & \frac{cos(\emptyset)}{cos(\theta)} \\ 0 & cos(\emptyset) & -sin(\emptyset) \\ 1 & sin(\emptyset) * tan(\theta) & cos(\emptyset) * tan(\theta) \end{bmatrix} * \begin{bmatrix} P \\ Q \\ R \end{bmatrix}$$

From these equations a singularity exists in the description of the Euler angular rates when:

$$cos(\theta) = 0$$

This singularity however, can be treated by applying the L'Hospital rule as $\left\{\theta \Rightarrow \frac{\pi}{2}\right\}$, see for instance (Regan, 1984:161). Although this singularity is solvable it can become computationally expensive. It has become more popular to rather use the so-called Quaternion transformation scheme that does not have such a singularity with respect to the description of the angular rates. Detailed description will be in the following section 3.5.12.

3.5.12 Quaternion

It is one of the common methods that is used to represent the attitude of rigid bodies such as projectiles. The attitude of a projectile is referring to its rotational orientation during its flight relative to a defined reference frame. The widely used quaternion representation is based on Euler's rotational theorem which states that the relative orientation of two coordinate systems can be described by only one rotation about a fixed axis as shown in Figure 17. However, a quaternion is composed of a rotational axis and a rotation angle, according to Euler's rotational theorem, and representing a coordinate transformation from frame to frame as: (Gro *et al.*, 2012).

$$q = \begin{bmatrix} qc \\ qx \\ qy \\ qz \end{bmatrix} = \begin{bmatrix} cos\frac{\theta}{2} \\ \|\vec{e}\| * sin\frac{\theta}{2} \end{bmatrix}$$

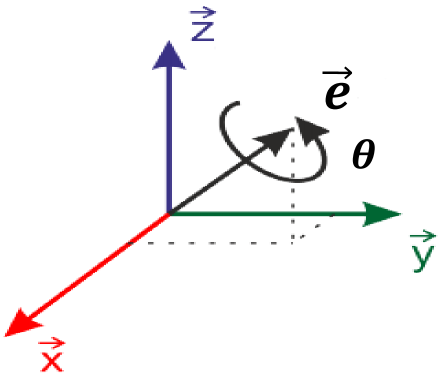

Figure 17: Concept of Euler's rotational theorem of a quaternion (Gro *et al.*, 2012)

" $\|\vec{e}\|$ is the normalised rotational axis (Euler axis) and θ is not the rotational angle but the transformation angle (Euler angle). Quaternions are widely used due to its advantages such as no singularity and computationally less intense compared to other attitude representations, such as Euler angles or a direction cosine matrix. The representation of relative orientation using Euler angles is easy to develop and to visualise, but computationally intense. Also, a singularity problem occurs when describing attitude kinematics in terms of Euler angles and therefore it is not an effective method for spacecraft attitude dynamics." (Gro *et al.*, 2012).

3.6 Projectile model

3.6.1 Introduction to the data required to define a specific projectile

For the present study two data files are used:

- AERODYN Providing the aerodynamic parameters.
- INERTIA Providing the inertia parameters.

In future another two models will be added:

- Rocket Providing the parameters to model rocket performance.
- Base Bleed Providing the parameters required to model Base Bleed performance.

Detail on how the inertia data is presented is given in paragraph 3.6.2. and detail for the aerodynamic data is given in paragraph 3.6.3.

3.6.2 Inertia Model

The inertia of the projectile is described by its moments of inertia relative to the centre of gravity as:

Moments of inertia $$[I] = \begin{bmatrix} I_{xx} & I_{xy} & I_{xz} \\ I_{yx} & I_{yy} & I_{yz} \\ I_{zx} & I_{zy} & I_{zz} \end{bmatrix}.$$

Additional data required to define projectile asymmetry is:

- The radial off-set in the center of gravity i.e. dYcg and dZcg.

And for possible future use provision is also made for:

- Axial position of the center of gravity i.e. Xcg.

This data is supplied in File "Inertia" as a function of projectile mass as shown in Table 3. This allows for changes that might be experienced along the trajectory, for example when fuel is consumed as in rocket and Base Bleed trajectory simulations.

Note that in the Inertia data file provision is made for a scale factor for each column. This is used during parametric studies where it might be required to analyse the effect of changes in certain parameters.

Table 3: Form of File "Inertia"

First two header lines are used to supply references information regarding data in file										Header 1
										Header 2
Mass	Ixx	Iyy	Izz	Ixy	Ixz	Iyz	dYcg	dZcg	Xcg	Header 3
1.0	1.0	1.0	1.0	1.0	1.0	1.0	1.0	1.0	1.0	Scale Factor
Data	Data	Data	Data	Data	Data	Data	Data	Data	Data	Line 4 – n
Data	Data	Data	Data	Data	Data	Data	Data	Data	Data	"
Data	Data	Data	Data	Data	Data	Data	Data	Data	Data	Line n

A detailed description of the data in each column in file "INERTIA" is given in Table 4 where the file structure is presented in a "Transposed" format.

Table 4: Description of the data in file "INERTIA"

COL	Coefficient	Description
1	Mass	Mass is used as independent parameter in inertia data interpolation
2	Ixx	Moment of inertia around the axial X-axis
3	Iyy	Moment of inertia around the transverse Y-axis
4	Izz	Moment of inertia around the transverse Z-axis
5	Ixy	Product of Inertia around X-Y axis
6	Ixz	Product of Inertia around X-Z axis
7	Iyz	Product of Inertia around Y-Z axis
8	dYcg	Radial off-set in the CoG in the Y-Axis direction
9	dZcg	Radial off-set in the CoG in the Z-Axis direction
10	Xcg	Axial position of the CoG from the nose tip

For the basic trajectory simulation of a symmetric projectiles the inertia parameters used are:

- Mass Projectile Mass
- Ixx Moment of Inertia around the Axial Axis - X
- Iyy Moment of Inertia around the Y-Axis
- Izz Moment of Inertia around the Y-Axis

The other inertia parameters shown in Table 3 and Table 4 are used to define the asymmetric properties used in the 6-DOF trajectory simulations. These parameters allow for:

- A radial off-set in the CoG from the axial axis of the projectile.

- Products of inertia to account for principle inertia axes that are not aligned with the axial geometric axis of the projectile as illustrated in Figure 18. See for example also (Glover, Hagan, 1971).

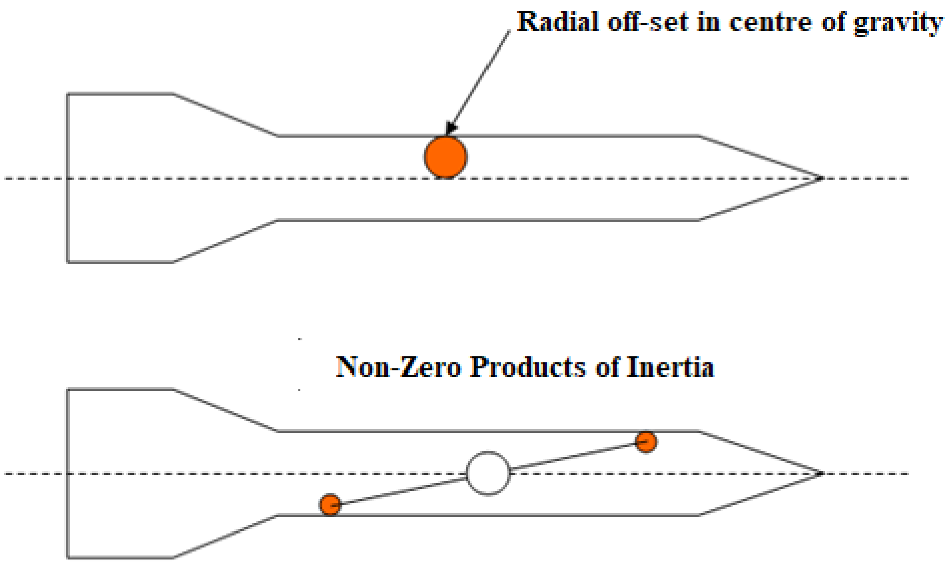

Figure 18: Illustration of asymmetric inertia properties

3.6.3 Aerodynamic Model

The aerodynamic model is described by the aerodynamic coefficients, following the approach presented by (Mccoy, 1998), see APPENDIX B. The aerodynamic data is supplied in a file, “AERODYN” with Mach number as the independent variable as defined in Table 5.

Table 5: Table to describe aerodynamic properties

COL	Coefficient	Description
1	Mach	Mach number used as independent parameter in aero data interpolation
2	Cd0	Drag coefficient at zero angle of attack
3	Cda2	Induced drag coefficient due to angle of attack
4	Cdb	Base drag coefficient used only with BB effect prediction
5	CLa	Lift curve slope i.e. $\left\{\frac{dCL}{d\alpha}\right\}$
6	CLa3	Non-linear lift coefficient
7	Cma	Pitch moment coefficient slope i.e. $\left\{\frac{dCm}{d\alpha}\right\}$
8	Cma3	Non-linear pitch moment coefficient

COL	Coefficient	Description
9	Cmq	Pitch damping moment coefficient
10	Cl	Roll moment: $Cl = \left\{\frac{dCl}{d\delta} * \delta\right\}$
11	Clp	Spin damping coefficient
12	Cypa	Magnus force coefficient
13	Cypa3	Non-linear Magnus force coefficient
14	Cmpa	Magnus moment coefficient
15	Cmpa3	Non-linear Magnus moment coefficient
16	Cn0	Asymmetric lift force coefficient at zero angle of attack
17	B1	Reference angle for asymmetric force
18	Cm0	Asymmetric pitch moment coefficient at zero angle of attack
19	B2	Reference angle for asymmetric moment

The aerodynamic parameters presented in columns 1-15 is used for the 6-DOF trajectory simulation of axial symmetric projectiles. The other parameters in columns 16-19 is used to describe asymmetric aerodynamic properties used in 6-DOF simulations.

The asymmetric aerodynamic properties can be presented by a so-called banana shape, as shown in Figure 19. (See for example (Glover, Hagan, 1971:167)). This allows for:

- A normal force (Cn0) at zero angle of attack and at a certain angle B1 relative to the body axis.
- A pitch moment (Cm0) at zero angle of attack at a certain angle B2 relative to the body axis, as shown in Figure 20.

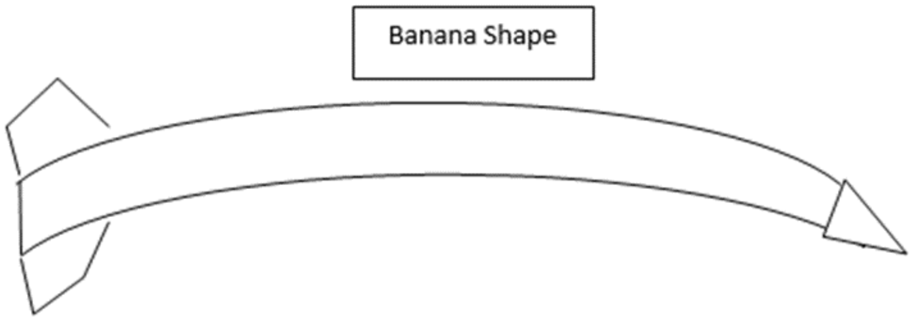

Figure 19: Illustration of asymmetric aerodynamic properties

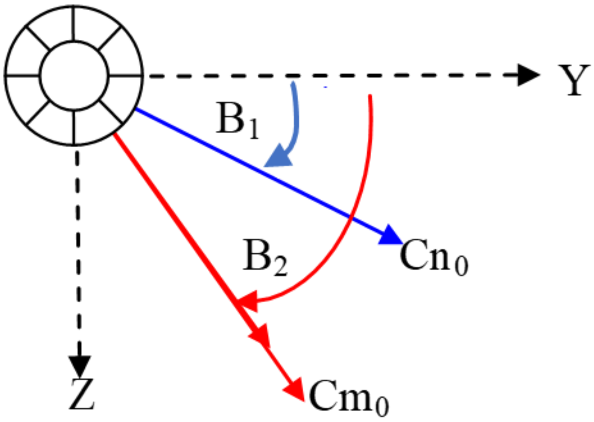

Figure 20: Illustration of orientation of aerodynamic asymmetries

3.7 Integration Method

A 6-DOF simulation model describes the motion of a projectiles during their flight through the atmosphere. The moving projectiles can translate and rotate. The six fundamental differential equations for a general body with asymmetries that allow the motion to be tracked are (Greenwoord, 1988):

$$
\begin{bmatrix} \frac{dP}{dt} \\ \frac{dQ}{dt} \\ \frac{dR}{dt} \\ \frac{du}{dt} \\ \frac{dv}{dt} \\ \frac{dw}{dt} \end{bmatrix} = \begin{bmatrix} \dfrac{M_X + (I_Y - I_Z) * Q * R + I_{YZ} * (R^2 - Q^2) - I_{XZ} * \left(P * Q + \frac{dR}{dt}\right) + I_{XY} * \left(P * R - \frac{dQ}{dt}\right)}{I_{XX}} \\ \dfrac{M_Y + (I_Z - I_X) * R * P + I_{XZ} * (P^2 - R^2) - I_{XY} * \left(Q * R + \frac{dP}{dt}\right) + I_{YZ} * \left(P * Q - \frac{dR}{dt}\right)}{I_{YY}} \\ \dfrac{M_Z + (I_X - I_Y) * P * Q + I_{XY} * (Q^2 - P^2) - I_{YZ} * \left(R * P + \frac{dQ}{dt}\right) + I_{XZ} * \left(Q * R - \frac{dP}{dt}\right)}{I_{ZZ}} \\ \dfrac{F_X}{Mass} - Q * w + R * v \\ \dfrac{F_Y}{Mass} - R * u + P * w \\ \dfrac{F_Z}{Mass} - P * v + Q * u \end{bmatrix}
$$

Where,

- Fx , Fy , Fz are the sum of all the forces causing the body to accelerate.
- Mx, My, Mz are the sum of the aerodynamic and thrust moments with respect to the center of mass.
- Mass is the total mass of the projectile.
- Ix, Iy, Iz, Ixy, Ixz, Iyz are the moments and products of inertia.
- P, Q, R are the angular velocities.

3.7.1 Runge-Kutta 4th order method

The equations of motion describing the projectile motion and angular rotation are integrated numerically. Runge-Kutta methods is a family of a single-point methods that can be used to solve systems of initial value of ordinary differential equation (ODEs) such as the equations of motion of the projectile (Hoffman, 1992).

These single-point methods use data available at one point (n), to advance the solution to point (n+1) as illustrated in Figure 21.

The fourth-order Runge-Kutta method has become a popular method for solving initial value ODEs and was selected for the numerical integration of the projectile equations of motion (Hoffman, 1992). In the algorithm below the time step of the integration $dt = t_{n+1} - t_n$.

$$x(t_{n+1}) = x(t_n) + \frac{dt}{6}(k_1 + 2k_2 + 2k_3 + k_4), \text{ where } t_n + 1 = t_n + dt$$

$$k_1 = \dot{x}(t_n, y_n) \equiv \text{state derivatives at } t_n$$

$$k_2 = \dot{x}(t_n + \frac{dt}{2}, x_n + \frac{dt}{2}k_1) \equiv \text{state derivatives at midpoint of interval using states advanced to the midpoint using Euler's method and } k_1 \text{ as the slope}$$

$$k_3 = \dot{x}(t_n + \frac{dt}{2}, x_n + \frac{dt}{2}k_2) \equiv \text{state derivatives at midpoint of interval using } k_2 \text{ as the slope}$$

$$k_4 = \dot{x}(t_n + dt, x_n + dt * k_3) \equiv \text{state derivatives at endpoint of interval using } k_3 \text{ as the slope}$$

Figure 21: RUNGE–KUTTA INTEGRATION FORMULA (Hawley & Blauwkamp, 2010)

To put it simply, “the commonly used fourth-order Runga-Kutta integration algorithm breaks each major integration interval into four minor integration steps as illustrated in Figure 22. Each step involves the calculation of the derivatives with an updated state. Note that time does not step uniformly through the minor steps. The advantage of using a higher-order algorithm, such as this one, is that the error shrinks by 0.4dt rather than by dt, as it does in a first-order algorithm, such as the Euler method” (Hawley & Blauwkamp, 2010). In each step the derivative is evaluated four times: Once at the initial point, twice at trial midpoints, and once at a trial endpoint. From these derivatives the final function value (shown as a filled dot) is calculated.

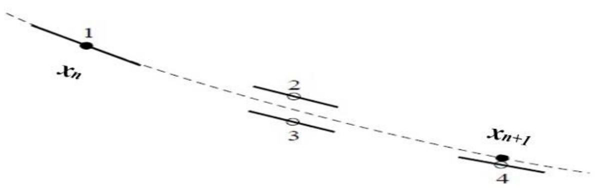

Figure 22: Fourth-order Runge-Kutta method (Press *et al.*, 1968).

In addition, the stability of integration strongly depends on the integration step size. Instability of the calculation of the trajectory can happen when too large initial integration step is set, or too large limits on integration errors are set. For this reason, careful analysis and choice of the steps of integration and limits of integration errors should be done by user (Curcin D. M., 2007).

<u>The reasons of choice:</u> The fourth-order Runga-Kutta integration method was selected because it is reasonably efficient (fast) and accurate. Since it is a single step method it allows for dynamical adjustment of the integration step if required. Outputs can easily be obtained at any timestep which is helpful during debugging and detail trajectory analysis.

3.8 Time Step

The accuracy of the trajectory prediction is dependent on a time step. The time step can be changed depending on the projectile type and its expected dynamic response. For instance, when calculating the trajectory of a spin stabilised projectile, a very small timestep might be required. This might also change along the trajectory as the velocity and spin rate changes. Rockets and mortars might use larger timesteps depending on the expected dynamic response (usually lower angular rates than the spin of a spin-stabilized projectiles).

The time step for the 6-DOF model was chosen by running several simulations and comparing the results with another 6-DOF model to achieve optimum time step for each kind of projectile. In addition, the stability of the projectiles during simulation time is a good indication of the precision of 6-DOF model. The reason for this is when a large time step is applied on the model the simulation will lose its numerical stability (tumble) and when the adequate small-time step is applied on the model the projectile will retain its stability, assuming the projectile is of stable design.

For example, to evaluate the time step limitation for an axially symmetric 155 mm artillery projectile, a couple of simulations were done by using different time step sizes. The smallest time step is 0.00005s and the largest time step is 0.1 s. Figure 23 shows the time step as the X-axis and the relative precision on the Y-axis. Where the relative precision means the value calculated by dividing results by the results obtained with the smallest time step (0.0005 s), which is the most precise result. The results are compared to the result of the smallest time step is illustrated in Figure 23 below.

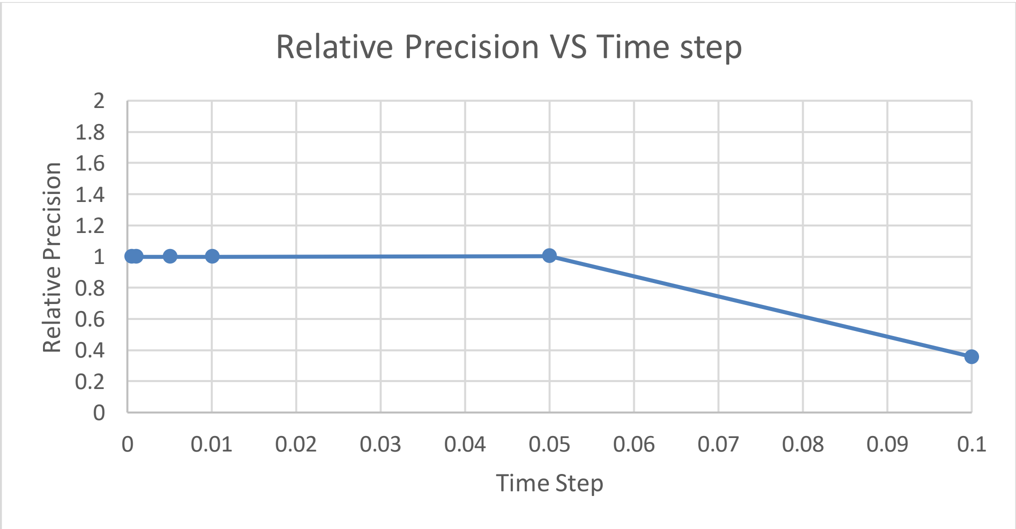

Figure 23: Relative precision vs time step

From Figure 23 above, the conclusions can be made are that for this case study the time step smaller than 0.05 s caused very long simulation times. A time steps longer than 0.05 s caused an unstable and inaccurate simulation. Moreover, the long simulation times observed when performing this case study on time steps.

CHAPTER 4: MODEL VERIFICATION

4.1 Introduction

This chapter shows the verification results obtained with the 6-DOF trajectory simulation model with those obtained from other simulation models as well as the results predicted by analytical solutions. The objective of the verification process is to demonstrate the accuracy of present 6-DOF model solutions so that it may be used with confidence in the case study in chapter 5 specifically, and for exterior ballistic simulation in general. According to (AIAA, 1998), “the verification process determines the correctness of the computational and programming implementation of the model. It examines the mathematics in the model through comparison with exact analytical results and checks for computer programming errors”.

In order to verify the accuracy of 6-DOF model, various case studies were selected. Firstly, the 6-DOF model results will be compared to analytical solutions. Secondly, it will be compared to results generated by other available simulation programs such as PMM, MPMM, 5-DOF, and 6-DOF. Lastly, it will be compared to results generated by the commercial program PRODAS V3 (PRODAS V3 Arrow Tech Associates).

4.2 Verification against Simplified Analytic Solutions

The equations of motion for the 6-DOF model described in Chapter I can be simplified and solved analytically in special cases when certain assumptions are made. Such solutions are approximations but provide a good estimate as long as the parameters match the assumptions made for each special case. The input parameters for the comparisons with analytic solutions and other simulation model are given in Table 6.

4.2.1 Overview of case studies selected for 6-DOF verification

4.2.1.1 Case 1: Spin Stabilised projectile in Vacuum

The results of this trajectory can be compared with analytic solutions and other simulation programs to verify implementation of gravity and earth rotation as well as the correct integration of accelerations to simulate the trajectory.

4.2.1.2 Case 2: Spin Stabilised Symmetric projectile with Initial Pitch

The results of this trajectory can be compared with analytic solutions and other simulation programs to verify implementation of major aerodynamic and inertia models.

4.2.1.3 Case 3: Spin Stabilised Asymmetric projectile with Initial Pitch

The results of this case can be compared with analytic solutions and other simulation programs to verify implementation of asymmetric aerodynamic and inertia models.

Table 6: Summary of parameters for case studies 1, 2, 3 for 6-DOF model verification – Spin Stabilized Projectile

Input parameters		case 1	case 2	case 3
Nominal Launch Condition	V0 [m/s]	900	900	900
	Height [m]	0	0	0
	Elev [deg]	60	60	60
	Pitch [deg]	0	5	5
	Yaw [deg]	0	0	0
	Spin [rad/s]	1824.15	1824.15	1824.15
	Spin [Deg/s]	104516.1	104516.1	104516.1
	Latitude [deg]	0	0	0
	Azimuth [deg]	0-270	0	0
	Wind	0	0	0
Sym Mass	Mass [kg]	45.0	45.0	45.0
	Ix [kgm^2]	0.148	0.148	0.148
	Iy=Iz [kgm^2]	1.797	1.797	1.797
Symmetric Aerodynamic Properties	Lref [m]	0.155	0.155	0.155
	Aref [m^2]	0.01887	0.01887	0.01887
	Cdo	0	0.25	0.25
	Cda2	0	0	0
	CLa	0	2.5	2.0
	Cma	0	3.65	3.65
	Cmq	0	-25.0	-25.0
	Cmpa	0	0.859	0.859
	Cl	0	0	0
	Clp	0	-0.03	-0.03
Rocket	Thrust [N]	0	0	0
	Isp [sec]	0	0	0
	BurnTime [sec]	0	0	0
Asymmetries	Ixy [kgm^2]	0	0	0.005
	dYcg [m]	0	0	0
	dZcg [m]	0	0	0
	Cm0	0	0	0
	Beta [deg]	0	0	0
	Asym Thrust Moment [Nm]	0	0	0
	Objective	Vacuum	Yaw Motion	Asymmetries

Note: The red is used to highlight certain input parameters for a specific case.

4.2.2 Individual case studies

4.2.2.1 Case 1: Trajectory in Vacuum

Assumptions

To simulate the trajectory in vacuum using the 6-DOF simulation programs the ICAO atmospheric density was scaled using:

- Atmospheric Density = ICAO(Density) * 0.000001

Summary of trajectory simulation results

The equations derived by (Regan, 1984) can be used to estimate the effect of earth rotation for various launch azimuths. The comparative results obtained with 6-DOF programs are shown in Table 7.

Table 7: Summary of Results for Case Study 1

Method	Analytic 1 Cons G	Analytic 2 Const G + Earth Rot	Point Mass	5DOF	6-DOF	PRESENT 6-DOF	Comment
Azimuth = 0.0 [i.e. due North]							
Time of Flight [sec]	158.9	159.9	158.9	160.9	160.9	161.0	Difference possibly due to different Gravity Models
Range [m]	71507.0	71967.0	71507.0	71953.0	71952.0	71991.4	
Drift Right Negative [m]	****	-481.0	****	-484.0	-484.0	-484.7	
Azimuth = 90.0 [i.e. due East]							
Range [m]	****	71974.0	****	71950.0	71948.0	71986.2	
Drift Right Negative [m]	****	0	****	0	0	0	
Azimuth = 180.0 [i.e. due South]							
Range [m]	****	71969.0	****	71953.0	71952.0	71991.4	
Drift Right Negative [m]	****	481.0	****	484.0	484.0	484.7	
Azimuth = 270.0 [i.e. due West]							
Range [m]	****	71967.0	****	71958.0	71956.0	71995.4	
Drift Right Negative [m]	****	0	****	0	0	0	
Azimuth = 360.0 [i.e. due North]							
Range [m]	71507.0	71967.0	71507.0	71953.0	71952.0	71991.4	
Drift Right Negative [m]	****	-481.0	****	-484.0	-484.0	-484.7	

The effect of earth rotation on the trajectory in vacuum is illustrated by the variation in drift as a function of launch azimuth. The variation in drift (i.e. drift to right at a given azimuth – drift for a launch towards north) is illustrated in Figure 24. Note that the analytic and 6-DOF results coincide.

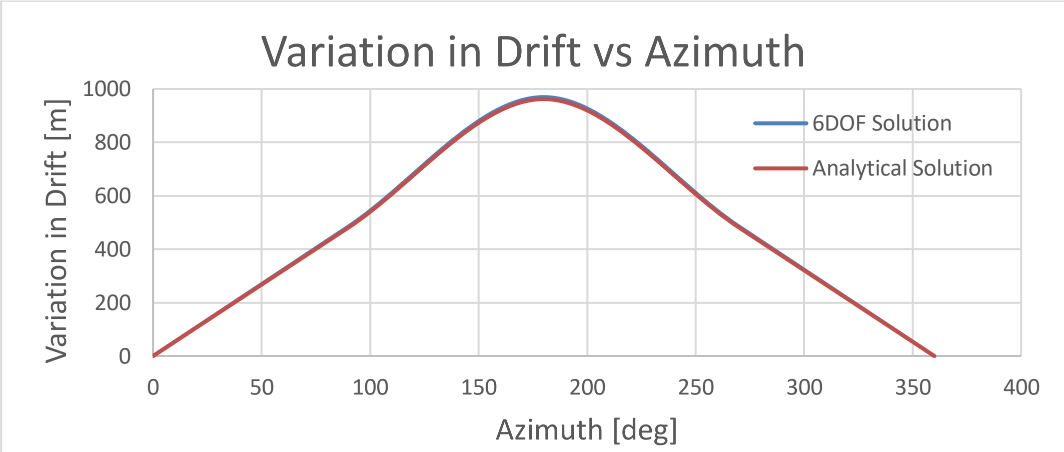

Figure 24: Case 1 variation in drift vs. launch azimuth to illustrate effect of Earth rotation

4.2.2.2 Case 2: Spin stabilised projectile with Constant Aero and Initial Pitch

Assumptions

For this case the standard ICAO MET is used with constant aerodynamic coefficients for a typical artillery projectile with initial yaw. This allow for evaluation of angular motion that can be compared to analytic solutions for short sections of the trajectory.

Summary of trajectory simulation results

The analytic solution is provided by the Tri-Cyclic motion (Murphy, 1963; Vaughn, 1969). These analytic equations were incorporated in program “Alf_Bet” and use it to calculate an analytic result for the angular motion of projectiles. This theory assumes constant velocity and is therefore only applicable to short sections of the trajectory. The comparative results obtained are shown in Table 8.

Table 8 : Summary of Results for Case Study 2

Method	Analytic 3 Tri-Cyclic	Point Mass	5DOF	6-DOF	PRESENT 6-DOF	Comment
Time of Flight [sec]		107.82	109.84	109.83	109.91	
Range [m]		25601.00	26442.00	26440.00	26482.00	
Drift Right Negative [m]		****	-2151.00	-2156.00	-2153.00	
Impact Velocity [m/s]		410.60	414.60	414.60	418.00	
Impact Angle [deg]		-71.60	-70.77	-70.77	-70.91	
Maximum Yaw [deg] first 0.25 sec	7.08	****	6.79	6.95	6.95	

The solution according to the analytic description of the Tri-Cyclic motion, using the Alf_Bet program is illustrated in Figure 25 for t = 0.25 sec. The comparison of the expected pitch versus yaw motion for first 0.25 sec is shown in Figure 26, and a maximum yaw of 6.95 deg is shown in Figure 27.

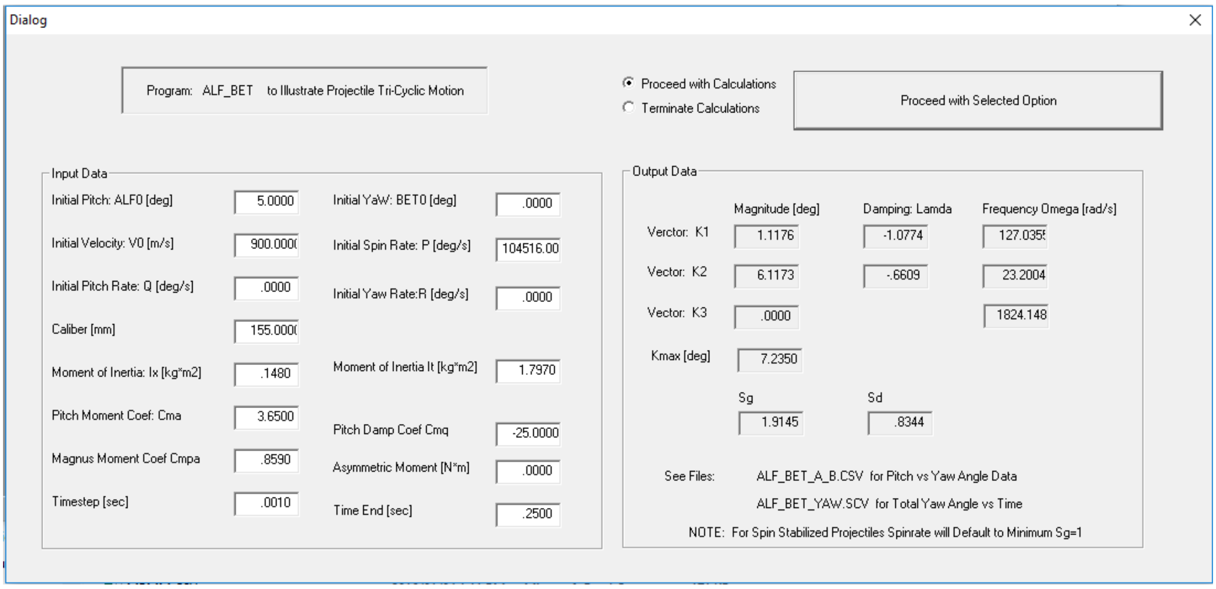

Figure 25: Analytic Tri-Cyclic solution: Case 2 – Initial Pitch of 5 deg

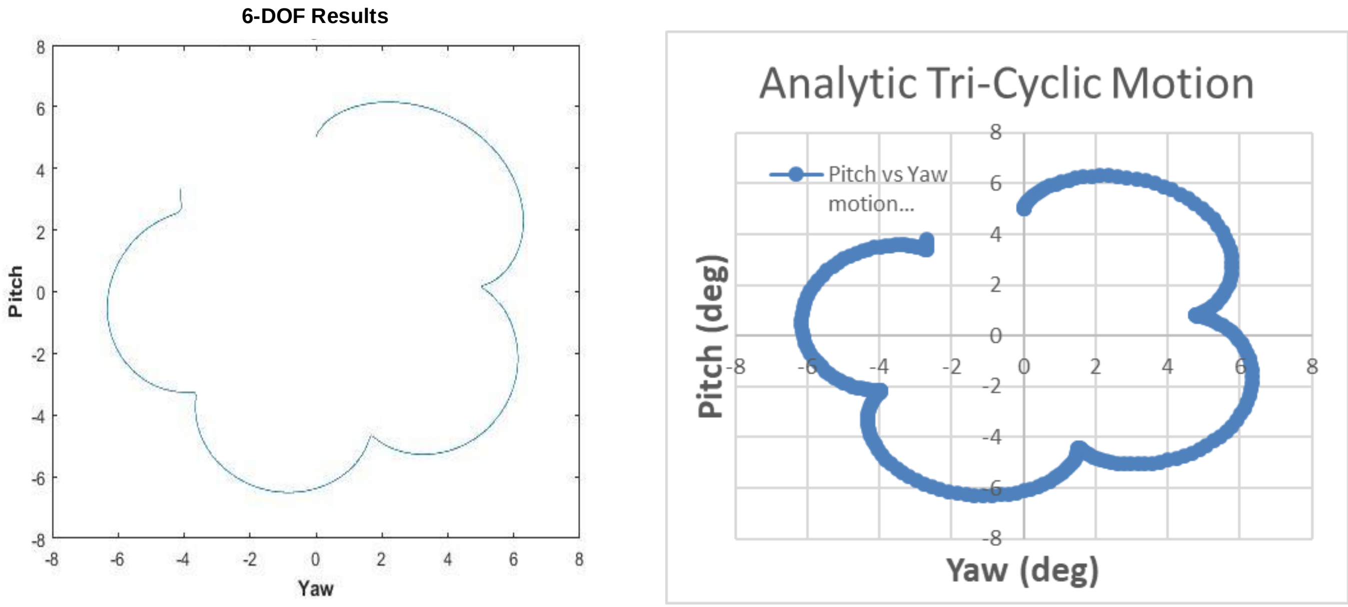

Figure 26: **Predicted Pitch-Yaw of 6-DOF and analytic solution for first 0.25 sec: Case 2 – Initial Pitch of 5 deg**

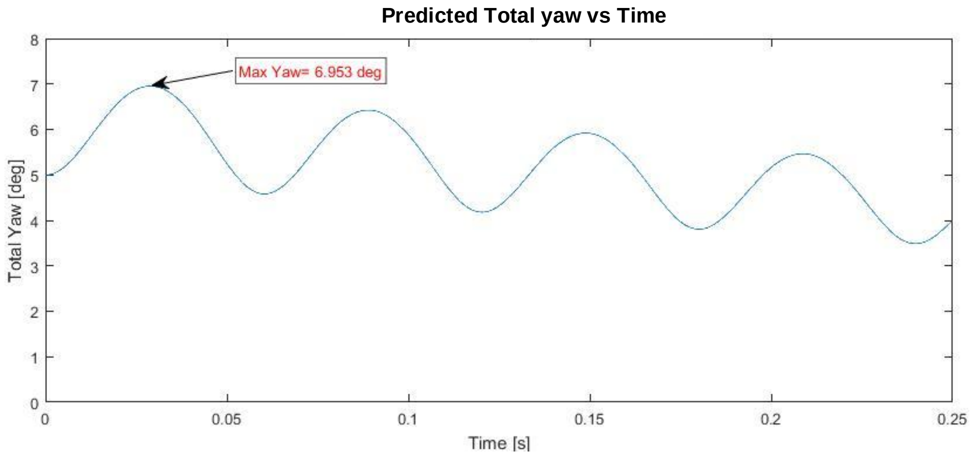

Figure 27: **Predicted Total Yaw for first 0.25 sec: Case 2 – Initial Pitch of 5 deg**

4.2.2.3 Case 3: Asymmetric Spin stabilised projectile with constant aero and initial pitch

Assumptions

For this case the standard ICAO MET is used with constant aerodynamic coefficient for a typical artillery projectile with initial pitch and asymmetric inertia properties presented by:

- Ixy = 0.005

For a spinning projectile the asymmetric moment due to a product of inertia of Ixy (Mz), is given by(Greenwoord,1988:391):

- Asymmetric Moment = $-\Omega^2$ * Ixy = -1824.152 * 0.005 = -16637.6 Nm

This allows for evaluation of angular motion that can be compared to analytic solutions for short sections of the trajectory. For the spinning symmetric projectile, the motion is characterised by the precession and nutation components. The contribution of the asymmetry is to add an additional component with a frequency that equals spin frequency. The comparative results obtained with the present 6-DOF model are shown in Table 9.

Summary of trajectory simulation results

Table 9: Summary of Results for Case Study 3

Method	Analytic 3 Tri-Cyclic	5DOF	6-DOF	Present 6-DOF	Comment
Time of Flight [sec]	****	109.84	109.90	109.97	The effect of asymmetry causes 41 m difference in range and 2 m in drift.
Range [m]	****	26442.00	26419.00	26460.00	
Drift Right Negative[m]	****	-2151.00	-2147.00	-2149.00	
Impact Velocity [m/s]	****	414.60	414.70	418.00	
Impact Angle [deg]	****	-70.77	-70.80	-70.94	
Maximum Yaw [deg] First 0.25 sec	13.3 Vector Sum 12.9 Pitch-Yaw	6.80 No Asym	9.50	9.60	Note: For the analytic solution the V remains constant

The solution according to the analytic description of the Tri-Cyclic motion as calculated, using the Alf_Bet program is illustrated in Figure 28, a comparison of the expected pitch versus yaw motion is shown in Figure 29, and the maximum yaw is shown in Figure 30.

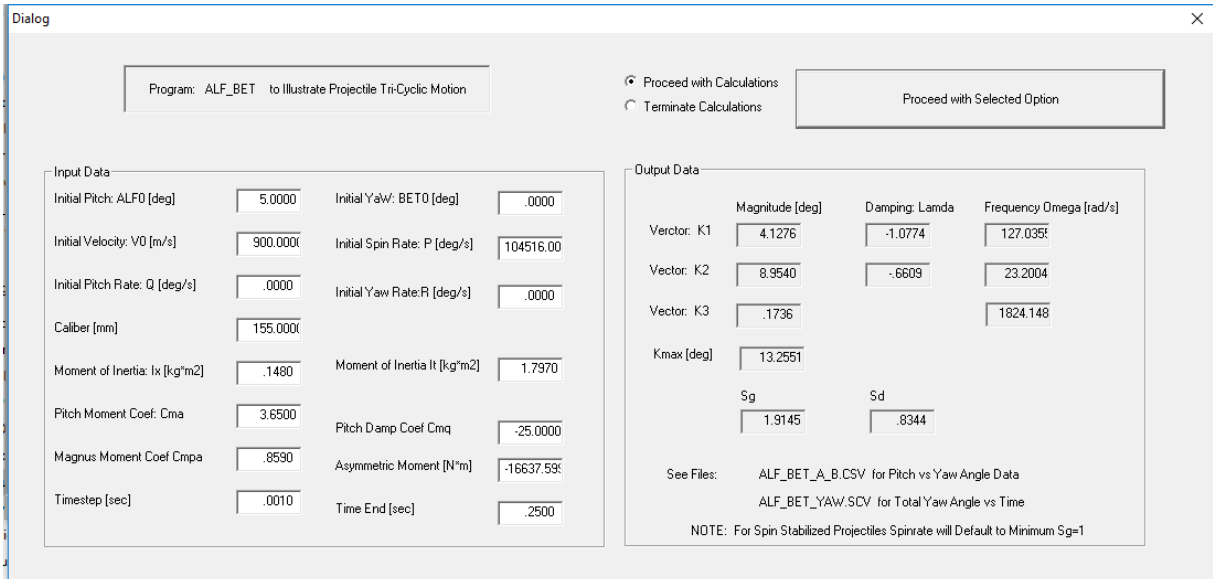

Figure 28: **Predicted Pitch-Yaw for first 0.25 sec: Case 3 – Initial Pitch of 5 deg**

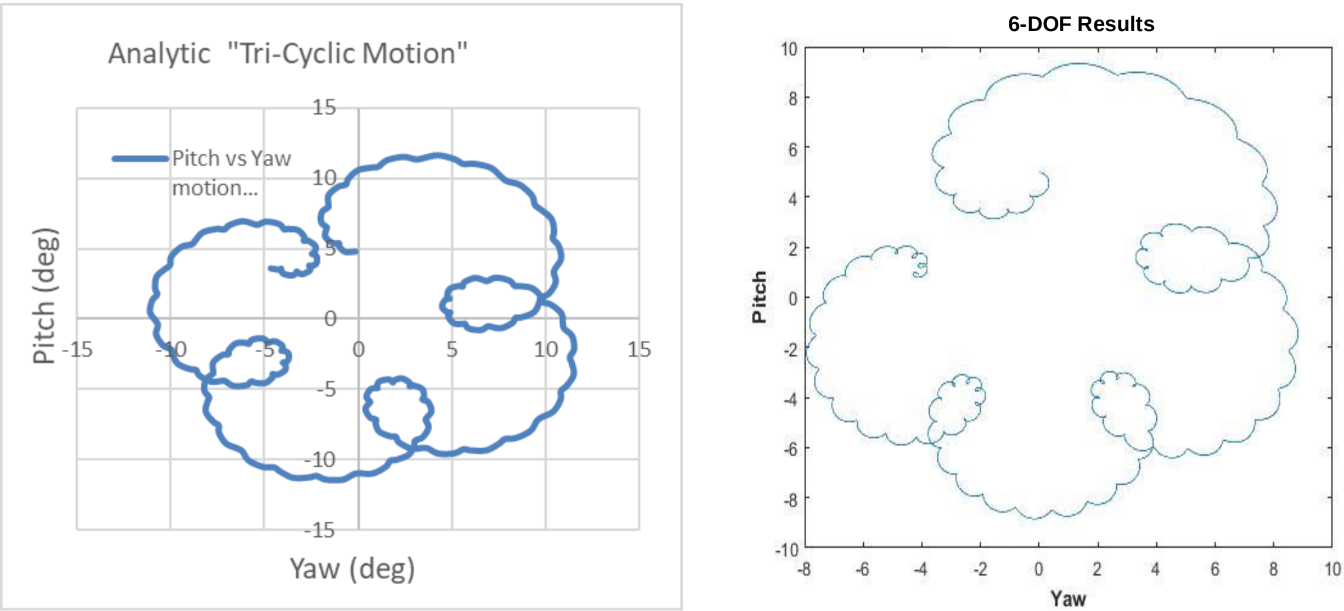

Figure 29: **Tri-Cyclic Solutions of the 6-DOF and analytic solution for an asymmetric spin stabilized projectile Case 3 – 0.25 sec**

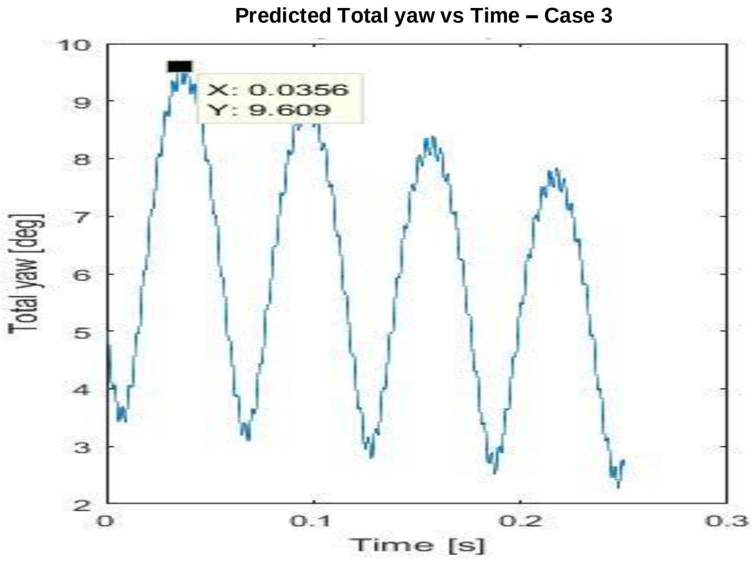

Figure 30: 6-DOF total yaw profile for Asymmetric Case 3– first 0.25 s

4.2.3 Results

These results of the three cases verified that the 6-DOFmodel has been coded correctly as they match very well in portion to the trajectory where the analytical solutions are sufficiently accurate. The results also show the correctness of the implementation of integration scheme, gravity, earth rotation, Coriolis effects, and the correctness of implementation of major symmetric and asymmetric aerodynamic and inertia models. Moreover, they verified that the model produces reliable trajectories for symmetric and asymmetric cases. This will verify correctness of simulation in general and provide confidence to proceed with case studies. The slight difference in the results between the present 6-DOF model and the analytical solutions are due to the fact that the analytical solutions are based on certain assumptions. The analytical solutions are approximations but provide a good estimate as long as the parameters fit the assumptions made for each special case. The close agreement of these results strongly suggest that the equations have been coded correctly in Matlab and that the program produces reliable trajectories for both symmetric and asymmetric cases.

4.3 Verification against other Simulation Models [PMM, 5DOF and 6-DOF]

As mentioned in the Chapter 2 of this research, the simulation models [PMM, 5-DOF, 6-DOF] were developed as tools to simulate the trajectory of projectiles. These models range from the extremely simple to the very complex models. The degree of complexity usually depends upon the degrees of freedom which the model is based on, and the specific simulation requirements. For these verification studies, the results obtained with the present 6-DOF model are compared to the results obtained by the PMM, 5-DOF, and 6-DOF models as implemented in the WinFast program. WinFast is the program used by RDM in trajectory analysis and the preparation of Range Tables. The results of the WinFast program has been verified against similar programs used internationally. The input parameters for the comparisons with simulation models are given in Table 10.

4.3.1 Overview of case studies selected for 6-DOF verification

4.3.1.1 Case 4: Fin Stabilised Symmetric Projectile without Spin

The results from this case study can be used to verify correct prediction of features like the natural pitch frequency of static stable (typical fin stabilised) missiles.

4.3.1.2 Case 5: Fin Stabilised Symmetric Projectile Spinning Through Resonance

The results from this case study can be used to verify spin-up and spin through resonance for a typical fin stabilised projectile.

4.3.1.3 Case 6: Fin Stabilised Asymmetric Projectile Experiencing Lock-In at Resonance

The results for this case study can be used to verify correct implementation of asymmetric properties and the experience of lock-in at resonance.

Table 10: Summary of parameters for case studies 4, 5, 6 for 6-DOF Verification – Fin stabilized projectile

Input parameters		Case 4	Case 5	Case 6
Nominal Launch Condition	V0 [m/s]	300	300	300
	Height [m]	0	0	0
	Elev [deg]	45	45	45
	Pitch [deg]	0	0	0
	Yaw [deg]	0	0	0
	Spin [rad/s]	0	0	0
	Latitude [deg]	0	0	0
	Azimuth [deg]	0	0	0
	Wind	0	0	0
Sym Mass	Mass [kg]	4.4	4.4	4.4
	Ix [kgm^2]	0.0034	0.0034	0.0034
	Iy=Iz [kgm^2]	0.0267	0.0267	0.0267
Symmetric Aerodynamic Properties	Lref [m]	0.081	0.081	0.081
	Aref [m2]	0.0052	0.0052	0.0052
	Cdo	0.15	0.15	0.15
	Cda2	3.125	3.125	3.125
	CLa	1.75	1.75	1.750
	Cma	-1.80	-1.80	-1.80
	Cmq	-54.0	-54.0	-54.0
	Cmpa	0	0	0
	Cl	0	0.003	.003
	Clp	0	-0.25	-0.25
Rocket	Thrust [N]	0	0	0
	Isp [sec]	0	0	0
	BurnTime [sec]	0	0	0
Asymmetries	Ixy [kgm^2]	0	0	0
	dYcg [m]	0	0	0
	dZcg [m]	0	0	0.001
	Cm0	0	0	0.05
	Beta [deg]	0	0	0
	Asym Thrust Moment [Nm]	0	0	0
	Objective	Point Mass	Spin through Resonance	Asymmetric Spin

Note: The red is used to highlight certain input parameters for a specific case.

4.3.2 Individual case studies

4.3.2.1 Case 4: Statically stable projectile with constant aero and no spin

Assumptions

For this case, typical data for an 81 mm mortar bomb is used. The trajectory can be compared to that of a typical 3-DOF point mass model, and 5/6-DOF models as shown in Table 11.

Summary of trajectory simulation results

Table 11: Summary of Results for Case Study 4

Method	Point Mass	5DOF	6-DOF	PRESENT 6-DOF	Comment
Time of Flight [sec]	37.20	37.38	37.39	37.40	Good correlation between results illustrating that 3DOF might be sufficient due to low impact of lateral forces.
Range [m]	5624.00	5638.00	5638.00	5639.00	
Drift Right Negative [m]	****	-4.50	-4.50	-4.60	
Impact Velocity [m/s]	196.70	196.50	196.50	197.40	
Impact Angle [deg]	-56.10	-56.20	-56.20	-56.36	

The angular motion of a static stable projectile is characterised by the natural pitch frequency given by (Regan, 1984):

$$\omega_N = \sqrt{-\left(\frac{M_\alpha}{I_T}\right)} = \sqrt{-\left(\frac{\rho * V^2 * A_{Ref} * L_{Ref} * Cm_\alpha}{2 * I_T}\right)}$$

$$= \sqrt{-(\frac{1.22488 * 300^2 * 0.00515 * 0.081 * -1.8}{2 * 0.0267})} = 39.5\, rad/s$$

At launch this gives: $\omega_N = 39.5\, rad/s$. The predicted natural pitch frequency along the trajectory is illustrated in Figure 31. The changes in ω_N are due to change in velocity and density along the trajectory.

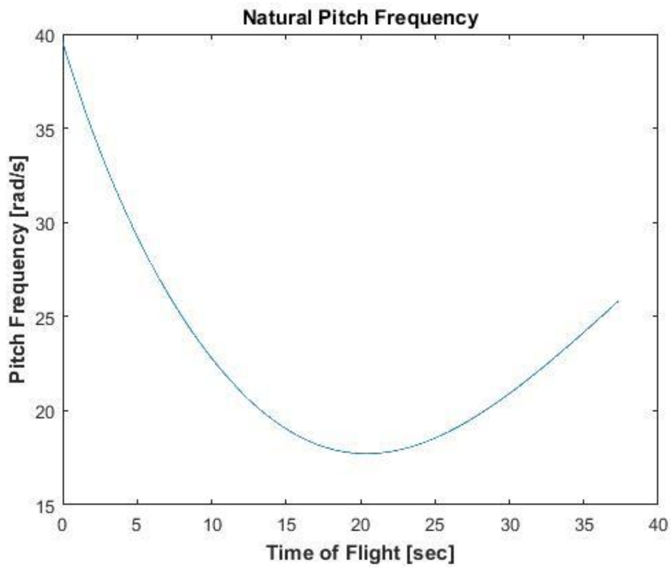

Figure 31: **Illustration of predicted natural pitch frequency of a statically stable projectile Case 4**

4.3.2.2 Case 5: Statically stable projectile spinning through resonance

Assumptions

For this case a spin or rolling moment is applied to force the projectile to spin through resonance, experienced when the spin rate become equal to the natural pitch frequency. The moment used in the simulation is:

$$Cl \quad = \quad 0.003$$

Summary of trajectory simulation results

Table 12: **Summary of Results for Case Study 5**

Method	Point Mass	5DOF	6-DOF	PRESENT 6-DOF	Comment
Time of Flight [sec]	37.20	37.38	37.39	37.38	Spin of statically stable missile cause slight drift to the left.
Range [m]	5624.00	5638.00	5638.00	5636.00	
Drift Right Negative [m]	****	-16.70	-16.70	-16.75	
Impact Velocity [m/s]	196.70	196.50	196.50	197.00	
Impact Angle [deg]	-56.10	-56.20	-56.20	-56.35	

Figure 32 illustrate how the spin rate increases until it passes through the natural pitch frequency (resonance) at about 2.5 sec and then settled at about 50 rad/s due to spin damping. Despite experiencing resonance there is no evidence of any change in the drag as the symmetric projectile passes through resonance as illustrated in Figure 33.

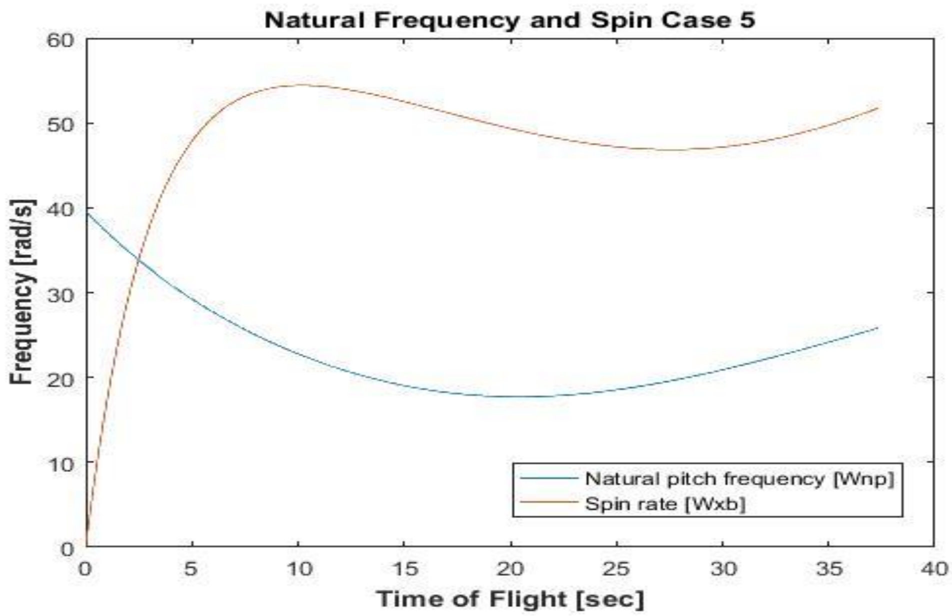

Figure 32: Natural pitch frequency and spin rate for symmetric projectile

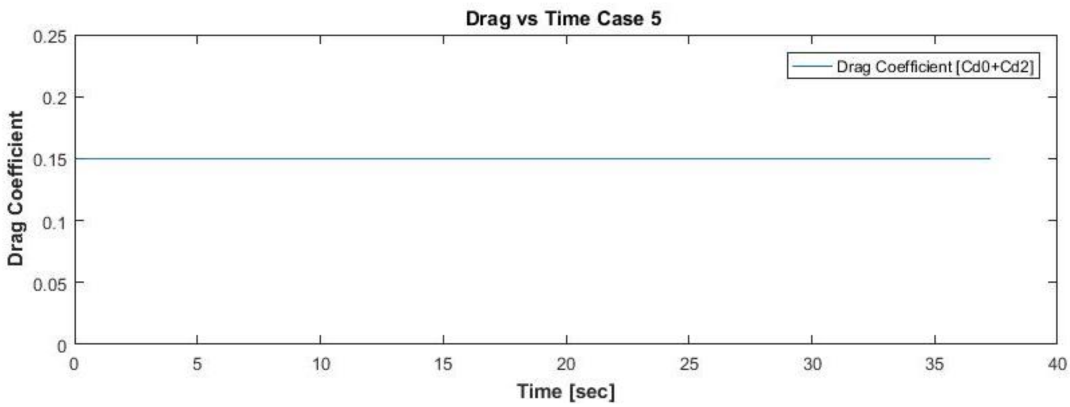

Figure 33: Drag profile for symmetric projectile spinning through resonance

4.3.2.3 Case 6: Asymmetric staticslly stable projectile spin through resonance

This case illustrates how an asymmetric projectile tend to lock-in when spinning through resonance, (i.e. when the spin rate = the natural pitch frequency). To illustrate this requires a specific combination of asymmetries.

Assumptions

For this case the selected combination of asymmetries are:

- A radial off-set in the CoG of 1 mm in the Z-body direction
- A pitch moment at zero angle of attack of Cm0 = 0.05 at an angle of ß=0 as illustrated in Figure 34.

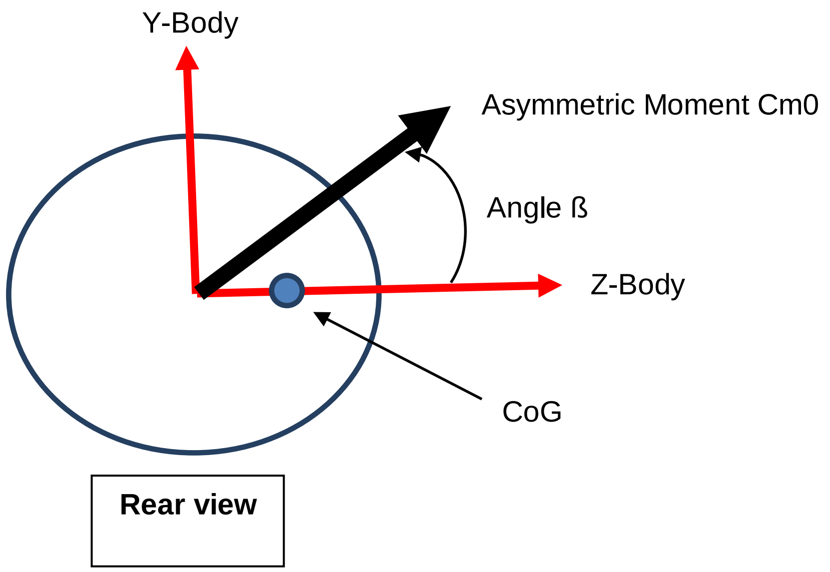

Figure 34: Illustration of asymmetries selected for Case 6

Summary of trajectory simulation results

Table 13: Summary of Results for Case Study 6

Method	Point Mass	5-DOF	6-DOF	PRESENT 6-DOF	Comment
Time of Flight [sec]	37.20	37.38	36.79	36.80	6-DOF prove its value for the simulation of asymmetric effects especially when resonance is encountered.
Range [m]	5624.00	5622.00	5480.00	5481.44	
Drift Right Negative[m]	****	-16.70	-0.43	-0.41	
Impact Velocity [m/s]	196.70	196.10	194.10	194.70	
Impact Angle [deg]	-56.10	-56.25	-56.10	-56.26	
Maximum Yaw [deg]	****	0.08	7.57	7.54	

The spin profile shown in Figure 35 illustrate how the projectile nearly lock-in when passing through resonance. During the dwell time close to the natural pitch frequency, the projectile will experience an increase in yaw due to the asymmetries. This is illustrated by the total yaw profile shown in Figure 36.

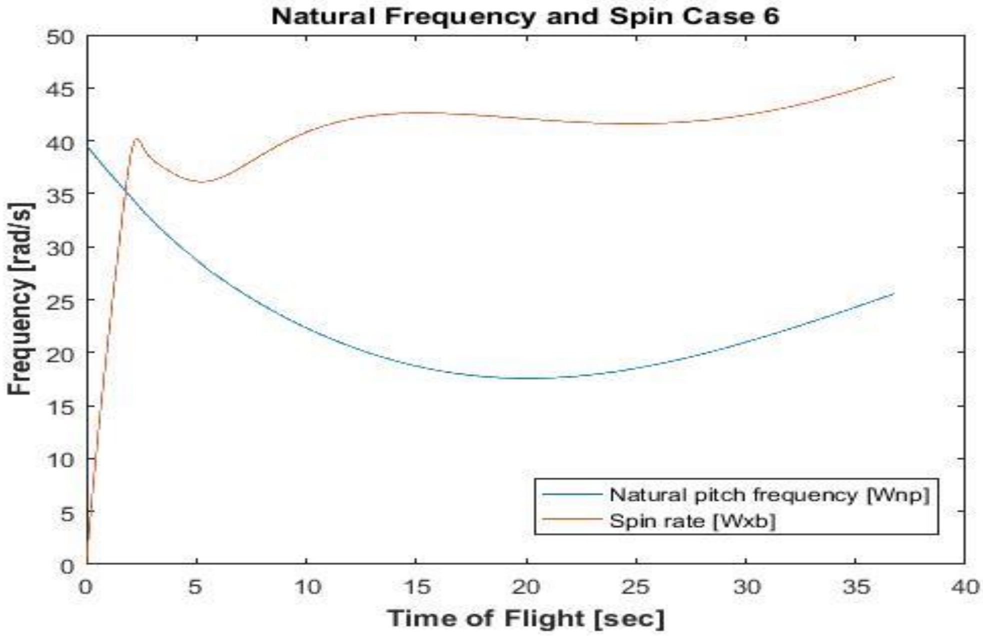

Figure 35: **Case 6 asymmetric projectile spinning through resonance**

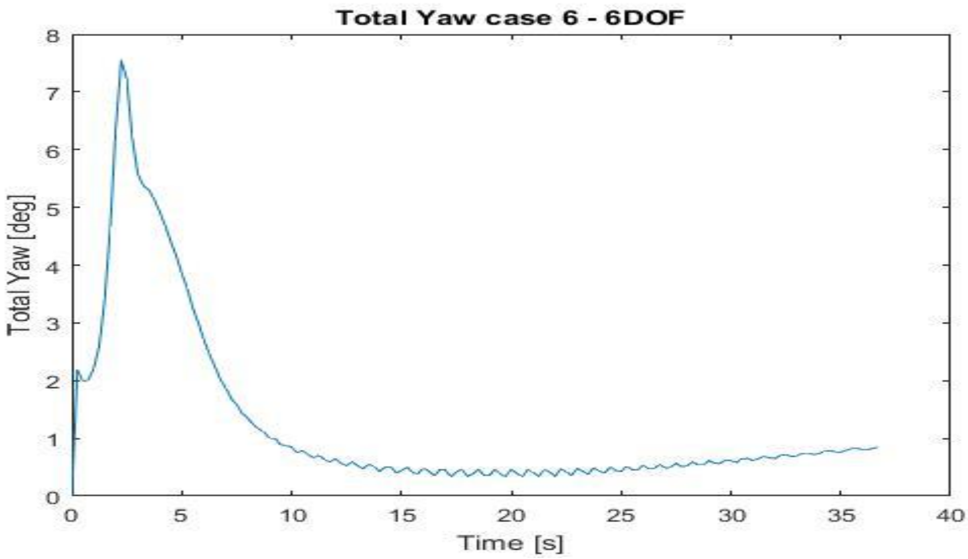

Figure 36: **Total yaw angular motion for asymmetric projectile - Case 6**

The increase in yaw experienced by an asymmetric projectile passing through resonance is associated with an increase in drag, as illustrated in Figure 37.

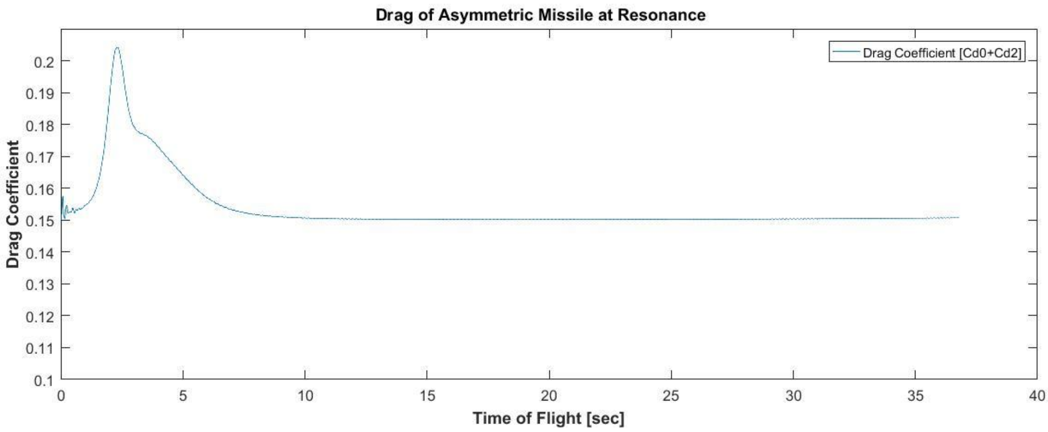

Figure 37: Increase in drag for asymmetric projectile at resonance

4.3.3 Results

These results illustrate that the 6-DOF model and WinFast program produce comparable results when starting with the same initial parameters. It also demonstrates the validity of the functions used in MATLAB to predict features like the natural pitch frequency and phenomena such as spin-up and spin through resonance for a typical fin stabilised projectile. Moreover, it demonstrates the validity of the function used in the 6-DOF model to accommodate the combination of asymmetries effects when the asymmetric projectile tends to lock-in.

4.4 Verification against PRODAS V3 (Arrow Tech Associates)

In this section, test cases have been defined to verify the 6-DOF model results by comparing it with results from the commercial PRODAS V3 simulation program. The reference program [PRODAS V3] have been validated and compared against a variety of experimental results and is widely used internationally. The objective of this verification is to demonstrate the accuracy of 6-DOF model solutions with that of PRODAS. This comparison between the present 6-DOF model and PRODAS was done using a 155 mm M107 artillery projectile (as the test projectile). In addition, all aerodynamic forces, moments coefficients and mass properties of the given projectile are calculated using PRODAS and then applied in the 6-DOF model. See Figure 38 for layout of projectile, and Table 14 for physical characteristics and main dimensions of the test projectile.

Table 15 specifies the aerodynamic characteristics of the test projectile computed using PRODAS V3 software.

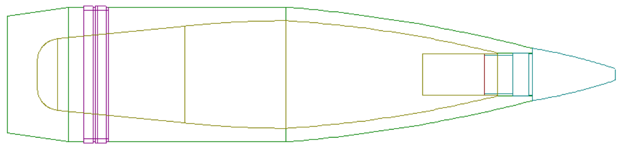

Figure 38: Contour sketch of the 155 mm M107 series projectile

Table 14: Physical characteristics of the 155 mm M107 series projectile

Projectile diameter	d	155.0000	mm
Fuze projectile mass	m	43.09620	kg
Center of gravity from nose	Xcg	458.3700	mm
Axial moment of inertia	Ix	0.142480	Kgm^2
Transverse moment of inertia	Iy	1.225615	Kgm^2

Table 15: Aerodynamic characteristics of the 155 mm M107 projectile (STANAG 4355, 2009).

Mach	Cd_0	Cd_{a2}	CL_a	CL_{a3}	C_{ypa}	C_{ma}	C_{mq}	Cl_p	Cl_d
0.4	0.1419	1.78	1.890	0	-0.71	3.336	-8.7	-0.02800	0
0.6	0.1431	1.79	1.901	0	-0.71	3.365	-8.5	-0.02788	0
0.7	0.1439	1.96	1.909	0	-0.72	3.388	-8.4	-0.02776	0
0.8	0.1487	2.18	1.933	0	-0.74	3.493	-8.4	-0.02754	0
0.9	0.1756	2.57	2.033	0	-0.79	3.737	-9.3	-0.02712	0
1.0	0.3239	3.27	2.328	0	-0.83	3.618	-11.4	-0.02643	0
1.2	0.3816	4.69	2.476	0	-0.65	3.403	-12.6	-0.02511	0
1.5	0.3466	3.72	2.621	0	-0.56	3.268	-13.0	-0.02370	0
2.0	0.2976	2.74	2.812	0	-0.51	3.058	-12.4	-0.02213	0
2.5	0.2607	2.18	2.865	0	-0.50	2.928	-11.7	-0.02028	0
3.0	0.2329	1.73	2.821	0	-0.50	2.874	-10.5	-0.01905	0

The verification was performed for initial velocities of 580 m/s and 950 m/s and quadrant elevation at 20°, 45°and 60° with both programs using standard meteorological conditions and the same projectile parameters. High and low initial velocity and varied quadrant elevation have been chosen to reflect a wide range of flight conditions.

Table 17 shows the test cases for the 155 mm M107 artillery projectile.

Table 16: Test case conditions

	155 mm 107 artillery projectile
Muzzle Velocity	• 580 m/s • 950 m/s
Quadrant Elevation	• 20 degrees • 45 degrees • 60 degrees
Spin Rate at muzzle	• 1176 rad/sec when MV equal 580 m/s • 1926 rad/sec when MV equal 950 m/s
meteorological conditions	• standard meteorological conditions, with no wind

Results and Discussion

Table 17 shows the comparison of the trajectory results from the 6-DOF model and the PRODAS V3 program. The trajectory results using a 6-DOF model and PRODAS V3 program are calculated using the muzzle velocity of 580 m/s and 950 m/s and the quadrant elevation at 20°, 45°, and 60°. The trajectory results for (time of flight, range, maximum height, drift to the right, terminal velocity, and terminal angle of attack), the relative $\delta_{\mathbf{r}}$ is compared.

Table 17: Comparison of Trajectory Results from 6-DOF and PRODAS

				Trajectory					
S/N	**Program**	**Muzzle Velocity [m/s]**	**Elevation Angle [deg]**	**Time of Flight [s]**	**Range [m]**	**Max Height [m]**	**Drift to the Right Negative [m]**	**Terminal Velocity [m/s]**	**Terminal Angle of Attack [m/s]**
1	**6-DOF**	580 m/s	20°	31.7	10878.0	1300.5	-132.5	298.1	-30.2
	PRODAS		20°	31.6	10837.0	1293.0	-134.3	297.8	-30.0
2	**6-DOF**	580 m/s	45°	60.8	14905.3	4675.5	-500.6	321.8	-56.3
	PRODAS		45°	60.5	14851.4	4654.2	-517.7	320.3	-56.1
3	**6-DOF**	580 m/s	60°	74.5	13107.5	6891.6	-810.7	333.3	-68.1
	PRODAS		60°	74.3	13056.4	6863.6	-827.5	331.0	-68.1
4	**6-DOF**	950 m/s	20°	45.7	19189.0	2700.7	-323.8	316.5	-40.1
	PRODAS		20°	45.4	19098.8	2680.0	-326.6	315.6	-39.8
5	**6-DOF**	950 m/s	45°	87.2	25770.3	9356.1	-1182.0	338.5	-65.8
	PRODAS		45°	86.7	25641.6	9296.8	-1185.7	335.9	-65.6
6	**6-DOF**	950 m/s	60°	108.7	24219.6	14010.0	-1834.0	352.8	-73.8
	PRODAS		60°	108.3	24106.0	13914.0	-1822.0	349.3	-73.7

Table 18 shows the relative differences observed between the present 6-DOF model and PRODAS results. For each test case and for each trajectory parameter listed in Table 18 (time of flight, range, maximum height, drift to the right, terminal velocity, and terminal angle of attack), the relative difference $\delta_{\mathbf{r}}$ is computed as follows:

$$\delta_{\mathbf{r}} = \frac{6 - \text{DOF results} - \text{PRODAS results}}{6 - \text{DOF results}}$$

Table 18: Relative Differences at the end point (expressed as a percentage)

S/N	Muzzle Velocity [m/s]	Elevation Angle [deg]	Trajectory Time of Flight [s]	Range [m]	Height [m]	Drift to the Right Negative [m]	Terminal Velocity [m/s]	Terminal Angle of Attack [m/s]
1	580 m/s	20°	0.32%	0.38%	0.58%	1.36%	0.10%	0.66%
2	580 m/s	45°	0.44%	0.36%	0.46%	2.70%	0.31%	0.35%
3	580 m/s	60°	0.25%	0.39%	0.40%	2.10%	0.70%	0.03%
4	950 m/s	20°	0.68%	0.47%	0.76%	0.86%	0.28%	0.75%
5	950 m/s	45°	0.60%	0.49%	0.63%	0.31%	0.77%	0.30%
6	950 m/s	60°	0.37%	0.47%	0.68%	0.65%	0.99%	0.14%

The differences obtained by the comparison in Table 18 for 155 mm M107 projectile shows that:

- Difference in range between +0.36% to +0.49%.
- Difference in time of flight between +0.25% to +0.68%.
- Difference in height between +0.4% to +0.68%.
- Difference in drift between - 0.31% to -2.7%.
- Difference in terminal velocity between +0.1% to +0.99%.
- Difference in angle of attack between +0.03% to +0.75%.

A comparison between the 6-DOF model and the PRODAS V3 program for the 155 mm M107 projectile can be seen in Figure 39 and Figure 40. For cases 4 to 6 in Table 17, the trajectory, drift, velocity, and drag profiles of 155 mm M107 projectile with muzzle velocity of 950 m/s, at 20°, 45°, and 60°, respectively, are shown in Figure 39.

For the cases 1 to 3 in Table 17, the trajectory, drift, velocity, and drag profiles of 155 mm M107 projectile with muzzle velocity of 580 m/s, at 20°, 45°, and 60°, respectively, are shown in Figure 40.

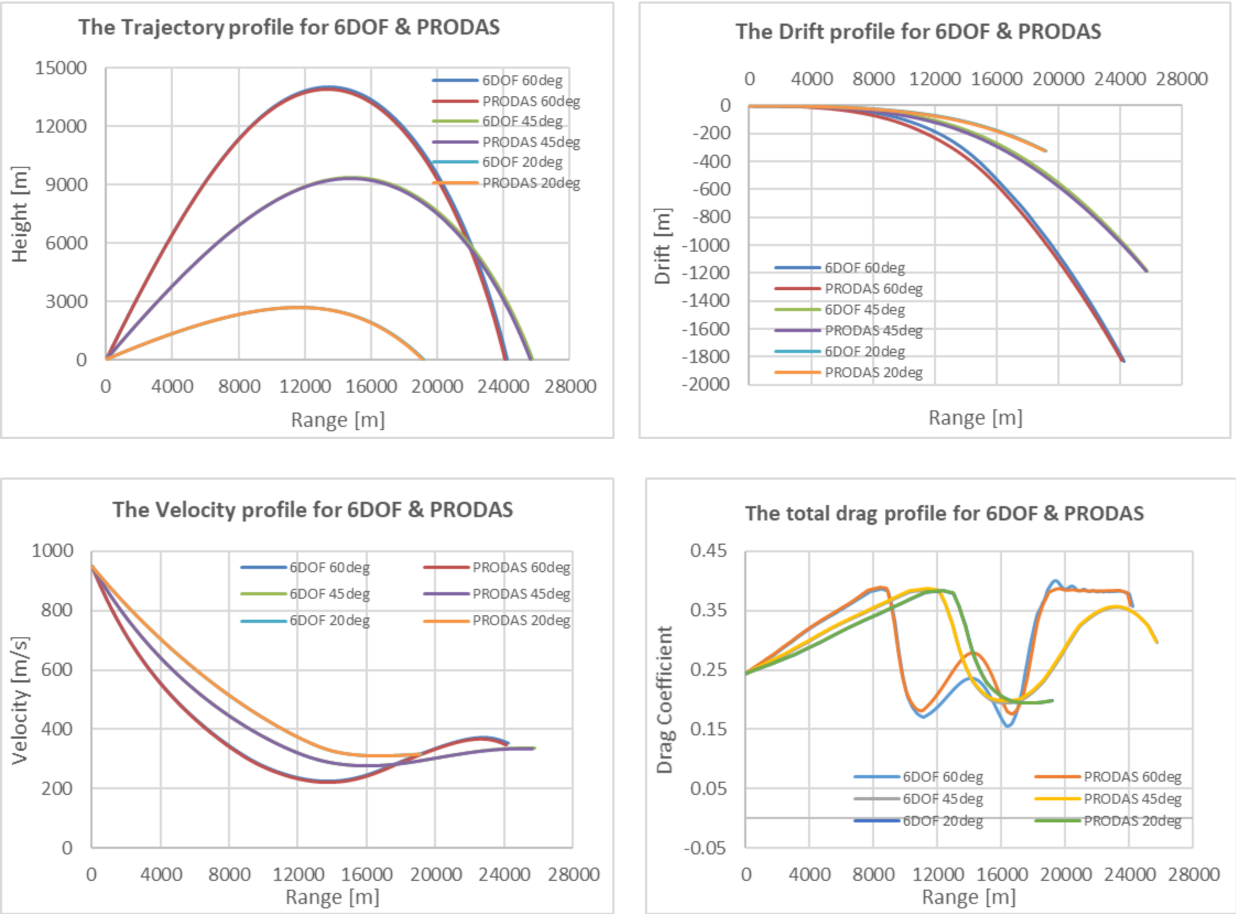

Figure 39: **Comparison of Output Results with muzzle velocity of 950 m/s, at 20°, 45°, and 60°, respectively, between 6-DOF model and PRODAS V3 program**

From the results of the present 6-DOF model and PRODAS V3 program as illustrated in Figure 39, the following is noted: The 155 mm M107 projectile, fired at 20° with muzzle velocity of 950 m/s, gives a range to impact at 19,189 m with a maximum height at almost 2,700 m. At 45°, the predicted range is 25,770 m and the height is 9,356 m, and at 60° gives 24,219.6 m and 14,010 m respectively. For the same set up, the PRODAS program results has slightly shorter range to impact points as shown in Table 17 and illustrated in Figure 39.

Moreover, the drift profile in Figure 39 shows that the drift of the 155 mm M107 projectile, fired with muzzle velocity of 950 m/s and at 20°, 45°, and 60°, always gives negative values (right) drift at about -323.8 m, -1182 m, -1834 m, respectively.

Furthermore, the velocity profile in Figure 39 shows that at elevation angle of 20°, the velocity decreases due to drag and gravity until it reaches the apex to the value of almost 310 m/s. Then, as the projectile accelerates after passing the apex, the velocity increases due to the dominance of gravity over the drag to the value of 316 m/s. At 45°, the velocity decreases to the value of almost 279 m/s and then increases to the value of 338.5 m/s. Moreover, at 60° the velocity decreases to value of 224 m/s and then increases to the value of 353 m/s.

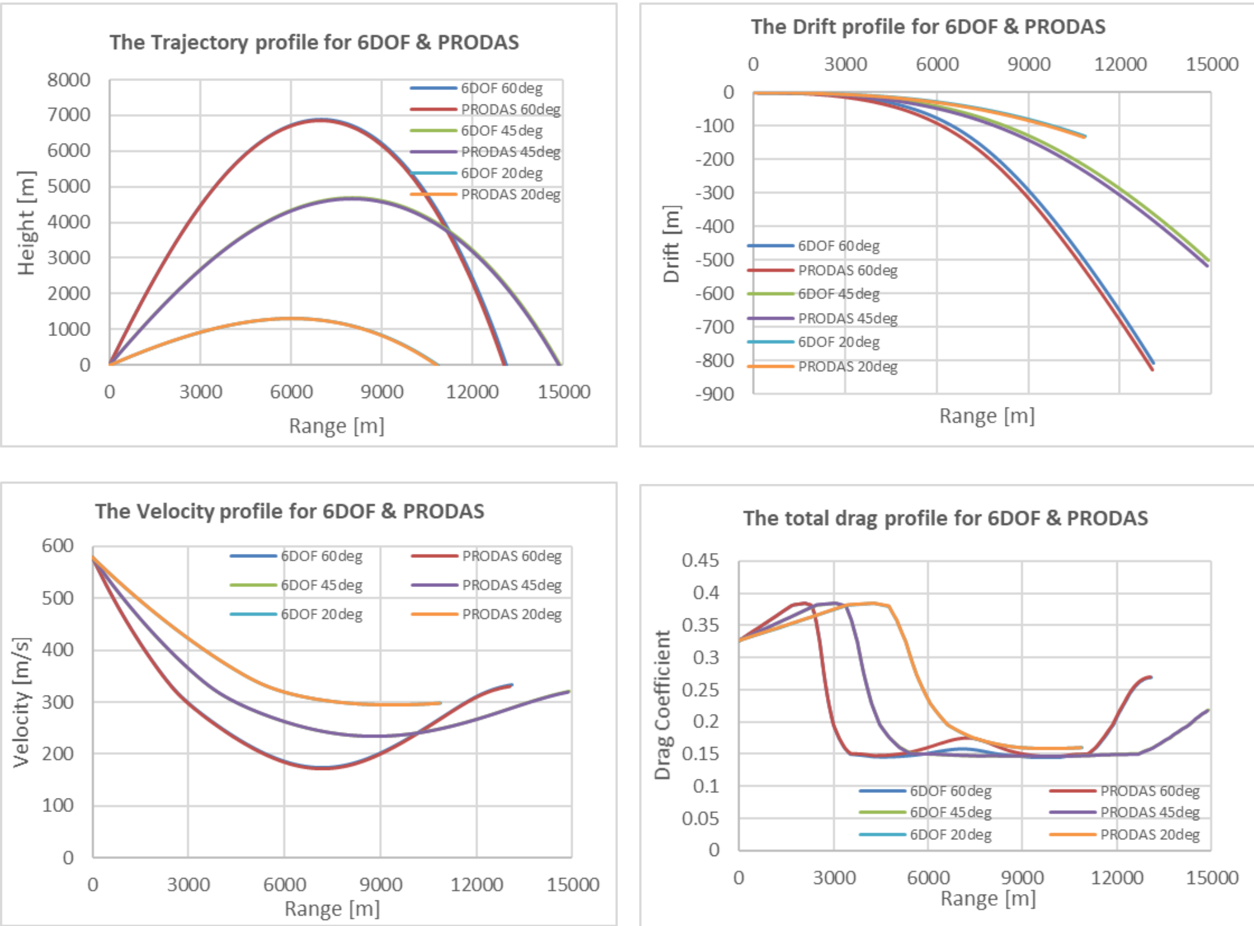

Figure 40: Comparison of Output Results with muzzle velocity of 580 m/s, at 20°, 45°, and 60°, respectively, between 6-DOF model and PRODAS V3 program

Figure 40 shows the comparison of results of the present 6-DOF model and PRODAS V3 program. For program the 155 mm M107 projectile fired at 20° with muzzle velocity of 580 m/s. This gives a range to impact at 10,878 m with a maximum height at almost 1300.5 m. At 45°, the predicted range is 14,905.3 m and the height is 4,675.5 m, and at 60° gives 13107.5 m and 6891.6 m respectively. In the same set up, the PRODAS program results has slightly shorter range to impact points as shown in Table 17 and illustrated in Figure 40.

Moreover, the drift profile in Figure 40 shows that the drift of the 155 mm M107 projectile, fired with muzzle velocity of 580 m/s and at 20°, 45°, and 60°, always gives negative values (right) drift at about -132.5 m, -500.6 m, -810 m, respectively, while the PRODAS program results has slightly higher drift to impact points as shown in Table 17. Furthermore, the velocity profile in Figure 40 shows that at elevation angle of 20°, the velocity decreases due to drag and gravity until it reaches the apex to the value of almost 294.6 m/s. Then, as the projectile accelerates after passing the apex, the velocity increases due to the dominance of gravity over the drag to the value of 298.1 m/s. At 45°, the velocity decreases to the value of 235.3 m/s and then increases to the value of 321.8 m/s. Moreover, at 60° the velocity decreases to value of 173 m/s and then increases to the value of 333.3 m/s.

4.4.1 Conclusion of 6-DOF model & PRODAS V3 program verification

The verification in 4.4.1 showed that the relative difference in range is significantly smaller when compared to the relative difference in drift. The relative differences between the results from the two programs are relatively small except probably for drift. The reason for the larger relative difference in drift can be attributed to the different approaches to implement the non-linear Magnus effects. However, in the battlefield the actual range differences (even in excess of 100 m) are much larger than the actual drift differences (at most 17 m). In practice, this is much less important than the range difference.

4.5 Conclusion of the 6-DOF model verification

This chapter showed the verification results obtained with the present 6-DOF trajectory simulation model by comparing it with results from other simulation programs as well as the results that are predicted by analytical solutions.

The first case showed comparison of the 6-DOF model results with the analytical solutions and other simulation models. The results of these cases verified that the present 6-DOF model has been coded correctly as they match very well in the portion of the trajectory where the analytical solutions are accurate enough. The results also show the correctness of the implementation of integration scheme, gravity, earth rotation, which gives rise to Coriolis effects, and the correctness of implementation of major symmetric and asymmetric aerodynamic and inertia models. Moreover, they verified that the model produces reliable trajectories for symmetric and asymmetric case.

The second set of studies showed comparison of the 6-DOF model results with WinFast program results. The results of these cases illustrate that the 6-DOF model and WinFast program produce comparable results when starting with the same initial parameters. It also demonstrates the validity of the functions used in MATLAB to predict features like the natural pitch frequency and phenomena such as spin-up, and spin through resonance for a typical fin stabilised projectile. Moreover, it demonstrates the validity of the function used in the present

6-DOF model to accommodate the combination of asymmetries effects when the asymmetric projectile tends to lock-in.

The last set of studies showed the 6-DOF model results compared to results generated by PRODAS V3 (Arrow Tech Associates). The results of these cases verified that the complicated six degrees of freedom (6-DOF) trajectory simulation model can be applied for the accurate prediction of short and long-range trajectories of high and low spin and fin-stabilised symmetric and asymmetric projectiles. Therefore, this study verifies the correctness of simulation in general, and provide confidence to proceed with case studies in chapter 5.

CHAPTER 5: CASE STUDY – MORTAR TRAJECTORIES

5.1 Introduction

The verification phase has now been discussed and it showed that the 6-DOF model is capable to accurately predict trajectories for symmetric and asymmetric projectiles. This chapter is divided into two sections. The first section provides a systematic study of the drag experienced by a mortar with asymmetries. The systematic study shows how unexpected flight behaviour may lead to a degradation in impact dispersion, and can be linked to small asymmetries.

The second section provides a diagnostic evaluation of real test data captured for mortar projectiles with asymmetries.

5.2 A Systematic Study of the Drag Experienced by a Mortar with Asymmetries

Mortar bombs are called fin-stabilised projectiles due to the existence of fins that provide stability during flight. Ideally, the spin rate of the mortar remains very constant during its flight. When mortars have mass and aerodynamic asymmetries, it will have a great impact on the angular motion. Flight test experience has indicated that mortars can exhibit unexpected flight behaviour leading to a degradation in impact dispersion. The systematic study shows how this behaviour can be linked to small asymmetries for a mortar spinning up to resonance, which is when the spin rate matches the natural pitch frequency of the mortar. For persistent roll resonance, also called "Lock-In", serious flight performance degradation can result in impact dispersions or catastrophic flight failure. In this systematic study, the focus is placed on aerodynamic and mass asymmetries. The study has shown that a combination of relatively small asymmetries can have a significant effect. These asymmetries can result from manufacturing tolerances or minor damage incurred during inter alia, storage, transport, and misuse.

The study focuses on two asymmetries, namely a radial offset in the center of gravity, and aerodynamic asymmetry. It also provides the expected drag profiles for a systematic combination of mortar asymmetries. This is obtained using a six-degree-of-freedom (6-DOF) trajectory simulation. The results presented in this section can be used by design development teams to link "abnormal drag profiles" as captured during dynamic firings with possible causes for the failure. It also provides guidelines regarding the allowable tolerances for mortar asymmetries.

5.2.1 Six-degree-of-freedom (6-DOF) trajectory simulation model

As previously stated in section 3.6.3, the 6-DOF trajectory model is developed by the author which include various types of asymmetry. These asymmetries can be illustrated as (Glover, Hagan, 1971):

- Skew (banana shaped) bomb.
- Radial off-set of the Centre of Gravity [CoG] from the axial axis.

Skew (banana shaped) bomb

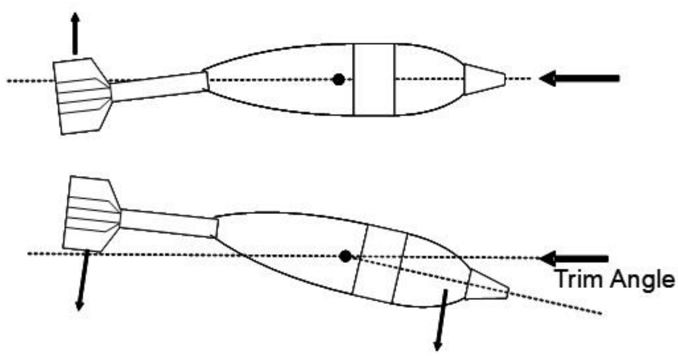

Figure 41: Illustration of a net force on a skew (banana shaped) bomb.

When the nose of a skew bomb is aligned with the flight path as shown in Figure 41, there will be "unbalanced moments" and being stable it will rotate until the moments around the CoG cancels out. At that point however, the bomb would experience a net force perpendicular to the flight path, meaning that it would deviate from its path. To simulate skewness, it is necessary to introduce a moment denoted by [Cm0] and normal force denoted by [Cn0] at zero yaw (Glover, Hagan, 1971) as shown in Figure 42.

- Normal Force at Zero Angle of Attack: Cn0 at various Angles [B1].
- Yaw Moment at Zero Angle of Attack: Cm0 at various Angles [B2].

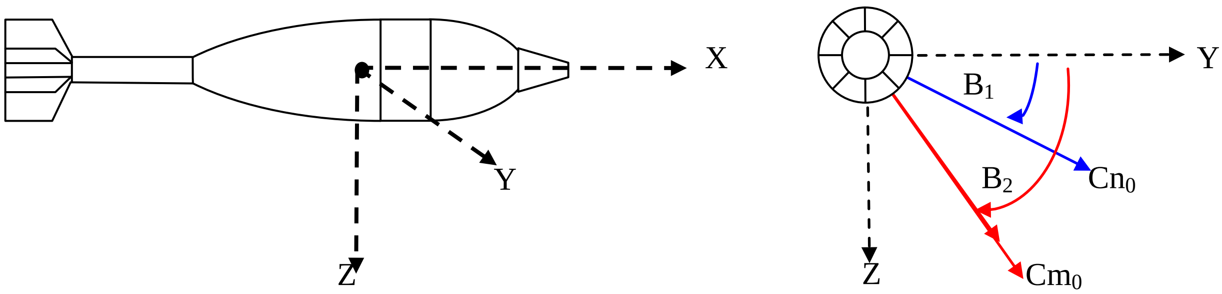

Figure 42: Definition of asymmetries used in the 6-DOF simulation

Radial off-set of the Centre of Gravity [CoG] from the axial axis

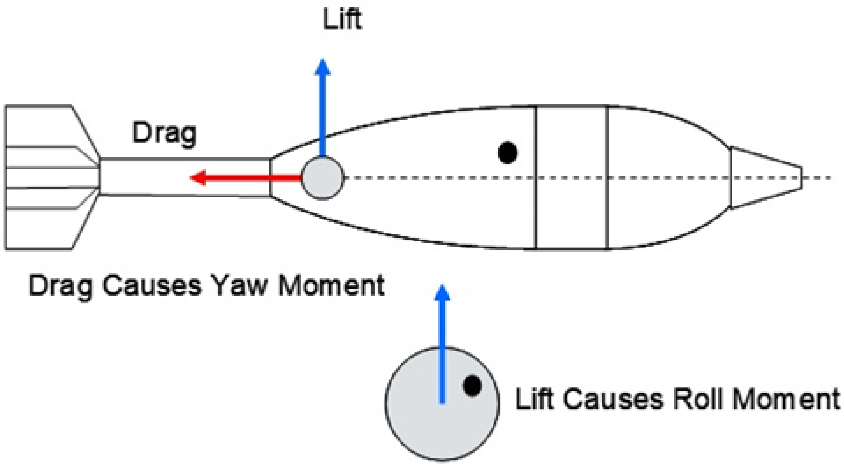

Figure 43: Illustration of a radial off-set of the centre of gravity

To simulate the effect of a radial off-set in the CoG the force and moment equations in the simulation program should account for the effects as illustrated in Figure 43. One of the interesting consequences of these asymmetries is that not only does it affect the yaw motion, but it also affects the spin of the bomb. This phenomena was studied extensively in statically stable re-entry vehicles (Glover, Hagan, 1971).

5.2.2 Methodology

This study focuses on two asymmetries, namely the radial offset in the centre of gravity, and aerodynamic asymmetry. The systematic study shows how these small asymmetries for a mortar can be linked to resonance. In addition, it provides the expected drag profile for a combination of various asymmetries, which exist in mortar projectiles. This is obtained using a six-degree-of-freedom (6-DOF) trajectory simulation-model developed by the author.

The simulations were done for a generic 81 mm mortar bomb. All aerodynamic forces, moments coefficients and mass properties of the given mortar bomb are calculated using the PRODAS simulation program.

5.2.3 Aerodynamic model

The nominal aerodynamic properties for the generic 81 mm bomb shown in Figure 44 was predicted, using the PRODAS.

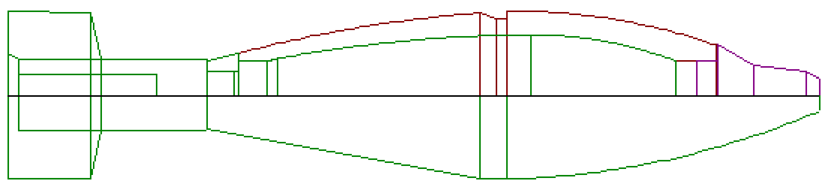

Figure 44: Model used in PRODAS program prediction

The mass properties and firing conditions of a generic 81 mm mortar bomb used in this study are summarised below in Table 19.

Table 19: Generic model and launch conditions as predicted, using the PRODAS program

Mass	4.4 kg
Axial Moment of Inertia	0.0034 kgm^2
Transverse Moment of Inertia	0.0267 kgm^2
Projectile Length	417.5 mm
Muzzle Velocity	280 m/s
Atmospheric Conditions	Standard ICAO MET Conditions
Altitude	Standard Sea Level
Launch angle	45 deg

5.2.3.1 Aerodynamic Coefficients

Knowing the aforementioned configuration, the aerodynamic coefficients for a generic 81 mm mortar bomb were predicted using PRODAS. The results of these predictions are shown in Table 20.

Table 20: Generic aerodynamic model for 81 mm mortar bomb

Mach	Cd0	Cda2	CLa	CLa3	Cma	Cmq	Clp
0.100	0.150	3.125	1.750	-1.300	-1.800	-50.000	-0.250
0.500	0.150	3.125	1.750	-1.300	-1.800	-50.000	-0.250
0.800	0.150	3.125	1.750	-1.300	-1.800	-50.000	-0.250
0.900	0.168	3.367	1.750	-2.300	-2.400	-54.200	-0.250
1.000	0.176	3.450	2.050	-2.300	-2.500	-56.100	-0.250

5.2.3.2 Case studies

The systematic study presented in this section will cover two different cases, being the following:

5.2.3.2.1 First case study

It has been shown that a combination of asymmetries can induce the spin rate which can approach the natural pitch frequency of the mortar bomb. This in return gives excessive yaw accompanied by an increase in aerodynamic drag. Therefore, simulations were done with small asymmetries and various roll moments as illustrated in Table 21. This case illustrates the effect of spinning through resonance, with asymmetries with various roll moments.

Table 21: Simulations with small asymmetries and various roll moments

Conditions	Cn0	B1 [deg]	Cm0	B2 [deg]	Ycg [mm]	Zcg [mm]	Cl (Roll Moment)
1	0.02	0	0.02	90	0	0.002	0.0000
2	0.02	0	0.02	90	0	0.002	0.0005
3	0.02	0	0.02	90	0	0.002	0.0015
4	0.02	0	0.02	90	0	0.002	0.0045
5	0.02	0	0.02	90	0	0.002	0.0050

5.2.3.2.2 Second case study

In this case, simulations are used for small asymmetries with various relative orientation. As discussed in case 1, it showed that one of the spin rates used in the simulations experienced a “Lock-in”, which was determined to be at CL= 0.0045 rad/s as shown in Table 21. The “lock-in” case is then tested against different radial positions of CoG offset as illustrated in Figure 45 and shown in Table 22. This case illustrates the effect of the relative orientation of asymmetries.

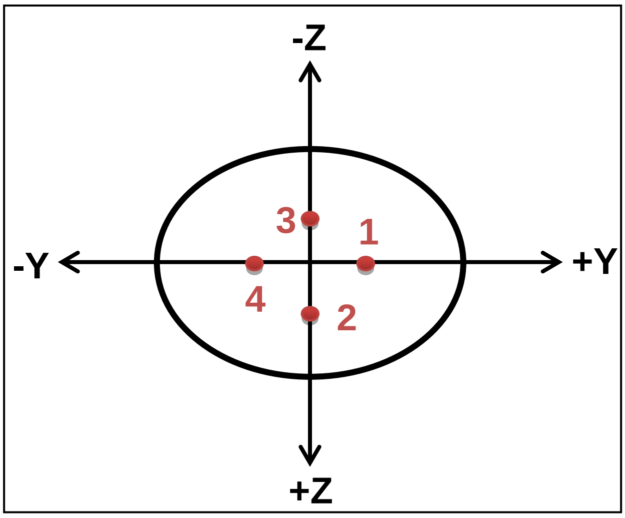

Figure 45: **The rear view of the mortar bomb to Illustrate various relative orientations of the position of radial CoG off-set.**

Table 22: **Simulations with small asymmetries and various relative orientation**

Conditions	Cn0	B1 [deg]	Cm0	B2 [deg]	Ycg [mm]	Zcg [mm]	Cl (Roll Moment)
1	0.02	0	0.02	90	0.000	0.002	0.0045 (The case of lock-in)
2	0.02	0	0.02	90	0.002	0.000	0.0045 (The case of lock-in)
3	0.02	0	0.02	90	0.000	-0.002	0.0045 (The case of lock-in)
4	0.02	0	0.02	90	-0.002	0.000	0.0045 (The case of lock-in)

5.2.4 Result and discussion

5.2.4.1 Case 1:

It has been shown that a combination of asymmetries can induce spin and whenever the spin rate approaches the natural pitch frequency of the mortar bomb, excessive yaw accompanied by an increase in drag is expected. Simulations were done with small asymmetries and various roll moments. In Figure 46 below, various spin rate profiles with the natural pitch frequency (denoted by WNB, which is considered in the body frame) are depicted.

It shows that a combination of asymmetries with spin rate equal to CL= 0.0045 rad/s forces the mortar to spin-up to resonance (i.e. spin frequency = natural yaw frequency). After passing through resonance, the spin rate starts to follow the natural yaw frequency and therefore remain in a state of resonance as shown in Figure 46. This resulted in developing high angles of incidence accompanied by severe lateral accelerations. The extent to which the dynamic behaviour is influenced during this period of resonance depends on the combination of asymmetries and the dynamic pressure at the onset of the resonance. This phenomenon is witnessed in the associated drag profile which shows a very high increase in drag as shown in Figure 47, Consequently, leading to (6%) shorter range as shown in Figure 48.

Then the spin rate is equal to CL=0.0050 rad/s, it shows that it forces the mortar to spin-up to resonance and then passes through resonance. The passing through resonance is revealed by the drag peak visible between T=1 and T=4 seconds as shown in Figure 47, Consequently, leading to (3%) shorter range as shown in Figure 48. Lastly, the other spin rate values forced the mortar to induce spin that is insufficient to reach resonance.

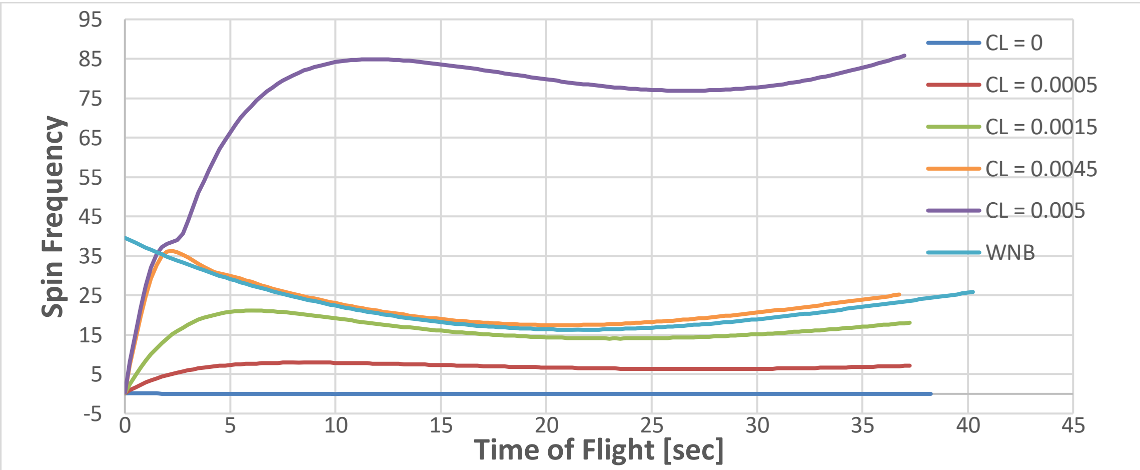

Figure 46: **Spin rate and natural yaw frequency with different conditions**

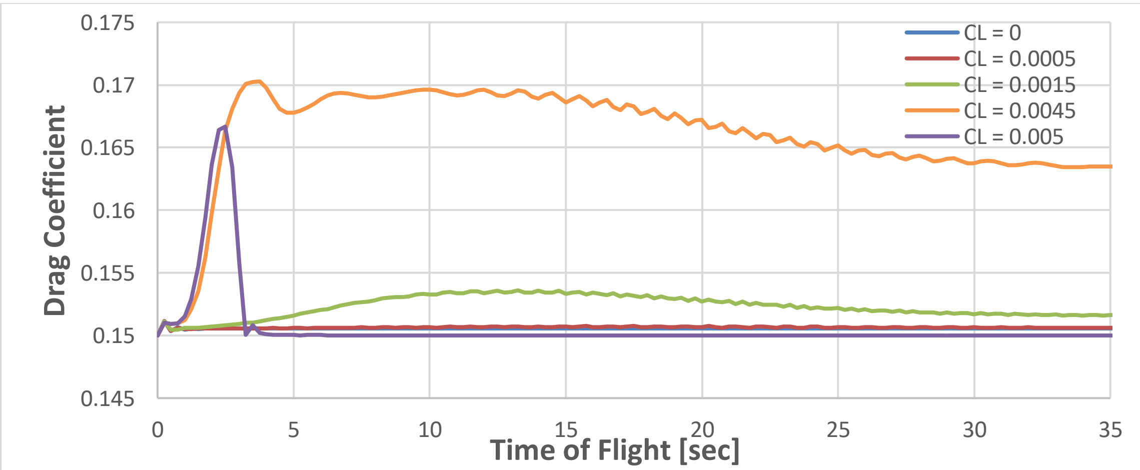

Figure 47: **Drag associated with various spin profiles**

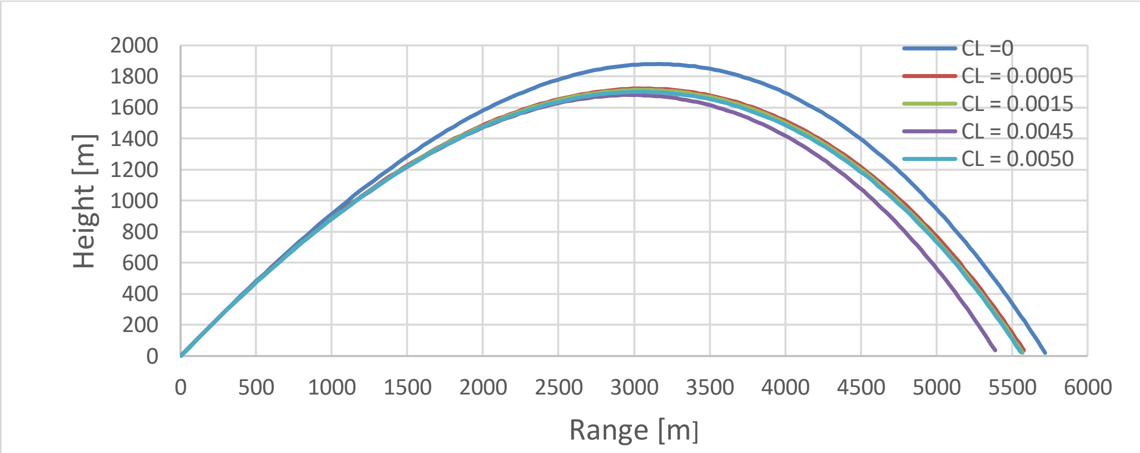

Figure 48: Range associated with various spin profiles

5.2.4.2 Case 2:

In this case, simulations are performed for small asymmetries with various relative orientation. As discussed in case 1, it showed that one of the spin rates used in the simulations experienced a "Lock-in", which was determined to be at CL= 0.0045 rad/s as shown in Table 21. The "lock-in" case is then tested against different radial positions of CoG offset as illustrated in Figure 45 and shown in Table 22. This case illustrates the effect of the relative orientation of asymmetries. When the radial position of CoG was set to a distance of 0.002 m in all the mentioned positions illustrated in Figure 45, the condition at the position of Zcg = 0.002 m and Ycg = 0 m showed that the spin rate got locked-in and therefore remained in a state of resonance as mentioned in case 1. On the other hand, other conditions showed that the spin rate accelerated through resonance fast enough to avoid being captured. This enabled reaching the steady state of spin with only a slight stimulus to its pitching motion, which is caused by passing through resonance as illustrated in Figure 49. This phenomena is witnessed in the associated drag profile which showed the drag peak visible at between T=1 and T=4 sec as shown in Figure 50, leading to a (3%) longer range compared to the lock-in conditions as shown in Figure 51.

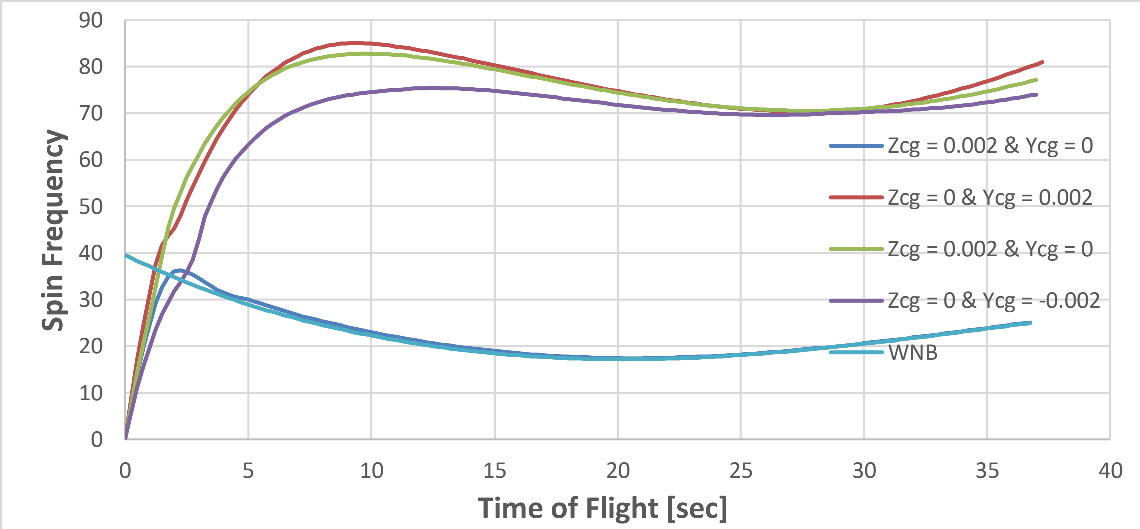

Figure 49: **Spin rate and natural yaw frequency with different conditions at first 15 [sec]**

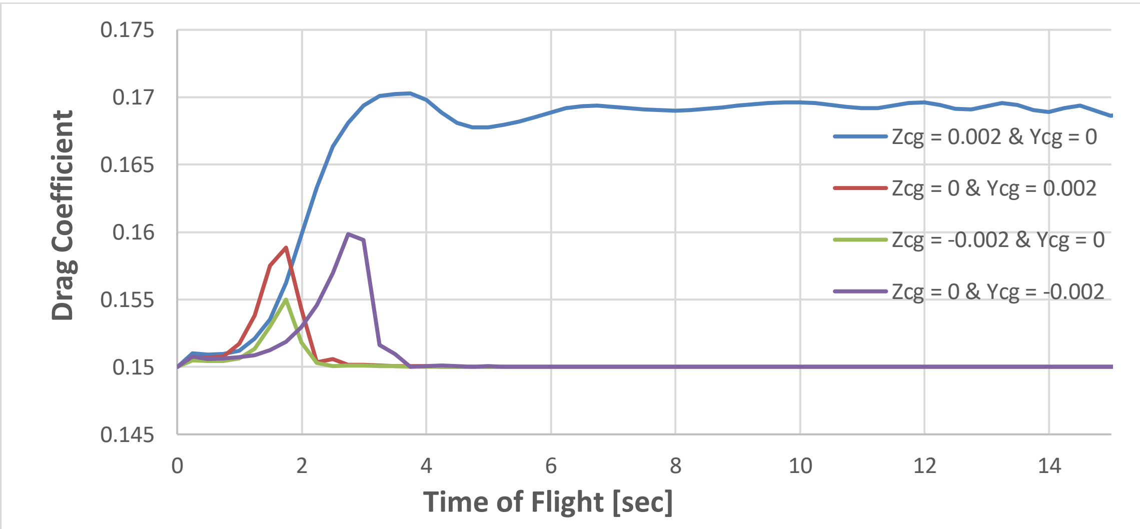

Figure 50: **Drag associated with various spin profiles at first 15 [sec]**

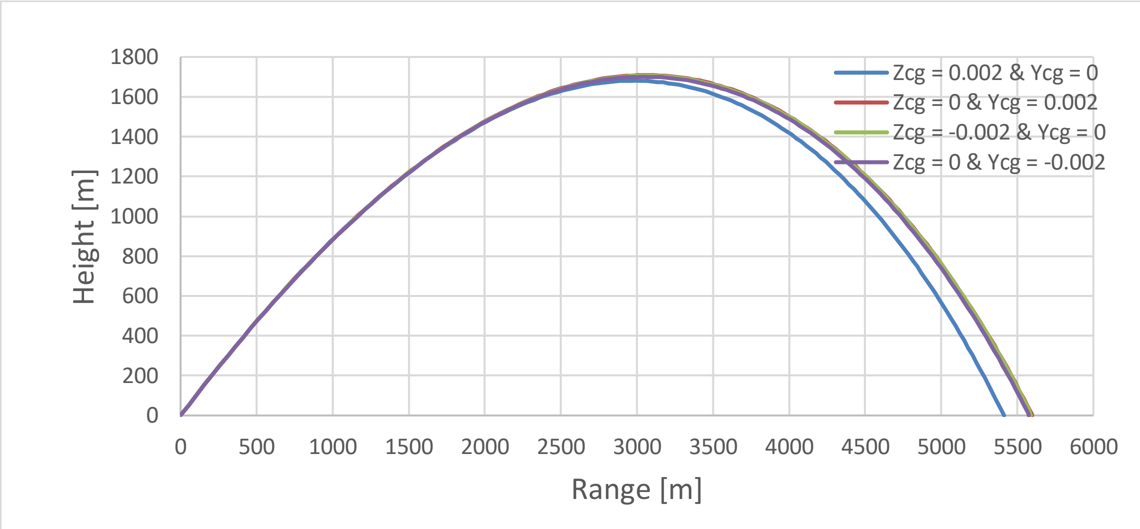

Figure 51: Range associated with various spin profiles

5.2.5 Conclusion of the systematic study

A generic 81 mm mortar bomb has been used in this systematic study. The study done in this section focused on aerodynamic and mass asymmetries. It has shown that a combination of relatively small asymmetries in mortar bombs can lead to unexpected flight performance and therefore a degradation in impact dispersion is likely occurring. In addition, the systematic study was based on two cases, one with small asymmetries and various roll moments, and the other with small asymmetries and variable positions of radial CoG offset. The section provided the expected drag profiles for both cases of combined asymmetries in mortar bombs by means of simulations.

As a result, relatively small asymmetries and especially skew-ness or the so-called banana shape can cause a significant variation in the lateral dispersion of a mortar bomb leading to unacceptable performance. On the other hand, larger inertia asymmetries (radial off-set in CoG) are required to have the same effect as the aerodynamic asymmetries. A combination of asymmetries can lead to the so-called "lock-in" where the bomb remains at a state of resonance and high drag leading to short-distance fallers.

A different relative position of the same asymmetries can lead to spin through resonance, so as to avoid the detrimental effects associated with "lock-in".

5.3 Apply 6-DOF model to reconstruct actual flight test data

In this section, the 6-DOF model program will be used to conduct cases studies to find possible causes for the flight behaviour of real test results captured during the dynamic firing of mortar bombs. This procedure, with reliable experimental results can greatly enhance the confidence of using the 6-DOF model. It also provided difficult trajectory simulation problems because it required predictions in abnormal conditions (asymmetric cases), where small asymmetries can greatly affect the overall trajectory. As previously stated in section 1.2, small asymmetries can cause unexpected flight behaviour which can lead to a degradation in impact dispersion. The correlation between the test data and predicted performance will be used to obtain insight in the accuracy of this simulation program, and conclude with comments on the adequacy of models to analyse stability and asymmetries captured.

5.3.1 Aerodynamic model

Apply the 6-DOF model to 81 mm mortar bombs, which are used in real fire tests. The aerodynamic forces, moments and mass properties of these bombs are used in the simulations.

The mass properties and firing conditions of the studied 81 mm mortar bomb are summarised below in Table 23.

Table 23: Generic model and launch conditions of the 81 mm mortar bomb

Mass	4.4 kg
Axial Moment of Inertia	0.0034 kgm^2
Transverse Moment of Inertia	0.0267 kgm^2
Projectile Length	417.5 mm
Atmospheric Conditions	Standard ICAO MET Conditions
Altitude	1070 m above mean sea level

5.3.2 Aerodynamic Coefficients

Knowing the aforementioned configuration, the aerodynamic coefficients for 81 mm mortar bomb are predicted using PRODAS program. The results of these predictions are shown in Table 24.

Table 24: Generic aerodynamic model for 81 mm mortar bomb

Mach	Cd0	Cd_{a2}	CL_a	CL_{a3}	C_{ma}	C_{mq}	Cl_p
0.010	0.157	3.125	1.750	-1.300	-1.800	-55.700	-0.250
0.500	0.178	3.125	1.750	-1.300	-1.800	-56.000	-0.250
0.600	0.168	3.125	1.750	-1.400	-1.800	-56.000	-0.250
0.800	0.173	3.125	1.750	-1.700	-2.100	-57.000	-0.250
0.880	0.244	4.250	1.800	-2.000	-2.200	-57.500	-0.250

5.3.3 Evaluation of 81 mm mortar bomb short fallers

The purpose of the following case study is to obtain insight in the accuracy of this simulation program in general, and to evaluate samples of short faller shots. All the samples are for an 81 mm mortar bomb that exhibited a drag increase as expected from spin through resonance, “lock-in”, or instability.

Figure 52 shows the drag profiles captured by radar in the experimental tests for shots A, B, C, and D that exhibited increase in drag.

Note that the major source of the experimental results was kindly supplied by RDM from tests conducted at Alkantpan test range and trajectory data was captured using a Weibel tracking radar (Weibel,2007).

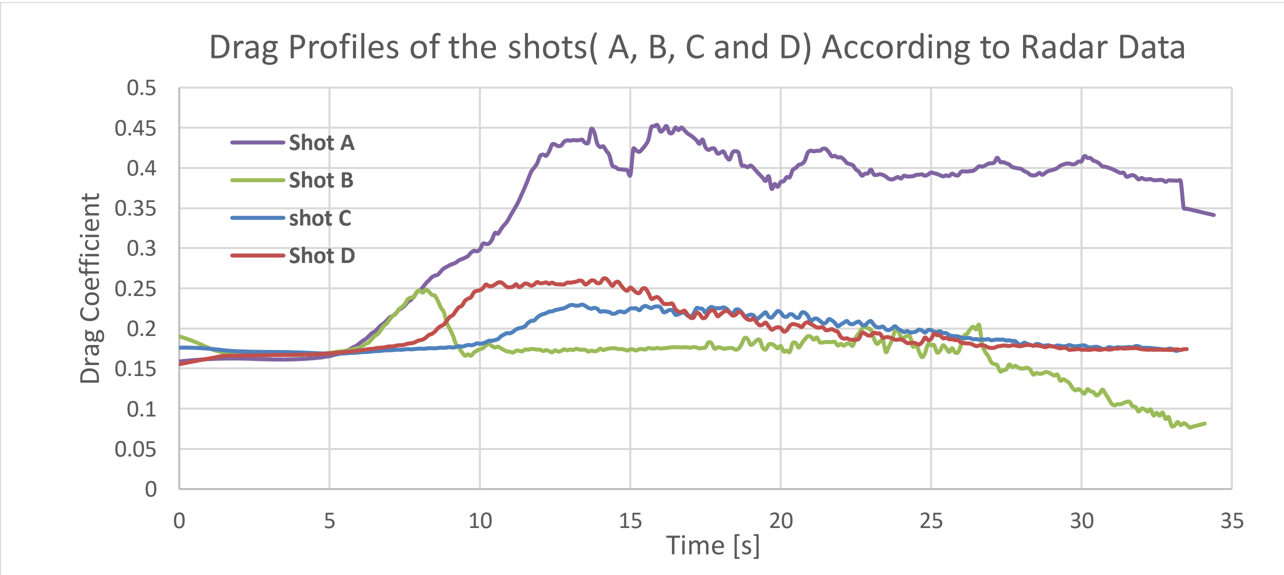

Figure 52: Drag profiles according to radar data for shot A, B, C, and D

5.3.4 Case studies

In this section, the 6-DOF model program will be used to conduct a case study to identify possible causes for the drag increment in real test results captured during the dynamic firing of mortar bombs.

5.3.4.1 Case study 1

In this case study, a computational investigation was completed on an 81 mm mortar bomb using the 6-DOF model to predict the drag profile of the shot A. It has been shown in the systematic studies and specifically in case 1 (condition 4), how a combination of asymmetries can affect angular motion whenever it approaches the natural pitch frequency of the mortar bomb. This in return gives excessive yaw accompanied by an increase in aerodynamic drag. This indicates what happened to Shot A.

Therefore, simulations were done with the mass properties and aerodynamic coefficients previously summarised in Table 23 and Table 24, respectively. Moreover, specific roll moment and small asymmetries were chosen for this case study as illustrated in Table 25. Were the roll moment and small asymmetries changed until a fit to the tracking radar data was found, which therefore gives a good prediction for the drag profile of shot A. Note that the initial velocity of the case 2, 3, and 4 was the average of a test group and the initial pitch and yaw of 5° was selected to allow for typical launch disturbances experienced by mortars.

Table 25: Simulation with initial conditions and aerodynamic asymmetries for case 1

<table>
<tr><th colspan="7">Initial fire conditions</th></tr>
<tr><th>cases</th><th>Mass [Kg]</th><th colspan="2">Initial Velocity [m/s]</th><th colspan="2">Elevation Angle [deg]</th><th>Initial Pitch [deg]</th><th>Initial Yaw [deg]</th></tr>
<tr><td>1</td><td>4.39</td><td colspan="2">276.86</td><td colspan="2">44.79</td><td>5</td><td>5</td></tr>
<tr><th colspan="8">Aerodynamic and mass asymmetries</th></tr>
<tr><th>cases</th><th>B1</th><th>Cm0</th><th>B2</th><th>Ycg [mm]</th><th>Zcg [mm]</th><th colspan="2">Cl (Roll Moment)</th></tr>
<tr><td>1</td><td>0</td><td>0.085</td><td>40</td><td>0</td><td>0.001</td><td colspan="2">0.00018</td></tr>
</table>

Results from this simulation were then compared to real test data for shot A as shown in Figure 53. The drag coefficient comparisons, shown in Figure 53, indicated good agreement with shot A. The 6-DOF model slightly above-predicts the magnitude of the drag coefficient at the first 12 seconds and slightly under-predicts after 12 seconds.

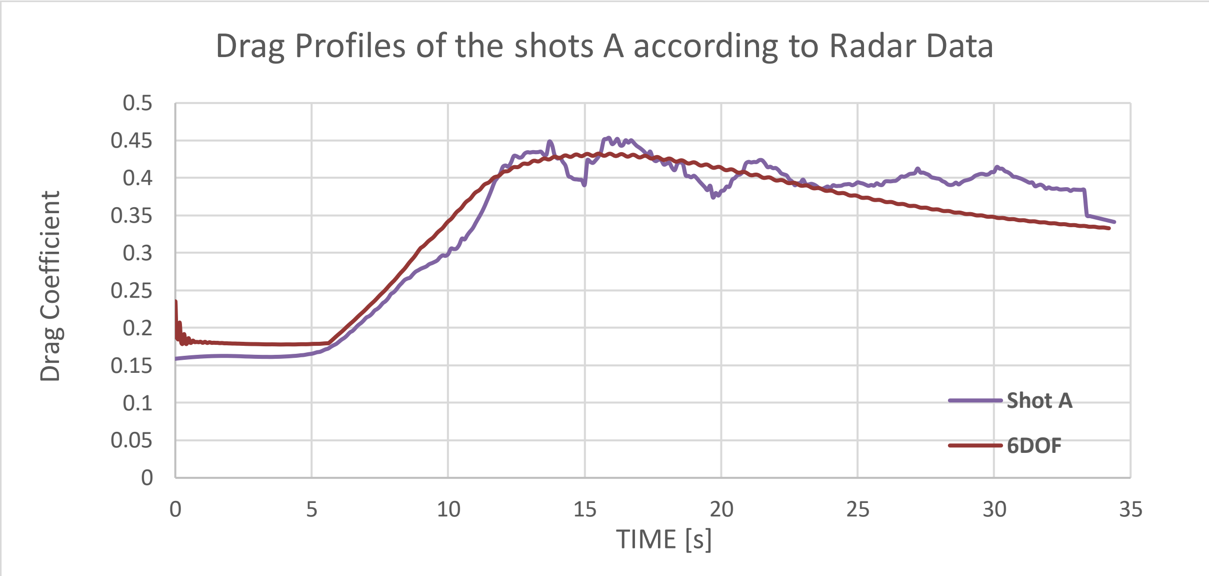

Figure 53 : **Drag coefficient comparisons for Case 1**

5.3.4.2 Case study 2

In this case study, a computational investigation was completed on an 81 mm mortar bomb using the 6-DOF model, to predict the drag profile of shot B. It has been shown in the systematic studies and especially in case 1 (condition 5), how a combination of asymmetries forces the mortar to spin-up to resonance and then pass through it. The passing through resonance is revealed by the drag peak visible between T= 1 and T= 4 seconds as shown in Figure 47. This indicates what happened to Shot B. Therefore, simulations were done with the mass properties and aerodynamic coefficients previously summarised in Table 23 and Table 24, respectively. Moreover, specific roll moment and small asymmetries chosen for this case study are illustrated in Table 26, which therefore gives a good prediction for the drag profile of shot B.

Table 26: **Simulation with initial conditions and aerodynamic asymmetries for case 2**

<table>
<tr><th colspan="7">Initial fire conditions</th></tr>
<tr><th>Case</th><th>Mass [Kg]</th><th colspan="2">Initial Velocity [m/s]</th><th>Elevation Angle [deg]</th><th>Initial Pitch [deg]</th><th>Initial Yaw [deg]</th></tr>
<tr><td>2</td><td>4.365</td><td colspan="2">278.04</td><td>44.625</td><td>5</td><td>5</td></tr>
<tr><th colspan="7">Aerodynamic and mass asymmetries</th></tr>
<tr><th>Case</th><th>B1</th><th>Cm0</th><th>B2</th><th>Ycg [mm]</th><th>Zcg [mm]</th><th>Cl (Roll Moment)</th></tr>
<tr><td>2</td><td>0</td><td>0.05</td><td>179</td><td>0</td><td>0.001</td><td>0.0019</td></tr>
</table>

Results from this simulation was then compared to real test data for shot B as shown in Figure 54. The drag coefficient comparisons, shown in Figure 54, indicate good agreement with shot B.

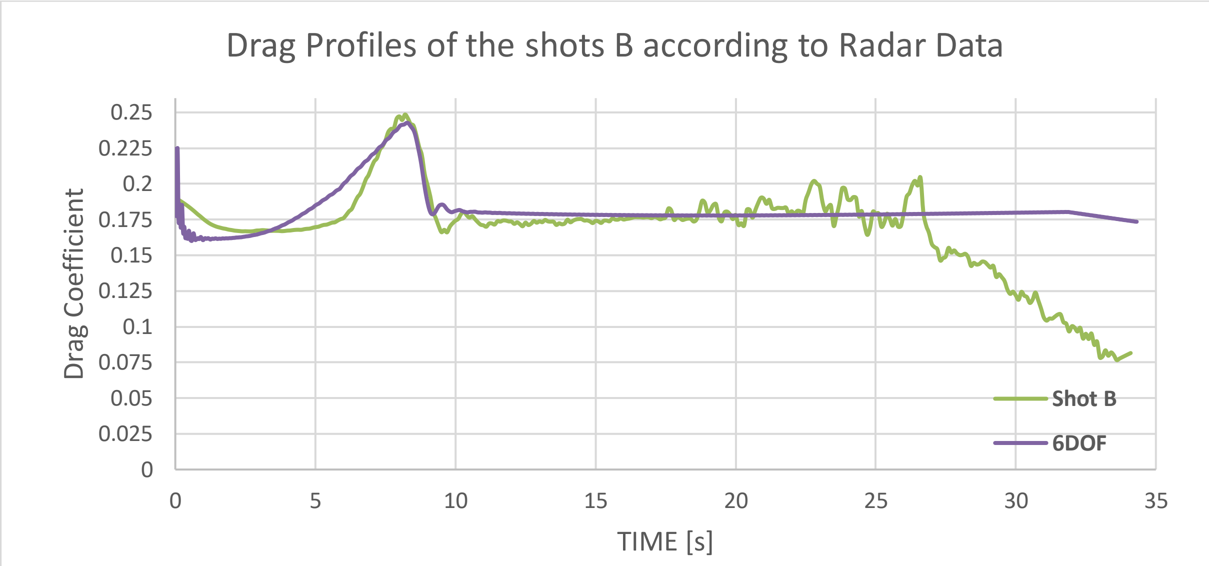

Figure 54: Drag coefficient comparisons for Case 2

5.3.4.3 Case study 3

In this case study, a computational investigation was completed on an 81 mm mortar bomb using the 6-DOF model, to predict the drag profile of shot C. It has been shown in the systematic studies and especially in case 1 (condition 3), how a combination of asymmetries forced the mortar to induce spin that is insufficient to reach resonance. This indicates to what happened to Shot C.

Therefore, simulations were done with the mass properties and aerodynamic coefficients previously summarised in Table 23 and Table 24, respectively. Moreover, specific roll moment and small asymmetries were chosen for this case study as illustrated in Table 27, which therefore gives a good prediction for the drag profile of shot C.

Table 27: Simulation with initial conditions and aerodynamic asymmetries for case 3

Initial fire conditions							
Case	Mass [Kg]	Initial Velocity [m/s]		Elevation Angle [deg]		Initial Pitch [deg]	Initial Yaw [deg]
3	4.365	278.04		44.79		5	5
Aerodynamic and mass asymmetries							
Case	Cn0	B1	Cm0	B2	Ycg [mm]	Zcg [mm]	Cl (Roll Moment)
3	0.01	0	0.0455	20	0	0.0003	0.00098

Results from this simulation was then compared to real test data for shot C as shown in Figure 55. The drag coefficient comparisons, shown in Figure 55, indicate good agreement with shot C.

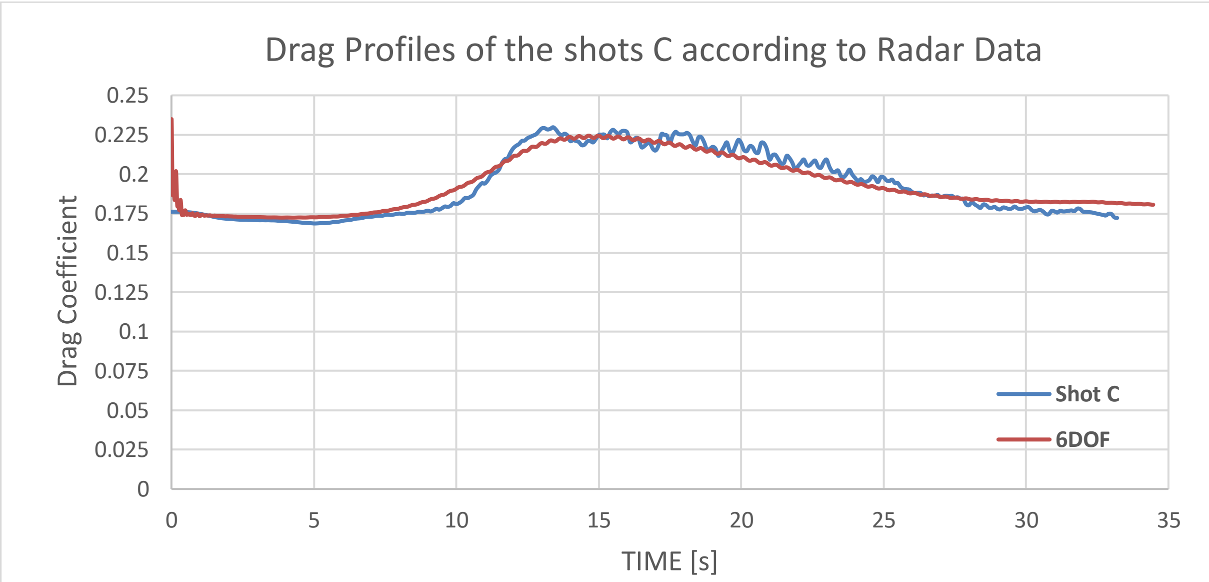

Figure 55: Drag coefficient comparisons for Case 3

5.3.4.4 Case study 4

In this case study, a computational investigation was completed on an 81 mm mortar bomb using the 6-DOF model, to predict the drag profile of shot D. Also, it has been shown in the systematic studies and especially in case 1 (condition 3), how a combination of asymmetries forced the mortar to induce spin that is insufficient to reach resonance. This indicates what happened to Shot D.

Therefore, simulations were done with the mass properties and aerodynamic coefficients previously summarised in Table 23 and Table 24. respectively. Moreover, specific roll moment and small asymmetries were chosen for this case study as illustrated in Table 28, which therefore gives a good prediction for the drag profile of shot D.

Table 28: Simulation with initial conditions and aerodynamic asymmetries for case 4

<table>
<tr><th colspan="8">Initial fire conditions</th></tr>
<tr><th>Case</th><th>Mass [Kg]</th><th colspan="2">Initial Velocity [m/s]</th><th colspan="2">Elevation Angle [deg]</th><th>Initial Pitch [deg]</th><th>Initial Yaw [deg]</th></tr>
<tr><td>4</td><td>4.35</td><td colspan="2">278.04</td><td colspan="2">44.625</td><td>5</td><td>5</td></tr>
<tr><th colspan="8">Aerodynamic and mass asymmetries</th></tr>
<tr><th>Case</th><th>B1</th><th>Cm0</th><th>B2</th><th>Ycg [mm]</th><th>Zcg [mm]</th><th colspan="2">Cl (Roll Moment)</th></tr>
<tr><td>4</td><td>0</td><td>0.06</td><td>120</td><td>0</td><td>0.0003</td><td colspan="2">0.0019</td></tr>
</table>

Results from this simulation was then compared to real test data for shot D as shown in Figure 56. The drag coefficient comparisons, shown in Figure 56, indicated good agreement with shot D.

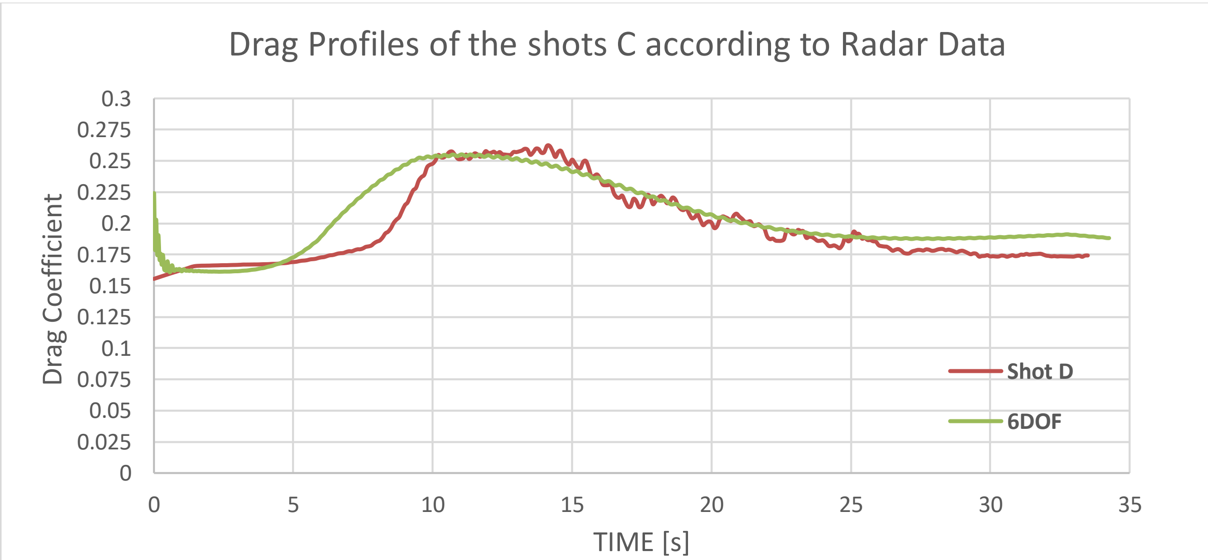

Figure 56: Drag coefficient comparisons for Case 4

5.3.5 Conclusion of the case studies

In this section, the 6-DOF model program was used to conduct case studies to identify possible causes for the flight behaviour of real test results captured during the dynamic firing of mortar bombs. A computational evaluation to predict the drag coefficient profiles of the given shots, was completed on an 81 mm mortar bomb using the 6-DOF model. The results of the case studies indicate good agreement with experimented results. The 6-DOF model has a slight difference in the predication of the drag coefficient profiles compared to the real test results. This is reasonable since the assumptions used in the calculation exclude the weather affects and other asymmetries affects. It is also important to note that the test data, as captured by the radar, also includes some error or uncertainty.

CHAPTER 6: CONCLUSION

6.1 Conclude that objectives set in Chapter 1 was reached.

A 6-DOF trajectory simulation model for predicting the behaviour of symmetric and asymmetric projectiles has been successfully implemented. This 6-DOF model was developed in MATLAB program, as outlined in chapter 3. The research summarised in this thesis began with complete detail on the theoretical models used to calculate forces and moments, as well as all the transformations between the various coordinate frames as shown in chapter 3.

Verification studies, which emphasise the overall ability of the 6-DOF model used in this verification, have been extensively reviewed in chapter 4. Various case studies were selected for the verification studies. The first cases showed a comparison of the 6-DOF model results with analytical solutions and other simulation models. The results of these cases verified that the present 6-DOFmodel has been coded correctly and verified that the model produces reliable trajectories for symmetric and asymmetric cases.

The second set of studies showed a comparison of the 6-DOF model results with WinFast program results. The results of these cases demonstrate the validity of the functions used in MATLAB to predict features like the natural pitch frequency and phenomena such as spin-up and spin through resonance for a typical fin stabilised projectile. Moreover, it demonstrates the validity of the function used in the present 6-DOF model to accommodate the combination of asymmetries effects when the asymmetric projectile tends to “lock-in”.

The last set of studies showed the 6-DOF model results compared to results generated by PRODAS V3 (Arrow Tech Associates). The results of these cases verified that the complicated six degrees of freedom (6-DOF) trajectory simulation model can be applied for the accurate prediction of short and long-range trajectories of high and low spin and fin-stabilised symmetric and asymmetric projectiles. Therefore, this verification studies verifies the correctness of simulation in general and provided confidence to proceed with the case studies in chapter 5.

The study done in chapter 5 focused on aerodynamic and mass asymmetries. It has shown that a combination of relatively small asymmetries in mortar bombs can lead to unexpected flight performance, and therefore a degradation in impact dispersion is likely to occur. In addition, the systematic study was based on two cases, one on small asymmetries and various roll moments, and the other on small asymmetries and variable positions of radial CoG offset. The studies provided the expected drag profiles for the combined asymmetries in mortar bombs by means of simulations.

Lastly, the 6-DOF model program was used to conduct case studies to identify possible causes for the flight behaviour of real test results captured during the dynamic firing of mortar bombs. A computational evaluation, to predict the drag coefficient profiles of the given shots, was completed on an 81 mm mortar bomb using the 6-DOF model. The results of the case studies indicated good agreement with experimented results. The 6-DOF results matches the radar data captured during the dynamic test reasonably well. The remaining differences is probably due to various factors in atmospheric data, as well as uncertainties associated with radar data.

6.2 Future work to be done

(1) Upgrade the 6-DOF model to include the influence of all the atmospheric conditions on a trajectory.

(2) Implementation of Rocket and Base Bleed models on 6-DOF trajectory simulation model as:

- Rocket Model — Providing the Parameters to model Rocket Performance.
- Base Bleed Model — Providing the Parameters required to model Base Bleed Performance.

(3) The 6-DOF trajectory simulation developed during this research proved adequate as a tool for research. In future, more work can be done to “Standardise” input and outputs through the development of user-friendly interfaces.

(4) Future research could focus on the identification of additional aerodynamic parameters not presently accounted for. An example would be yaw moments due to a pitch angle as experienced by a missile with canted fins and downwash.

(5) Sensitivity studies to advise on allowable tolerance in the design and manufacturing processes.

REFERENCES

Baranowski, L. 2013. Effect of the mathematical model and integration step on the accuracy of the results of computation of artillery projectile flight parameters. *Bull. Polish Acad. Sci.* 61(2):475–484.

Curcin, M. 2007. ProMoS-6DoF – Projectile Motion Simulation – Six DoF model.

Diebel, J. 2006. Representing Attitude: Euler Angles, Unit Quaternions, and Rotation Vectors. Stanford.

Duncan, L.D. & Ensey, R.J. 1964. Six Degree of Freedom Digital Simulation Model for Unguided Fin-Stabilized Rockets. Defence Documentation Center for Scientific and Technical Information: Alexandria, Virginia.

Dykes, J. 2011. Projectile linear theory for aerodynamically asymmetric projectiles. *Proc. Inst. Mech. Eng. Part G J. Aerosp. Eng.* 228(11):2094–2107.

Fann, C.M. 2006. DEVELOPMENT OF AN ARTILLERY ACCURACY MODEL. Naval Postgraduate School Monterey.(Thesis)

Fresconi, F., Cooper, G., Celmins, I., DeSpirito, J., & Costello, M. 2010. Flight mechanics of a novel guided spin-stabilized projectile concept. *Proc. Inst. Mech. Eng. Part G J. Aerosp. Eng.* 226(3):327–340.

Gkritzapis, D.N., Panagiotopoulos, E.E., Margaris, D.P., & Papanikas, D.G. 2007. A Six Degree of Freedom Trajectory Analysis of Spin - Stabilized Projectiles A Six Degree of Freedom Trajectory Analysis of Spin- Stabilized Projectiles, in: International Conference of Computational Methods in Sciences and Engineering. Corfu.

Glover, L.S. & Hagan, J.C. 1971. The Motion of Ballistic Missiles, Technical Memorandum TG 1164. Silver Spring.

Greenwood, D.T. 1988. Principles of Dynamics. 2nd ed. Prentice-Hall International: London.

Gro, K., Berlin, A., & May, G. 2012. Introduction into quaternions for spacecraft attitude representation. :1–16.

AIAA Guide for the verification and validation of computational fluid dynamics simulations. AIAA G-077e1998; 1998.

Hawley, P.A. & Blauwkamp, R.A. 2010. Six-Degree-of-Freedom Digital Simulations for Missile Guidance, Navigation, and Control. *Johns Hopkins APL Tech. Dig. (Applied Phys. Lab.* 29(1):71–84.

Hoffman, J.D. 1992. Numerical Methods for Engineers and Scientists. 2nd Editio ed. Marcel Dekker, Inc: New York.

ISO 2533, ICAO (the International Civil Aviation Organization). May 1975. The International Standard Atmosphere (ISA), 1st Edition.

Wertz, J . 1978. Spacecraft Attitude Determination and Control. Springer Netherlands.

Mccoy, R.L. 1998. Modern Exterior Ballistics: The Launch and Flight Dynamics of Symmetric Projectiles. Schiffer Military History: Atglen.

Murphy, C.H. 1963. Free Flight Motion of Symmetric Missiles. BRL Report No.1216, Aberdeen Proving Ground.

Nielsen, J.N. 1988. The Present Status and the Future of Missile Aerodynamics.

Press, W.H., Teukolsky, S.A., Vetterling, W.T., & Flannery, B.P. 1968. Numerical Recipes in C: The Art of Scientific Computing. 2nd Editio ed. Cambridge University Press: Cambridge.

PRODAS Arrow Tech Associated. 2013. Arrow Tech Software Products Featuring PRODAS V3.5. South Burington, VT.

Rasmussen, M. L., Kirk, D. B.: “On the Pitching and Yawing Motion of a Spinning Symmetric Missile Governed by an Arbitrary Nonlinear Restoring Moment”, NASA TN D-2135, 1964.

Regan, F.J. 1984. Re-Entry Vehicle Dynamics. AIAA education series.

STANAG 4061 (Edition 4) - Adoption of a Standard Ballistic Meteorological Message. 2000. Brussels.

STANAG 4355 (Edition 3) - The Modified Point Mass and Five Degree of Freedom Trajectory Models. 2006. Brussels.

STANAG 4537 (Edition 3) - Sub-Group 2 Sharable (Fire Control) Software Suite (S4). 2010. Brussels.

STANAG 4082 MET (Edition 3) - Adoption of a Standard Computer Meteorological Message. 2012. Brussels.

STANAG 2211 - Geodetic Datums, Ellipsoids, Grids and Grid References. 2016. Brussels.

Sterne, T.E. 1944. On jump due to bore clearance. ," Ballistic Research Laboratories Report No.491. Aberdeen Proving Ground.

Thuresson, M. 2015. Development and evaluation of a six degrees of freedom model of a 155 mm artillery projectile. KTH Royal Institute of Technology.

Vaughn, H.R. 1969. A Detailed Development of the Tricyclic Theory. Sandia Laboratory, Albuquerque.

Venegas, J. 2018. Inter-Comparison of Forward Radiative Transfer Computer Models [WWW Document]. URL https://digitalcommons.calpoly.edu/cgi/viewcontent.cgi?referer=https://www.google.co.za/&httpsredir=1&article=1232&context=star.

Walters, R.K. & Engebos, B.F. 1968. An Improved Method of Error Control for Runge-Kutta Numerical Integration. 2nd Editio ed. United States Army Electronic Command: White Sands Missile Range.

Weibel. 2007. External Control Interface: WinTrack File Formats. Allerod, Denmark.

Wey, P., Corriveau, D., Saitz, T.A., De Ruijter, W., & Stromback, P. 2016. BALCO 6/7-DoF Trajectory Model., in: 29th International Symposium on Ballistics. pp. 151–162.

Zipfel, P.H. 2007. Modelling and Simulation of Aerospace Vehicle Dynamics. 2nd Edition ed. American Institute of Aeronautics and Astronautics, Inc.: Reston.

APPENDIX A: BALLISTIC METEOROLOGICAL MESSAGE

A.1 Standard Ballistic Meteorological Message

This meteorological message provides MET data as a function of the so-called line number. The line number is linked to the apex height of the planned trajectory. The data provided for each line represents an average atmospheric condition for the trajectory as shown in Table 31 and descripted in Table 29 and Table 30. This format of atmospheric conditions is usually used in conjunction with so-called Range Tables (RT) and is ideally suited for "hand calculations" of the influence of atmospheric conditions on a trajectory. Please note that there are two versions of the Ballistic MET message (STANAG 4082, 2012; STANAG 4061, 2000):

- METB2 Is for surface to air trajectories.
- METB3 Is for surface to surface trajectories as in artillery applications.

Table 29: Format for the Standard Ballistic MET message

METB3QLaLaLaLoLoLo	First Heading Line
YYGoGoGoGHHHPPP	Second Heading Line
00DDFFTTTddd 01DDFFTTTddd ZZ… " 15DDFFTTTddd	MET data for Line Numbers 00 to 15
99999	Last line indicating End-of-File/Data

Table 30: Description of data and information in the METB3 File

Description of parameters in heading lines	
Q	Octant of the globe where this message is for
	0 Northern Hemisphere 0° to 90° West
	1 Northern Hemisphere 0° to 180° West
	2 Northern Hemisphere 180° to 90° East
	3 Northern Hemisphere 90° to 0° East
	4 Not Used
	5 Southern Hemisphere 0° to 90° West
	6 Southern Hemisphere 90° to 180° West
	7 Southern Hemisphere 180° to 90° East
	8 Southern Hemisphere 90° to 0° East
	9 Used when the centre of area of application is not indicated by latitude and longitude
LaLaLa	Latitude of the center of area of application in tens, units and tenths of degrees.
LoLoLo	Longitude of the center of area of application in tens, units and tenths of degrees. For longitudes of 100 degrees or greater the hundreds digit is omitted. The user should add it according to the octant of the globe.
YY	Day of the month on which the period of validity of the message commences (GMT)
GoGoGo	Time of commencement of the period of validity in whole hours and tenths (GMT; 000 to 239)
G	Duration of validity period in hours, from 1 to 8; G=9 designates 12 hours
HHH	Height of the meteorological datum plane (MDP) above mean sea level (MSL) in tens of meters.
PPP	Pressure at the MDP expressed as a percentage, to the nearest 0.1 per cent, of the standard pressure (1013.25 mBar); the initial digit is omitted when the pressure is standard or above
Description of MET data for each Line Number	
ZZ	Line number identifying a LINE in the message running from 00 to 15.
DD	Direction from which the ballistic wind is blowing; measured clockwise from true North and expressed in hundreds of mils (6400 mils = 360 degrees). Encoded from 01 to 64 and encoded as 00 when the wind speed is zero
FF	Speed of ballistic wind in tens and units of knots.
TTT	Ballistic temperature: expressed as a percentage of standard; to the nearest 0.1 per cent. The initial digit is omitted when the ballistic temperature is standard or above.
ddd	Ballistic density expressed as a percentage of standard; to the nearest 0.1 per cent. The initial digit is omitted when the ballistic density is standard or above.
99999	Optional to indicates the termination of a message

Table 31: METB3 Line numbers and corresponding zone boundaries (STANAG 4061, 2000)

Line Number	Height [m]	Zone Number	Boundaries [m]
00	Surface	01	0 – 200
01	200	02	200 – 500
02	500	03	500 – 1000
03	1000	04	1000 – 1500
04	1500	05	1500 – 2000
05	2000	06	2000 -3000
06	3000	07	3000 – 4000
07	4000	08	4000 – 5000
08	5000	09	5000 – 6000
09	6000	10	6000 – 8000
10	8000	11	8000 – 10000
11	10000	12	10000 – 12000
12	12000	13	12000 -14000
13	14000	14	14000 – 16000
14	16000	15	16000 - 18000
15	18000	16	18000 – 20000
16	20000	17	20000 – 22000
17	22000	18	22000 – 24000
18	24000	19	24000 – 26000
19	26000	20	26000- 28000
20	28000	21	28000 - 30000
21	30000		

It is important to note that the Ballistic MET message contains lines of average meteorological conditions for a trajectory with an apex height associated with a specific line number. To compile the ballistic MET message, it is therefore necessary to combine the influence of each atmospheric layer towards this average value, using weighting factors for density, temperature and wind as shown in Table 32, Table 33, and Table 34.

Table 32: Density weighting factors for each MET line and associated height

LINE NO:	SCALE FACTORS 1 to 21																				
1.00	1.00	0.00	0.00	0.00	0.00	0.00	0.00	0.00	0.00	0.00	0.00	0.00	0.00	0.00	0.00	0.00	0.00	0.00	0.00	0.00	0.00
2.00	0.30	0.70	0.00	0.00	0.00	0.00	0.00	0.00	0.00	0.00	0.00	0.00	0.00	0.00	0.00	0.00	0.00	0.00	0.00	0.00	0.00
3.00	0.15	0.24	0.61	0.00	0.00	0.00	0.00	0.00	0.00	0.00	0.00	0.00	0.00	0.00	0.00	0.00	0.00	0.00	0.00	0.00	0.00
4.00	0.11	0.16	0.28	0.46	0.00	0.00	0.00	0.00	0.00	0.00	0.00	0.00	0.00	0.00	0.00	0.00	0.00	0.00	0.00	0.00	0.00
5.00	0.08	0.12	0.20	0.21	0.38	0.00	0.00	0.00	0.00	0.00	0.00	0.00	0.00	0.00	0.00	0.00	0.00	0.00	0.00	0.00	0.00
6.00	0.06	0.09	0.14	0.14	0.14	0.44	0.00	0.00	0.00	0.00	0.00	0.00	0.00	0.00	0.00	0.00	0.00	0.00	0.00	0.00	0.00
7.00	0.05	0.07	0.11	0.11	0.10	0.22	0.35	0.00	0.00	0.00	0.00	0.00	0.00	0.00	0.00	0.00	0.00	0.00	0.00	0.00	0.00
8.00	0.04	0.06	0.10	0.09	0.09	0.17	0.17	0.29	0.00	0.00	0.00	0.00	0.00	0.00	0.00	0.00	0.00	0.00	0.00	0.00	0.00
9.00	0.04	0.05	0.09	0.08	0.08	0.14	0.14	0.14	0.24	0.00	0.00	0.00	0.00	0.00	0.00	0.00	0.00	0.00	0.00	0.00	0.00
10.00	0.03	0.05	0.08	0.07	0.07	0.13	0.11	0.11	0.10	0.27	0.00	0.00	0.00	0.00	0.00	0.00	0.00	0.00	0.00	0.00	0.00
11.00	0.03	0.04	0.07	0.06	0.06	0.11	0.10	0.19	0.08	0.14	0.20	0.00	0.00	0.00	0.00	0.00	0.00	0.00	0.00	0.00	0.00
12.00	0.03	0.04	0.07	0.07	0.06	0.11	0.10	0.08	0.08	0.13	0.11	0.14	0.00	0.00	0.00	0.00	0.00	0.00	0.00	0.00	0.00
13.00	0.03	0.04	0.07	0.06	0.06	0.10	0.09	0.08	0.08	0.12	0.09	0.08	0.10	0.00	0.00	0.00	0.00	0.00	0.00	0.00	0.00
14.00	0.03	0.04	0.06	0.06	0.06	0.10	0.09	0.09	0.08	0.12	0.09	0.07	0.05	0.06	0.00	0.00	0.00	0.00	0.00	0.00	0.00
15.00	0.03	0.04	0.07	0.06	0.06	0.10	0.09	0.08	0.07	0.12	0.09	0.07	0.05	0.03	0.04	0.00	0.00	0.00	0.00	0.00	0.00
16.00	0.03	0.05	0.06	0.06	0.06	0.10	0.10	0.08	0.07	0.12	0.09	0.06	0.04	0.03	0.02	0.04	0.00	0.00	0.00	0.00	0.00
17.00	0.03	0.04	0.07	0.06	0.05	0.10	0.09	0.08	0.07	0.12	0.09	0.07	0.05	0.03	0.01	0.01	0.04	0.00	0.00	0.00	0.00
18.00	0.03	0.04	0.07	0.06	0.05	0.10	0.09	0.08	0.07	0.11	0.09	0.07	0.04	0.03	0.02	0.01	0.02	0.02	0.00	0.00	0.00
19.00	0.03	0.04	0.06	0.07	0.06	0.10	0.09	0.08	0.08	0.11	0.09	0.07	0.05	0.03	0.02	0.01	0.02	0.02	0.01	0.00	0.00
20.00	0.02	0.04	0.06	0.06	0.06	0.11	0.09	0.09	0.08	0.13	0.10	0.06	0.04	0.03	0.00	0.00	0.00	0.01	0.01	0.01	0.00
21.00	0.02	0.03	0.06	0.05	0.06	0.10	0.09	0.08	0.07	0.11	0.09	0.06	0.05	0.03	0.03	0.01	0.01	0.01	0.01	0.00	0.02

Table 33: Temperature weighting factors for each MET line and associated height

LINE NO:	SCALE FACTORS 1 to 21																				
1	1	0	0	0	0	0	0	0	0	0	0	0	0	0	0	0	0	0	0	0	0
2	0.27	0.73	0	0	0	0	0	0	0	0	0	0	0	0	0	0	0	0	0	0	0
3	0.13	0.2	0.67	0	0	0	0	0	0	0	0	0	0	0	0	0	0	0	0	0	0
4	0.08	0.12	0.25	0.55	0	0	0	0	0	0	0	0	0	0	0	0	0	0	0	0	0
5	0.05	0.1	0.2	0.21	0.44	0	0	0	0	0	0	0	0	0	0	0	0	0	0	0	0
6	0.04	0.04	0.09	0.11	0.13	0.59	0	0	0	0	0	0	0	0	0	0	0	0	0	0	0
7	0.02	0.04	0.07	0.09	0.11	0.26	0.41	0	0	0	0	0	0	0	0	0	0	0	0	0	0
8	0.01	0.03	0.05	0.04	0.1	0.19	0.23	0.35	0	0	0	0	0	0	0	0	0	0	0	0	0
9	0.01	0.01	0.02	0.03	0.03	0.09	0.13	0.24	0.44	0	0	0	0	0	0	0	0	0	0	0	0
10	0.01	0.01	0.02	0.03	0.03	0.09	0.13	0.24	0.44	0.3	0	0	0	0	0	0	0	0	0	0	0
11	0.01	0.01	0.02	0.03	0.03	0.09	0.13	0.24	0.44	0.3	0	0	0	0	0	0	0	0	0	0	0
12	0.01	0.01	0.02	0.03	0.03	0.09	0.13	0.24	0.44	0.3	0	0	0	0	0	0	0	0	0	0	0
13	0.01	0.01	0.02	0.03	0.03	0.09	0.13	0.24	0.44	0.3	0	0	0	0	0	0	0	0	0	0	0
14	0.01	0.01	0.02	0.03	0.03	0.09	0.13	0.24	0.44	0.3	0	0	0	0	0	0	0	0	0	0	0
15	0.01	0.01	0.02	0.03	0.03	0.09	0.13	0.24	0.44	0.3	0	0	0	0	0	0	0	0	0	0	0
16	0.01	0.01	0.02	0.03	0.03	0.09	0.13	0.24	0.44	0.3	0	0	0	0	0	0	0	0	0	0	0
17	0.01	0.01	0.02	0.03	0.03	0.09	0.13	0.24	0.44	0.3	0	0	0	0	0	0	0	0	0	0	0
18	0.01	0.01	0.02	0.03	0.03	0.09	0.13	0.24	0.44	0.3	0	0	0	0	0	0	0	0	0	0	0
19	0.01	0.01	0.02	0.03	0.03	0.09	0.13	0.24	0.44	0.3	0	0	0	0	0	0	0	0	0	0	0
20	0.01	0.01	0.02	0.03	0.03	0.09	0.13	0.24	0.44	0.3	0	0	0	0	0	0	0	0	0	0	0
21	0.01	0.01	0.02	0.03	0.03	0.09	0.13	0.24	0.44	0.3	0	0	0	0	0	0	0	0	0	0	0

Table 34: Wind weighting factors for each MET line and associated height

LINE NO:	SCALE FACTORS 1 to 21																				
1	1	0	0	0	0	0	0	0	0	0	0	0	0	0	0	0	0	0	0	0	0
2	0.2	0.8	0	0	0	0	0	0	0	0	0	0	0	0	0	0	0	0	0	0	0
3	0.09	0.19	0.72	0	0	0	0	0	0	0	0	0	0	0	0	0	0	0	0	0	0
4	0.06	0.12	0.26	0.56	0	0	0	0	0	0	0	0	0	0	0	0	0	0	0	0	0
5	0.04	0.08	0.15	0.2	0.53	0	0	0	0	0	0	0	0	0	0	0	0	0	0	0	0
6	0.03	0.05	0.08	0.09	0.12	0.63	0	0	0	0	0	0	0	0	0	0	0	0	0	0	0
7	0.02	0.03	0.07	0.07	0.08	0.2	0.53	0	0	0	0	0	0	0	0	0	0	0	0	0	0
8	0.02	0.02	0.06	0.06	0.06	0.14	0.19	0.45	0	0	0	0	0	0	0	0	0	0	0	0	0
9	0.02	0.02	0.05	0.05	0.05	0.12	0.13	0.2	0.36	0	0	0	0	0	0	0	0	0	0	0	0
10	0.01	0.02	0.02	0.04	0.03	0.07	0.08	0.09	0.09	0.55	0	0	0	0	0	0	0	0	0	0	0
11	0	0	0.01	0.04	0.03	0.08	0.08	0.09	0.09	0.2	0.38	0	0	0	0	0	0	0	0	0	0
12	0	0.01	0.01	0.02	0.04	0.07	0.07	0.07	0.08	0.17	0.16	0.3	0	0	0	0	0	0	0	0	0
13	0	0.01	0.01	0.01	0.03	0.07	0.07	0.07	0.07	0.15	0.14	0.13	0.24	0	0	0	0	0	0	0	0
14	0	0.01	0.01	0.01	0.02	0.07	0.07	0.07	0.07	0.13	0.13	0.13	0.1	0.18	0	0	0	0	0	0	0
15	0	0.01	0.01	0.01	0.02	0.07	0.07	0.07	0.07	0.12	0.12	0.11	0.1	0.08	0.14	0	0	0	0	0	0
16	0.02	0.02	0.03	0.03	0.03	0.07	0.07	0.08	0.05	0.14	0.1	0.08	0.07	0.05	0.03	0.12	0	0	0	0	0
17	0.02	0.02	0.03	0.05	0.05	0.06	0.08	0.08	0.06	0.13	0.09	0.08	0.06	0.05	0.03	0.03	0.09	0	0	0	0
18	0.03	0	0.03	0.03	0.03	0.08	0.1	0.08	0.08	0.13	0.13	0.1	0.08	0.05	0	0	0.03	0.05	0	0	0
19	0.02	0.02	0.04	0.04	0.06	0.09	0.08	0.08	0.08	0.15	0.1	0.08	0.05	0.03	0.02	0.02	0.02	0.02	0.02	0	0
20	0.03	0.02	0.05	0.05	0.05	0.07	0.07	0.06	0.06	0.09	0.08	0.07	0.06	0.05	0.02	0.02	0.02	0.03	0.02	0.09	0
21	0.03	0.03	0.03	0.03	0	0.07	0.07	0.05	0.05	0.09	0.09	0.1	0.05	0.03	0.05	0.03	0.04	0.03	0.02	0.02	0.06

Where computer MET or atmospheric data as a function of height is required for trajectory simulations, such data has to be converted into the “Ballistic MET” format in order to it with firing tables.

A.2 Standard Artillery Computer Meteorological Message

The format of this meteorological message is defined in (STANAG 4082, 2012). This is the MET data usually used with trajectory simulation programs. This MET data essentially supply the average atmospheric conditions for certain zones, where the zones are linked to a specific atmospheric height as shown in Table 37 and descripted in Table 35 and Table 36.

Table 35: Format for the Standard Artillery Computer MET - METCM

METCMQLaLaLaLoLoLoYYGoGoGo HHHPPP	One Heading Line
00DDDFFF TTTTRRRR 01DDDFFF TTTTRRRR ZZ… “ 26DDDFFF TTTTRRRR d	MET data for Line Numbers 00 to 26
99999	Last line indicating End-of-File/Data

Table 36: Description of data and information in the METCM File

Description of parameters in heading line		
Q	Octant of the globe where this message is for	
0	Northern Hemisphere	0° to 90° West
1	Northern Hemisphere	0° to 180° West
2	Northern Hemisphere	180° to 90° East
3	Northern Hemisphere	90° to 0° East
4	Not Used	
5	Southern Hemisphere	0° to 90° West
6	Southern Hemisphere	90° to 180° West
7	Southern Hemisphere	180° to 90° East
8	Southern Hemisphere	90° to 0° East
9	Used when the centre of area of application is not indicated by latitude and longitude	
LaLaLa	Latitude of the centre of area of application in tens, units and tenths of degrees.	
LoLoLo	Longitude of the centre of area of application in tens, units and tenths of degrees. For longitudes of 100 degrees or greater the hundreds digit is omitted. The user should add it according to the octant of the globe.	
YY	Day of the month on which the period of validity of the message commences (01 to 31)	
GoGoGo	Time of commencement of the period of validity in whole hours and tenths (GMT; 000 to 239)	
G	Duration of validity period in hours, from 1 to 8; G=9 designates 12 hours	
HHH	Height of the meteorological datum plane (MDP) above mean sea level (MSL) in tens of meters.	
PPP	Pressure at the MDP expressed as a percentage, to the nearest 0.1 per cent, of the standard pressure (1013.25 mBar); the initial digit is omitted when the pressure is standard or above	
Description of MET data for each Line Number		
ZZ	Line number identifying a LINE in the message running from 00 to 26.	
DDD	Direction from which the ballistic wind is blowing; measured clockwise from true North and expressed in tens of mils (6400 mils = 360 degrees). Encoded from 001 to 640 and encoded as 000 when the wind speed is zero	
FFF	Mean wind speed of the zone in knots.	
TTTT	Mean virtual temperature of the zone to the nearest 0.1 K.	
RRRR	Zone midpoint pressure in millibar.	

Table 37: METCM Line numbers and corresponding zone boundaries

Line Number	Height [m]	Zone Number	Boundaries [m]
00	Surface	01	0 – 200
01	200	02	200 – 500
02	500	03	500 – 1000
03	1000	04	1000 – 1500
04	1500	05	1500 – 2000
05	2000	06	2000 -2500
06	2500	07	2500 – 3000
07	3000	08	3000 – 3500
08	3500	09	3500 – 4000
09	4000	10	4000 – 4500
10	4500	11	4500 – 5000
11	5000	12	5000 – 6000
12	6000	13	6000 - 7000
13	7000	14	7000 – 8000
14	8000	15	8000 - 9000
15	9000	16	9000 - 10000
16	10000	17	10000 – 11000
17	11000	18	11000 – 12000
18	12000	19	12000 -13000
19	13000	20	13000 – 14000
20	14000	21	14000 – 15000
21	15000	22	15000 – 16000
22	16000	23	16000 – 17000
23	17000	24	17000 - 18000
24	18000	25	18000 – 19000
25	19000	26	19000 - 20000
26	20000		

APPENDIX B: INTERPRETATION OF AERODYNAMIC PARAMETERS

The aerodynamic coefficients used are defined, using the following convention, see also (Mccoy, 1998).

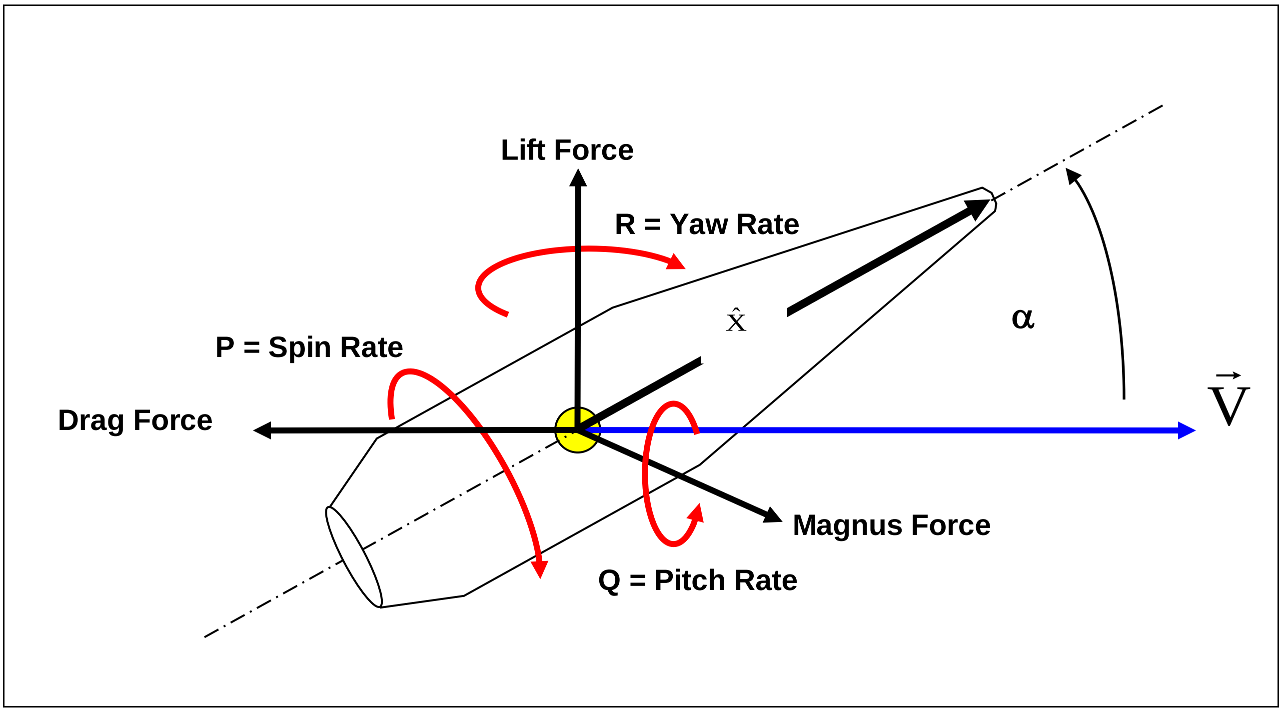

Drag Force:

$$D = \left\{\frac{1}{2} * \rho * V^2 * S\right\} * \left\{Cd_0 + Cd_{a^2} * \sin^2(\alpha)\right\}$$

Drag Force Vector:

$$\vec{D} = -\left\{\frac{1}{2} * \rho * S\right\} * \left\{Cd_0 + Cd_{a^2} * \sin^2(\alpha)\right\} * V * \vec{V}$$

NOTE: $\sin(\alpha) = \frac{|\vec{V} \otimes \hat{x}|}{V}$

Lift Force:

$$L = \left\{\frac{1}{2} * \rho * V^2 * S\right\} * \left\{\sin(\alpha)\right\} * \left\{CL_a + CL_{a^3} * \sin^2(\alpha)\right\}$$

Lift Force Vector:

$$\vec{L} = \left\{\frac{1}{2} * \rho * S\right\} * \left\{CL_a + CL_{a^3} * \sin^2(\alpha)\right\} * \left\{\vec{V} \otimes \left(\hat{x} \otimes \vec{V}\right)\right\}$$

To convert from LIFT and DRAG components to AXIAL and NORMAL components, use:

Axial Force = Lift * sin(α) - Drag * cos(α)

Normal Force = Lift * cos(α) + Drag * sin(α)

Magnus Force:

$$\mathrm{Fmag} = \left\{\frac{1}{2}*\rho*V^2*S\right\}*\left(\frac{P*d}{2*V}\right)*\{\sin(\alpha)\}*\left\{Cy_{pa} + Cy_{pa^3}*\sin^2(\alpha)\right\}$$

Magnus Force Vector:

$$\vec{\mathrm{F}}\mathrm{mag} = \left\{\frac{1}{2}*\rho*V*S\right\}*\left(\frac{P*d}{2*V}\right)*\left\{Cy_{pa} + Cy_{pa^3}*\sin^2(\alpha)\right\}*(\vec{V}\otimes\vec{X})$$

Roll Moment:

$$M\delta = \left\{\frac{1}{2}*\rho*V^2*S\right\}*\{d*Cl\}, \quad \text{where } [Cl = Cl_\delta*\delta]$$

Roll Moment Vector:

$$\vec{M}\delta = \left\{\frac{1}{2}*\rho*V^2*S\right\}*\{d*Cl\}*\vec{X}$$

Pitch Moment:

$$M\alpha = \left\{\frac{1}{2}*\rho*V^2*S\right\}*\{d*\sin(\alpha)\}*\left\{Cm_a + Cm_{a^3}*\sin^2(\alpha)\right\}$$

Pitch Moment Vector:

$$\vec{M}\alpha = \left\{\frac{1}{2}*\rho*V*S*d\right\}*\left\{Cm_a + Cm_{a^3}*\sin^2(\alpha)\right\}*(\vec{V}\otimes\hat{X})$$

Magnus Moment:

$$\mathrm{Mmag} = \left\{\frac{1}{2}*\rho*V^2*S\right\}*\left(\frac{p*d^2}{2*V}\right)*[\sin(\alpha)]*\left\{Cm_{pa} + Cm_{pa^3}*\sin^2(\alpha)\right\}$$

Magnus Moment Vector:

$$\vec{\mathrm{M}}\mathrm{mag} = \left\{\frac{1}{2}*\rho*V*S\right\}*\left(\frac{p*d^2}{2*V}\right)*\left\{Cm_{pa} + Cm_{pa^3}*\sin^2(\alpha)\right\}*\left[\hat{X}\otimes\left(\vec{V}\otimes\hat{X}\right)\right]$$

Spin Damping Moment:

$$\mathrm{Mp} = \left\{\frac{1}{2}*\rho*V^2*S\right\}*\left\{\left(\frac{p*d^2}{2*V}\right)*Cl_P\right\}$$

Spin Damping Moment Vector:

$$\vec{\mathrm{M}}\mathrm{p} = \left\{\frac{1}{2}*\rho*V^2*S\right\}*\left\{\left(\frac{p*d^2}{2*V}\right)*Cl_P\right\}*\hat{X}$$

Pitch Damping Moment:

$$\mathrm{Mq} = \left\{\frac{1}{2}*\rho*V^2*S\right\}*\left\{\frac{d^2}{2*V}\right\}*\left\{Cm_q*q + Cm_{d\alpha\alpha/d}*\left(\frac{d\alpha}{dt}\right)\right\}$$

Pitch Damping Moment Vector:

$$\vec{\mathrm{M}}\mathrm{q} = \left\{\frac{1}{2}*\rho*V^2*S\right\}*\left\{\frac{d^2}{2*V}\right\}*\left\{\begin{array}{l} Cm_q*\left(\hat{X}\otimes\left(\frac{d\hat{X}}{dt}\right)\right) \quad + \\ Cm_{d\alpha\alpha/d}*\left[\left(\hat{X}\otimes\left(\frac{d\hat{X}}{dt}\right)\right)-\left(\hat{X}\otimes\left(\frac{1}{V}*\frac{d\vec{V}}{dt}\right)\right)\right]\end{array}\right\}$$

$$\approx \left\{\frac{1}{2}*\rho*V^2*S\right\}*\left\{\frac{d^2}{2*V}\right\}*\left\{Cm_q + Cm_{d\alpha\alpha/d}\right\}*\left(\hat{X}\otimes\left(\frac{d\hat{X}}{dt}\right)\right)$$

Note: $\left(\frac{d}{2*V}\right)$ is used to obtain non-dimensional data for angular rates. This affects: Magnus Force, Magnus Moments, Spin Damping Moments and Pitch Damping Moments.